Imaging early brain characteristics of alzheimer's disease

Imaging early brain characteristics of Alzheimer's disease: Structure, function and symptomatology

Roy Willem Elisabeth van Hooren

Colophon

Cover design:	Nynke Dijkstra
Lay-out:	Publiss | publiss.nl
Print:	Ridderprint | ridderprint.nl

IMAGING EARLY BRAIN CHARACTERISTICS OF ALZHEIMER'S DISEASE
Structure, function and symptomatology

PROEFSCHRIFT

ter verkrijging van de graad van doctor aan de Universiteit Maastricht,
op gezag van de Rector Magnificus, Prof. dr. Pamela Habibović
volgens het besluit van het College van Decanen,
in het openbaar te verdedigen
op donderdag 15 december 2022 om 13:00 uur

door

Roy Willem Elisabeth van Hooren
Geboren op 10 mei 1993 te Valkenburg A/D Geul

Promotores

Dr. H.I.L. Jacobs

Prof. Dr. F.R.J. Verhey

Copromotor

Dr. M. van Egroo

Beoordelingscommissie

Prof. Dr. D.E.J. Linden (voorzitter)

Dr. M. van Boxtel

Prof. Dr. M. van Buchem (Leiden University Medical Center)

Prof. Dr. B.A. Poser

Prof. Dr. K. Reetz (RWTH Aachen University, Germany)

TABLE OF CONTENTS

Chapter 1	General introduction, thesis aims and outline	7
Chapter 2	Inter-network connectivity and amyloid-beta linked to cognitive decline in preclinical Alzheimer's disease: A longitudinal cohort study *Alzheimer's Research & Therapy, 2018*	25
Chapter 3	Elevated norepinephrine metabolism is linked to cortical thickness in the context of Alzheimer's disease pathology *Neurobiology of Aging, 2021*	57
Chapter 4	Associations between the magnetization transfer-weighted MRI signal at 7T and microstructural characteristics of the locus coeruleus and its projections *In prep*	83
Chapter 5	Validity and reliability of template-based and manual segmentation approaches of the locus coeruleus in vivo at 7T *In prep*	101
Chapter 6	Associations between locus coeruleus integrity and nocturnal awakenings in the context of Alzheimer's disease plasma biomarkers: A 7T MRI study *Alzheimer's Research & Therapy, 2021*	125
Chapter 7	General discussion	155
Addendum	Impact paragraph	172
	Summary	176
	Nederlandse samenvatting	178
	Published work	181
	PhD defenses at the school for Mental Health and Neuroscience	182
	Dankwoord – Acknowledgments	183
	Over de auteur – About the author	188

GENERAL INTRODUCTION, THESIS AIMS AND OUTLINE

CHAPTER 1

GENERAL INTRODUCTION

Alzheimer's disease (AD) is a neurodegenerative disease and the most common form of dementia [1]. It is estimated to affect at least 55 million people worldwide today and this number is projected to exceed 152 million by 2050, barring medical breakthroughs in prevention or treatment of the disease [2, 3]. In addition to the devastating consequences of the disease for the patients and their caretakers, it is estimated that the global economic impact resulting from informal, social and medical care related to dementia could rise to over 2 trillion US$ by 2030 [4].

AD dementia is characterized by the gradual onset and progression of clinical symptoms that typically include the well-known memory deficits, but also lesser-known cognitive and behavioral impairments, such as language problems, impaired reasoning skills and changes in personality. These symptoms are severe enough to impair the patient in their daily functioning [5]. In addition, mild cognitive impairment (MCI) due to AD has been recognized as a prodromal stage of the disease in which the patient displays clinical symptoms of AD to a milder extent and is generally able to maintain their independent functioning in daily life [6]. Furthermore, increasing amounts of research are being done towards preclinical AD, in which hallmark AD pathologies are detected, but no clinical symptoms are present [7].

According to prevailing theories, these hallmark pathologies of AD are toxic protein aggregations; extracellular amyloid-beta (Aβ) plaques and intracellular neurofibrillary tau tangles that are assumed to contribute to downstream neurodegeneration and cognitive decline [5, 8-12]. The amyloid cascade hypothesis describes a possible sequence in which these pathologies contribute to the pathophysiological process of AD. In essence, the amyloid cascade hypothesis posits that pathologic cleavage of the amyloid precursor protein is the catalyst that sets in motion a series of events that involve the accumulation of Aβ plaques, which trigger the hyperphosphorylation of tau, resulting in the accumulation of neurofibrillary tangles and neurodegeneration [13]. This is reflected in research showing that tau pathology tracks well with neurodegeneration and cognition, while accumulating evidence suggests that Aβ works synergistically with tau pathology to worsen its deleterious effects on neurodegeneration and cognition [14-18]. Given the idea that Aβ is at the start of the AD pathophysiological process, many clinical trials have attempted to reduce Aβ burden in AD with the aim of slowing or reversing cognitive decline, however satisfactory treatment strategies do not currently exist for the disease [19].

The amyloid cascade hypothesis has been dominating the field, however recent failures of clinical trials targeting Aβ suggest that AD's etiology may be more complex. The deposition of tau pathology may appear before Aβ pathology, meaning that while there is evidence that Aβ plaques exacerbate tau pathology, their presence may not be a necessary requirement for tau pathology to develop [17, 18, 20]. While the exact etiology underlying the development of AD pathology remains to be further elucidated, the temporal and spatial progression of Aβ and tau pathology in the brain has been thoroughly described in the seminal Thal phases and Braak stages[A], respectively, and begins decades before the onset of clinical symptoms [8, 9, 20-22]. Furthermore, we know that the earliest phases of the AD pathophysiology start before levels of Aβ and tau pathology reach the cerebrospinal fluid (CSF) or positron emission tomography detection (PET) thresholds [9] (figure 1). As a result of the long pathophysiological process of AD and the late detection of AD pathology, disease-modifying treatments may be applied too late in the disease process and this has been cited as a factor contributing to the failure of pharmaceutical trials in AD [22].

We therefore aim to explore additional in vivo pathways for early detection of brain changes associated with Aβ and tau pathology to improve the participant selection process and efficacy of clinical trials targeting AD, potentially before the preclinical stage.

A. The **Thal phases** describe the temporal and spatial progression of Aβ deposition in the brain [21]:

Phase 1: Widespread neocortical deposits

Phase 2: Additional allocortical deposits

Phase 3: Diencephalon and striatum deposits

Phase 4: Deposits in select brainstem nuclei

Phase 5: Deposits in additional brainstem nuclei and cerebellar deposits

The **Braak stages** describe this progression for tau pathology [8, 20, 23]:

Stage a-c: Pretangle material in brainstem nuclei, predominantly in the locus coeruleus

Stage 1a-b: Pretangle material in the cortex, predominantly in the transentorhinal region

Stage I-II: Neurofibrillary tangles in the allocortical layers of the transentorhinal region

Stage III-IV: Neurofibrillary tangles in the neocortical layers of the transentorhinal region and entorhinal cortex

Stage V-VI: Widespread neurofibrillary tangles in neocortical association areas

Figure 1. Model describing the temporal progression of Alzheimer's disease biomarkers and cognitive symptoms

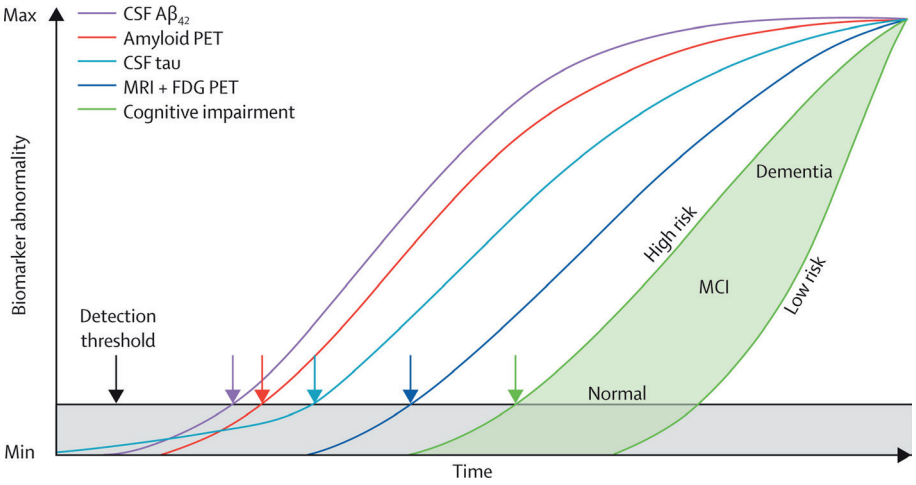

Note. The colored lines represent different modalities for the detection of the AD pathophysiological process. The detection threshold in this figure represents at which degree of biomarker abnormality we are currently able to detect each respective modality and this is plotted against a time variable on the x-axis. The focal point of this figure in the context of this thesis is the fact that the earliest detectable biomarkers, Aβ and tau, start building up before the CSF or PET detection threshold. We aim to investigate brain, cognition and behavior changes associated with Aβ and tau potentially before this detection threshold.

This figure was reprinted from The Lancet Neurology volume 12, issue 2, Jack et al. (2013) "Tracking pathophysiological processes in Alzheimer's disease: an updated hypothetical model of dynamic biomarkers", Pages 207-216, Copyright (2013), with permission from Elsevier.

DETECTING EARLY BRAIN CHANGES ASSOCIATED WITH AMYLOID-BETA AND TAU PATHOLOGY

One brain characteristic associated with Aβ pathology is neuronal excitability, as animal studies have revealed a distinct link between the presence of Aβ clusters and neuronal hyperexcitability in the vicinity of these clusters [24-26]. This has been described as a bi-directional association in which Aβ modulates neuronal activity, but the release of Aβ is simultaneously activity-dependent, resulting in a vicious cycle of increasing hyperactivity [26]. One of the earliest places where Aβ has been shown to accumulate in humans is in densely connected large-scale brain networks that maintain an intrinsic level of activity throughout the lifespan, such as the default mode network[B] [27, 28]. Resting-state functional magnetic resonance imaging (rs-fMRI)[C] has revealed that functional connectivity in these large-scale

brain networks is altered as a function of Aβ load in cognitively normal older persons [29], suggesting that Aβ may disrupt functioning of the networks, or that these networks adapt as response to Aβ pathology. Furthermore, the organization within and between these functional brain networks support cognitive functioning [30-34] and a dose-response relationship between Aβ and cognition has been reported in cognitively normal adults [35]. However, **it is still unclear whether functional connectivity between these large-scale networks is associated with Aβ burden and whether this connectivity conveys information about the Aβ-related rate of cognitive decline.**

B. The **default mode network (DMN)** is a functional brain network with hubs in the prefrontal, parietal and temporal lobes. It is characterized by its heightened activity in the absence of external stimuli and is thought to support cognitive functions including autobiographical memory retrieval and conceptualization [36, 37].

C. Functional magnetic resonance imaging (fMRI) is a noninvasive technique capable of measuring localized changes in blood oxygenation, which is coupled to the underlying neuronal activity [38]. While cautious interpretation is warranted due to the indirect association between the fMRI signal and neuronal activity, fMRI provides a convenient proxy measure to study brain function with great spatial detail. By investigating the temporal correlations of the fMRI signal between brain regions in participants at rest (**resting-state)**, we can study the organization of functional brain networks [39].

As mentioned previously, brain changes in AD are not only associated with Aβ, but also tau pathology. Post-mortem research has shown that an early form of aberrant tau species, namely tau pretangles, are present in the brainstem locus coeruleus (LC) (figure 2) as early as Braak stage a-c (also referred to as Braak stage 0) [20, 40] and volume loss in the LC is seen as early as Braak stage I [20, 41], implicating the LC in the very early stages of the disease. Importantly, the LC is a structure with widespread projections to the rest of the brain and forms the main source of cerebral noradrenaline (NA) [42]. There is evidence that metabolites[D] of NA are increased in AD and that this increase of metabolites is linked to higher levels of AD pathology [43-47]. Specifically, elevated metabolites of noradrenaline contribute to increased production of hyperphosphorylated tau in the LC, which contributes to the selective vulnerability of the LC to tau accumulation and related atrophy [46]. Furthermore, hyperphosphorylated tau is prone to propagation[E] to

connected brain regions [46, 48-50], suggesting that the LC-NA system may be a catalyst in spreading tauopathy to the rest of the brain. While previous research has described the involvement of elevated NA metabolites in the production and spreading of tau pathology, **it is still unclear whether these elevations are also associated with the downstream effects of tau on brain structure.**

D. The NA metabolic pathway produces a number of **metabolites**, including 3-Methoxy-4-hydroxyphenylglycol (MHPG) and 3,4-dihydroxyphenylglycolaldehyde (DOPEGAL). Specifically, DOPEGAL is upstream of MHPG in the NA metabolic pathway and has been reported to stimulate cleavage of tau into aggregation-prone forms [44, 46, 51].

E. The **propagation** of tau has been described as prion-like, meaning that the spreading of pathologic tau can induce the same type of abnormalities in other tau proteins, resulting in a self-amplifying cascade [48].

Figure 2. Visualization of the locus coeruleus in the brainstem and its projections to the rest of the brain

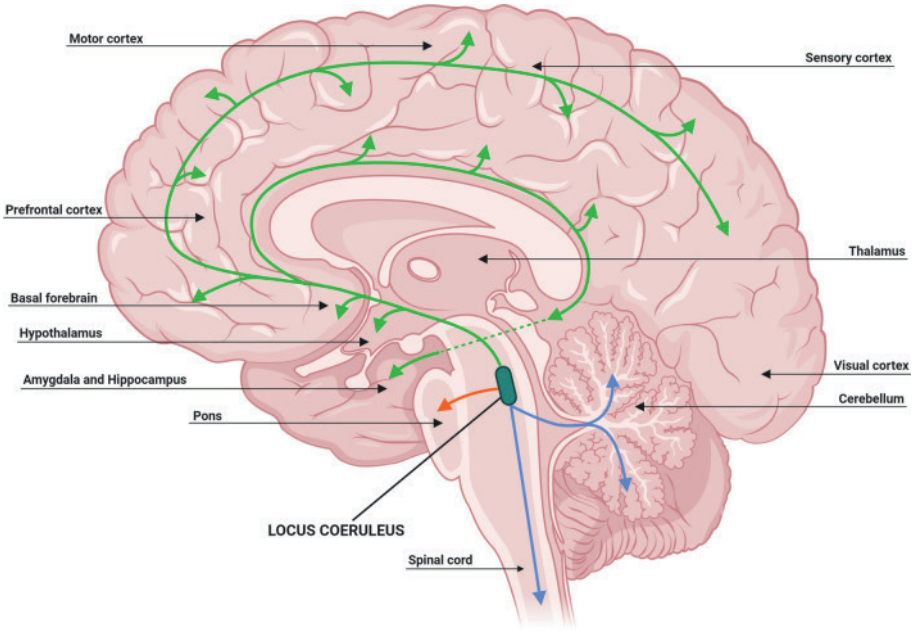

Reprinted with permission from Acta Neuropathologica volume 141, Matchett et al. (2021) "The mechanistic link between selective vulnerability of the locus coeruleus and neurodegeneration in Alzheimer's disease", Pages 631-650 under CC BY 4.0 licence.

The LC and its projections have an important modulatory role in arousal, attention and learning, but also plays a pivotal role in the sleep-wake cycle [52-56]. Sleep disturbances occur as early as in the 5th decade of life [57], and have been reported to be a risk factor for the development of cognitive impairment and (preclinical) AD later in life [58, 59]. Furthermore, accumulating evidence suggests that sleep is linked to clearance of metabolites like Aβ and tau from the brain [60, 61]. Disturbed sleep may therefore lead to a feedback loop, whereby neurodegeneration resulting from the reduced clearance of AD pathology leads to further increased sleep disturbances [62]. Furthermore, animal studies have shown that disturbed sleep induces an acceleration of tauopathy in the LC [63]. Given the predisposition of the LC to early tau pathology and associated volume loss [20, 40] and the important role of the LC in the regulation of sleep and wakefulness [54-56], the combined information about the structural integrity of the LC and sleep disturbances may contain valuable information about early processes related to AD pathology. Post-mortem research in humans has provided evidence supporting the link between the presence of tau pathology in the LC and antemortem sleep disturbances in preclinical stages of AD [64], however, **it has not been established in vivo whether there is a link between LC degeneration, AD pathology and sleep quality.**

Direct visualization of the LC in vivo is challenging due to its small size and proximity to pulsation of arteries and cerebrospinal fluid dynamics, introducing physiological noise. However, modern MRI developments from our lab allowed us visualize the LC at ultra-high resolution using 7 Tesla MRI scanners utilizing a specialized LC signal-sensitive MRI sequence, called magnetization transfer turbo flash (MT-TFL) [65]. With this sequence we can visualize the LC as a hyperintense signal in the brainstem (figure 3) and this signal has been generally interpreted as a proxy measure of LC integrity [66-70]. Furthermore, recent work indicated converging evidence[F] between autopsy LC tau tangle density and MRI-based LC integrity, suggesting that LC integrity may also signal early tau-related processes [71]. While autopsy data shows no neuronal loss until Braak stage IV, the LC does show volume loss in the earlier Braak stages [41], potentially reflecting other morphological changes, such as the loss of dendritic arborization or density of projections towards the rest of the brain. The fact that LC integrity was able to correlate early with tau pathology may indicate that LC integrity reflects some of these early morphological changes. **Further**

insight into the microstructural correlates of LC integrity are necessary to fully understand the biological process underlying LC volume loss in preclinical AD. Neurite Density and Dispersion Orientation Imaging (NODDI) and correlational tractography[G] are techniques that allow us to investigate these microstructural properties in vivo [72, 73].

F. In a sample consisting of both cognitively unimpaired participants and participants with varying degrees of cognitive impairment, in vivo measures of LC integrity have been shown to correlate with PET measures of tau in the temporal regions and part of the parietal lobe. Consistent with the temporal ordering of Braak staging, this association was limited to the entorhinal cortex in a subset of cognitively unimpaired individuals. Furthermore, LC integrity was able to predict retrospective cognitive decline.

Autopsy data provided **converging evidence**, showing that LC tangle density was associated with both cortical tangle density and Braak staging, while it was also able to predict antemortem cognitive decline.

The association between LC tangle density and Braak staging was present even at a clinical dementia rating of 0, while some individuals showed lower LC integrity in the absence of detectable PET measures of tau, suggesting that these LC measures may signal early tau-related processes [71].

G. NODDI is a diffusion MRI technique that can be utilized to measure microstructural properties of dendrites and axons (neurites). It achieves this by estimating the neurite density and orientation dispersion (arborization) indices. These indices can be interpreted as measures of neuronal complexity [72]. **Correlational tractography** can be used to determine the integrity of white matter tracts. [73, 74]

Figure 3. Example of in vivo visualization of the locus coeruleus using the magnetization transfer turbo flash sequence at 7 Tesla magnetic resonance imaging

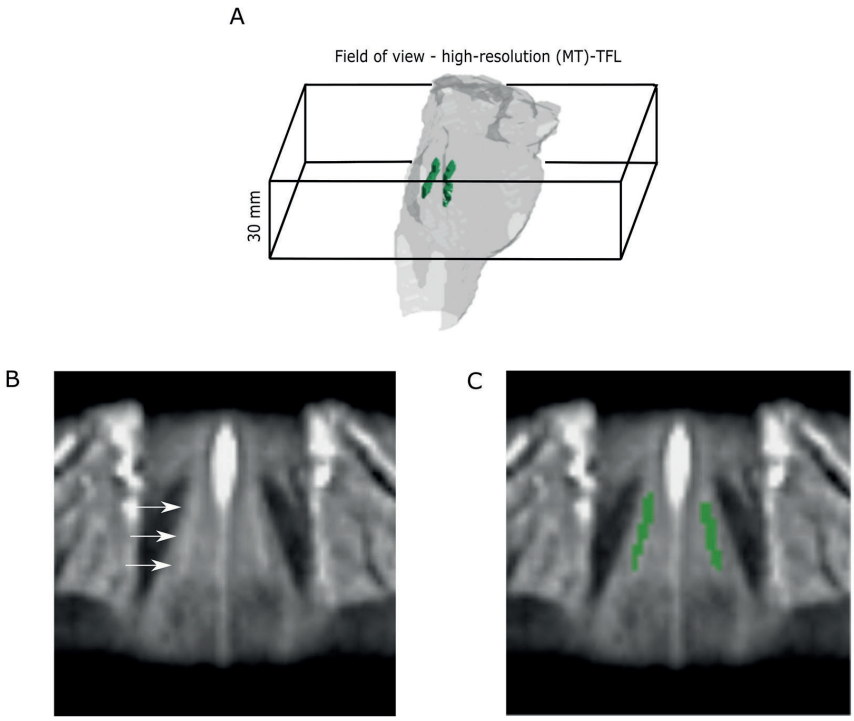

Note. A) The location of LC is visualized in the pons of the brainstem **B)** and is visible as a long, thin and hyperintense region on the MT-TFL scan, indicated by the white arrows. **C)** The LC is bilaterally segmented in green.

Reprinted with permission from eLife volume 9, Jacobs et al. (2020) "Dynamic behavior of the locus coeruleus during arousal-related memory processing in a multi-modal 7T fMRI paradigm" under CC BY 4.0 licence. Parts D-H of the original figure have been cropped out.

Finally, LC imaging is a relatively new field where new methods are continuously emerging. An important first step in order to evaluate and harmonize these efforts would be to assess the different approaches that researchers utilize to define the LC on MRI images. Previous studies have tried to establish an association between aging and LC integrity, though it is still unclear what the exact nature of this association is. Some data suggest a positive association between aging and LC integrity [75], whereas others find an inverted U-curve pattern for this association [71, 76, 77] or no association at all [78]. While differences in sample characteristics and MRI field strength may account for some of these discrepancies, **it is unclear to what extent the discrepancies between these findings may be due to divergent approaches to LC delineation.**

THESIS AIMS AND OUTLINE

Based on animal and histology work, we identified early AD pathology-related processes in the brain. We aim to examine these processes in vivo by using MRI and to determine their potential value as markers of the AD pathophysiological process in early stages of the disease. This aim serves the ultimate goal of improving the selection of at-risk participants for studies towards early intervention in AD, potentially in the preclinical phase. We can summarize this dissertation in the following chapters and research questions:

Chapter 2 ***What is the association between connectivity among functional brain networks and rate of cognitive decline, and does it depend on amyloid-beta burden?***

Aβ has been associated with alterations to the connectivity of brain networks that support cognitive functioning. Furthermore, Aβ has a dose-response relationship with cognition in healthy adults. In this chapter, we aimed to explore synergistic effects between inter-network functional connectivity, amyloid-beta, and memory decline in healthy older adults and individuals with preclinical, prodromal, or clinical Alzheimer's disease.

Chapter 3 ***Are noradrenaline metabolite levels associated with neurodegeneration, and is there a modifying role of hallmark Alzheimer's disease pathologies?***

Alzheimer's disease is characterized by high noradrenaline metabolite levels that may be associated with Alzheimer's disease pathology. The locus coeruleus is the main site for cerebral noradrenaline synthesis and volume loss in the locus coeruleus occurs as early as Braak stage 1. This study aims to investigate the association between noradrenergic turnover and brain morphology, and the modifying effect of Alzheimer's disease pathology in a memory clinic sample with cognitively impaired and unimpaired individuals.

Chapter 4 ***Is lower LC integrity associated with morphological changes in LC neurites or the integrity of LC projections?***

Locus coeruleus-sensitive MRI sequences at 7T MRI have been successful at imaging the locus coeruleus in-vivo at ultra-high-

resolution. However, the contribution of neuropil changes to the MT signal remains unclear. In this study we aimed to investigate the association between MT-weighted locus coeruleus signal and microstructural properties of the locus coeruleus and its projections, using Neurite Orientation Dispersion and Density Imaging and tractography in a healthy population across the lifespan.

Chapter 5 **What are the differences in reliability and validity among *different approaches of delineating the LC in vivo?***

The locus coeruleus is one of the first brain regions to accumulate hyperphosphorylated tau. Therefore, being able to image the integrity of the locus coeruleus in vivo in humans may provide valuable information about the earliest AD-related processes. However, different approaches to define the anatomical boundaries of the LC are in use, often leading to very different shapes and volumes of the LC. We compared the reliability of three different approaches for delineating the locus coeruleus in-vivo in the same sample of healthy individuals across the lifespan.

Chapter 6 ***Are subjective reports of sleep-wake disturbances related to structural integrity of the locus coeruleus and does this relate to Alzheimer's disease biomarkers?***

The locus coeruleus is the nexus of the first accumulations of Alzheimer's disease-related tau pathology and plays a key role in sleep-wake regulation. However, the associations between in vivo assessment of locus coeruleus integrity and Alzheimer's disease-related sleep alterations have not yet been investigated. Here, we investigated whether MRI-assessed locus coeruleus structural integrity relates to subjective sleep-wake measures of nocturnal awakening in the context of Alzheimer's disease plasma biomarkers in cognitively unimpaired older individuals.

Finally, we present the discussion of our findings and their implications for future directions in **chapter 7.**

REFERENCES:

1. Finder, V.H., *Alzheimer's Disease: A General Introduction and Pathomechanism.* Journal of Alzheimer's Disease, 2010. **22**: p. S5-S19.
2. Patterson, C., *World alzheimer report 2018.* 2018.
3. Gauthier, S., et al., *World Alzheimer Report 2021: Journey through the diagnosis of dementia.* Alzheimer's Disease International, 2021.
4. El-Hayek, Y.H., et al., *Tip of the Iceberg: Assessing the Global Socioeconomic Costs of Alzheimer's Disease and Related Dementias and Strategic Implications for Stakeholders.* J Alzheimers Dis, 2019. **70**(2): p. 323-341.
5. McKhann, G.M., et al., *The diagnosis of dementia due to Alzheimer's disease: Recommendations from the National Institute on Aging-Alzheimer's Association workgroups on diagnostic guidelines for Alzheimer's disease.* Alzheimer's & Dementia, 2011. **7**(3): p. 263-269.
6. Albert, M.S., et al., *The diagnosis of mild cognitive impairment due to Alzheimer's disease: Recommendations from the National Institute on Aging-Alzheimer's Association workgroups on diagnostic guidelines for Alzheimer's disease.* Alzheimer's & Dementia, 2011. **7**(3): p. 270-279.
7. Jack, C.R., et al., *NIA-AA Research Framework: Toward a biological definition of Alzheimer's disease.* Alzheimer's & Dementia, 2018. **14**(4): p. 535-562.
8. Braak, H. and E. Braak, *Neuropathological stageing of Alzheimer-related changes.* Acta neuropathologica, 1991. **82**(4): p. 239-259.
9. Jack, C.R., et al., *Tracking pathophysiological processes in Alzheimer's disease: an updated hypothetical model of dynamic biomarkers.* The Lancet Neurology, 2013. **12**(2): p. 207-216.
10. Jagust, W.J. and E.C. Mormino, *Lifespan brain activity, beta-amyloid, and Alzheimer's disease.* Trends Cogn Sci, 2011. **15**(11): p. 520-6.
11. Mulder, C., et al., *Amyloid-β (1–42), total tau, and phosphorylated tau as cerebrospinal fluid biomarkers for the diagnosis of Alzheimer disease.* Clinical chemistry, 2010. **56**(2): p. 248-253.
12. Price, J.L., et al., *The distribution of tangles, plaques and related immunohistochemical markers in healthy aging and Alzheimer's disease.* Neurobiology of aging, 1991. **12**(4): p. 295-312.
13. Hardy, J.A. and G.A. Higgins, *Alzheimer's Disease: The Amyloid Cascade Hypothesis.* Science, 1992. **256**(5054): p. 184-185.
14. Arriagada, P.V., et al., *Neurofibrillary tangles but not senile plaques parallel duration and severity of Alzheimer's disease.* Neurology, 1992. **42**(3): p. 631-631.
15. Hanseeuw, B.J., et al., *Association of amyloid and tau with cognition in preclinical Alzheimer disease: a longitudinal study.* JAMA neurology, 2019. **76**(8): p. 915-924.
16. Mattsson, N., et al., *Plasma tau in Alzheimer disease.* Neurology, 2016. **87**(17): p. 1827-1835.
17. Jin, M., et al., *Soluble amyloid β-protein dimers isolated from Alzheimer cortex directly induce Tau hyperphosphorylation and neuritic degeneration.* Proceedings of the National Academy of Sciences, 2011. **108**(14): p. 5819-5824.

18. Bloom, G.S., *Amyloid-β and Tau: The Trigger and Bullet in Alzheimer Disease Pathogenesis.* JAMA Neurology, 2014. **71**(4): p. 505-508.
19. Knopman, D.S., D.T. Jones, and M.D. Greicius, *Failure to demonstrate efficacy of aducanumab: An analysis of the EMERGE and ENGAGE trials as reported by Biogen, December 2019.* Alzheimer's & Dementia, 2021. **17**(4): p. 696-701.
20. Braak, H., et al., *Stages of the Pathologic Process in Alzheimer Disease: Age Categories From 1 to 100 Years.* Journal of Neuropathology & Experimental Neurology, 2011. **70**(11): p. 960-969.
21. Thal, D.R., et al., *Phases of Aβ-deposition in the human brain and its relevance for the development of AD.* Neurology, 2002. **58**(12): p. 1791-1800.
22. Mehta, D., et al., *Why do trials for Alzheimer's disease drugs keep failing? A discontinued drug perspective for 2010-2015.* Expert Opinion on Investigational Drugs, 2017. **26**(6): p. 735-739.
23. Braak, H. and E. Braak, *On areas of transition between entorhinal allocortex and temporal isocortex in the human brain. Normal morphology and lamina-specific pathology in Alzheimer's disease.* Acta Neuropathol, 1985. **68**(4): p. 325-32.
24. Bero, A.W., et al., *Neuronal activity regulates the regional vulnerability to amyloid-β deposition.* Nature Neuroscience, 2011. **14**(6): p. 750-756.
25. Ovsepian, S.V. and V.B. O'Leary, *Neuronal Activity and Amyloid Plaque Pathology: An Update.* Journal of Alzheimer's Disease, 2016. **49**: p. 13-19.
26. Busche, M.A. and A. Konnerth, *Neuronal hyperactivity – A key defect in Alzheimer's disease?* BioEssays, 2015. **37**(6): p. 624-632.
27. Palmqvist, S., et al., *Earliest accumulation of β-amyloid occurs within the default-mode network and concurrently affects brain connectivity.* Nature Communications, 2017. **8**(1): p. 1214.
28. Buckner, R.L., et al., *Molecular, Structural, and Functional Characterization of Alzheimer's Disease: Evidence for a Relationship between Default Activity, Amyloid, and Memory.* The Journal of Neuroscience, 2005. **25**(34): p. 7709-7717.
29. Sheline, Y.I. and M.E. Raichle, *Resting State Functional Connectivity in Preclinical Alzheimer's Disease.* Biological Psychiatry, 2013. **74**(5): p. 340-347.
30. Andrews-Hanna, J.R., et al., *Disruption of large-scale brain systems in advanced aging.* Neuron, 2007. **56**(5): p. 924-35.
31. Buckley, R.F., et al., *Functional network integrity presages cognitive decline in preclinical Alzheimer disease.* Neurology, 2017.
32. Damoiseaux, J.S., et al., *Reduced resting-state brain activity in the "default network" in normal aging.* Cerebral Cortex, 2008. **18**(8): p. 1856-1864.
33. Fornito, A., et al., *Competitive and cooperative dynamics of large-scale brain functional networks supporting recollection.* Proceedings of the National Academy of Sciences, 2012. **109**(31): p. 12788-12793.
34. Kelly, A.M., et al., *Competition between functional brain networks mediates behavioral variability.* Neuroimage, 2008. **39**(1): p. 527-37.
35. Farrell, M.E., et al., *Association of Longitudinal Cognitive Decline With Amyloid Burden in Middle-aged and Older Adults: Evidence for a Dose-Response Relationship.* JAMA Neurology, 2017. **74**(7): p. 830-838.

36. Raichle, M.E., *The brain's default mode network.* Annual review of neuroscience, 2015. **38**: p. 433-447.
37. Buckner, R.L., J.R. Andrews-Hanna, and D.L. Schacter, *The brain's default network: anatomy, function, and relevance to disease.* Ann N Y Acad Sci, 2008. **1124**: p. 1-38.
38. Heeger, D.J. and D. Ress, *What does fMRI tell us about neuronal activity?* Nature Reviews Neuroscience, 2002. **3**(2): p. 142-151.
39. Fox, M.D., et al., *The human brain is intrinsically organized into dynamic, anticorrelated functional networks.* Proceedings of the National Academy of Sciences, 2005. **102**(27): p. 9673-9678.
40. Ehrenberg, A.J., et al., *Quantifying the accretion of hyperphosphorylated tau in the locus coeruleus and dorsal raphe nucleus: the pathological building blocks of early Alzheimer's disease.* Neuropathology and applied neurobiology, 2017. **43**(5): p. 393-408.
41. Theofilas, P., et al., *Locus coeruleus volume and cell population changes during Alzheimer's disease progression: A stereological study in human postmortem brains with potential implication for early-stage biomarker discovery.* Alzheimer's & Dementia, 2017. **13**(3): p. 236-246.
42. Matchett, B.J., et al., *The mechanistic link between selective vulnerability of the locus coeruleus and neurodegeneration in Alzheimer's disease.* Acta Neuropathologica, 2021. **141**(5): p. 631-650.
43. Sheline, Y.I., et al., *Higher Cerebrospinal Fluid MHPG in Subjects With Dementia of the Alzheimer Type: Relationship With Cognitive Dysfunction.* The American Journal of Geriatric Psychiatry, 1998. **6**(2): p. 155-161.
44. Raskind, M.A., et al., *Norepinephrine and MHPG Levels in CSF and Plasma in Alzheimer's Disease.* Archives of General Psychiatry, 1984. **41**(4): p. 343-346.
45. Jacobs, H.I.L., et al., *Alzheimer's disease pathology: pathways between central norepinephrine activity, memory, and neuropsychiatric symptoms.* Mol Psychiatry, 2019.
46. Kang, S.S., et al., *Norepinephrine metabolite DOPEGAL activates AEP and pathological Tau aggregation in locus coeruleus.* The Journal of Clinical Investigation, 2020. **130**(1): p. 422-437.
47. Weinshenker, D., *Long Road to Ruin: Noradrenergic Dysfunction in Neurodegenerative Disease.* Trends in Neurosciences, 2018. **41**(4): p. 211-223.
48. Goedert, M., D.S. Eisenberg, and R.A. Crowther, *Propagation of Tau Aggregates and Neurodegeneration.* Annual Review of Neuroscience, 2017. **40**(1): p. 189-210.
49. Ahmed, Z., et al., *A novel in vivo model of tau propagation with rapid and progressive neurofibrillary tangle pathology: the pattern of spread is determined by connectivity, not proximity.* Acta neuropathologica, 2014. **127**(5): p. 667-683.
50. Jacobs, H.I., et al., *Structural tract alterations predict downstream tau accumulation in amyloid-positive older individuals.* Nature neuroscience, 2018. **21**(3): p. 424-431.
51. Eisenhofer, G., I.J. Kopin, and D.S. Goldstein, *Catecholamine metabolism: a contemporary view with implications for physiology and medicine.* Pharmacological reviews, 2004. **56**(3): p. 331-349.
52. Ehlers, M.R. and R.M. Todd, *Genesis and maintenance of attentional biases: The role of the locus coeruleus-noradrenaline system.* Neural Plasticity, 2017. **2017**.

53. Sara, S.J., *The locus coeruleus and noradrenergic modulation of cognition.* Nature Reviews Neuroscience, 2009. **10**(3): p. 211-223.
54. Berridge, C.W. and B.D. Waterhouse, *The locus coeruleus–noradrenergic system: modulation of behavioral state and state-dependent cognitive processes.* Brain Research Reviews, 2003. **42**(1): p. 33-84.
55. Oh, J., et al., *The role of co-neurotransmitters in sleep and wake regulation.* Molecular Psychiatry, 2019. **24**(9): p. 1284-1295.
56. Oh, J.Y., et al., *Subcortical Neuronal Correlates of Sleep in Neurodegenerative Diseases.* JAMA Neurology, 2022. **79**(5): p. 498-508.
57. Carrier, J., et al., *Sleep slow wave changes during the middle years of life.* European Journal of Neuroscience, 2011. **33**(4): p. 758-766.
58. Bubu, O.M., et al., *Sleep, cognitive impairment, and Alzheimer's disease: a systematic review and meta-analysis.* Sleep, 2017. **40**(1): p. zsw032.
59. Shi, L., et al., *Sleep disturbances increase the risk of dementia: a systematic review and meta-analysis.* Sleep medicine reviews, 2018. **40**: p. 4-16.
60. Xie, L., et al., *Sleep drives metabolite clearance from the adult brain.* science, 2013. **342**(6156): p. 373-377.
61. Holth, J.K., et al., *The sleep-wake cycle regulates brain interstitial fluid tau in mice and CSF tau in humans.* Science, 2019. **363**(6429): p. 880-884.
62. Lucey, B.P., *It's complicated: The relationship between sleep and Alzheimer's disease in humans.* Neurobiology of Disease, 2020. **144**: p. 105031.
63. Zhu, Y., et al., *Chronic Sleep Disruption Advances the Temporal Progression of Tauopathy in P301S Mutant Mice.* The Journal of Neuroscience, 2018. **38**(48): p. 10255-10270.
64. Ehrenberg, A.J., et al., *Neuropathologic Correlates of Psychiatric Symptoms in Alzheimer's Disease.* Journal of Alzheimer's Disease, 2018. **66**: p. 115-126.
65. Priovoulos, N., et al., *High-resolution in vivo imaging of human locus coeruleus by magnetization transfer MRI at 3T and 7T.* NeuroImage, 2018. **168**: p. 427-436.
66. Keren, N.I., et al., *Histologic validation of locus coeruleus MRI contrast in post-mortem tissue.* NeuroImage, 2015. **113**: p. 235-245.
67. Kitao, S., et al., *Correlation between pathology and neuromelanin MR imaging in Parkinson's disease and dementia with Lewy bodies.* Neuroradiology, 2013. **55**(8): p. 947-953.
68. Priovoulos, N., et al., *Unraveling the contributions to the neuromelanin-MRI contrast.* Brain Structure and Function, 2020. **225**(9): p. 2757-2774.
69. Sasaki, M., et al., *Neuromelanin magnetic resonance imaging of locus ceruleus and substantia nigra in Parkinson's disease.* NeuroReport, 2006. **17**(11).
70. Trujillo, P., et al., *Quantitative magnetization transfer imaging of the human locus coeruleus.* NeuroImage, 2019. **200**: p. 191-198.
71. Jacobs, H.I.L., et al., *In vivo and neuropathology data support locus coeruleus integrity as indicator of Alzheimer's disease pathology and cognitive decline.* Science Translational Medicine, 2021. **13**(612): p. eabj2511.
72. Zhang, H., et al., *NODDI: practical in vivo neurite orientation dispersion and density imaging of the human brain.* Neuroimage, 2012. **61**(4): p. 1000-1016.

73. Yeh, F.-C., D. Badre, and T. Verstynen, *Connectometry: A statistical approach harnessing the analytical potential of the local connectome.* NeuroImage, 2016. **125**: p. 162-171.
74. Yeh, F.-C., et al., *Differential tractography as a track-based biomarker for neuronal injury.* NeuroImage, 2019. **202**: p. 116131.
75. Betts, M.J., et al., *In vivo MRI assessment of the human locus coeruleus along its rostrocaudal extent in young and older adults.* NeuroImage, 2017. **163**: p. 150-159.
76. Liu, K.Y., et al., *In vivo visualization of age-related differences in the locus coeruleus.* Neurobiology of Aging, 2019. **74**: p. 101-111.
77. Shibata, E., et al., *Age-related Changes in Locus Ceruleus on Neuromelanin Magnetic Resonance Imaging at 3 Tesla.* Magnetic Resonance in Medical Sciences, 2006. **5**(4): p. 197-200.
78. Ye, R., et al., *An in vivo probabilistic atlas of the human locus coeruleus at ultra-high field.* NeuroImage, 2021. **225**: p. 117487.

INTER-NETWORK CONNECTIVITY AND AMYLOID-β LINKED TO COGNITIVE DECLINE IN PRECLINICAL ALZHEIMER'S DISEASE: A LONGITUDINAL COHORT STUDY

CHAPTER 2

Published in Alzheimer's Research & Therapy (2018)

Roy W.E. van Hooren
Joost M. Riphagen
Heidi I.L. Jacobs
For the Alzheimer's Disease Neuroimaging Initiative

ABSTRACT

Background: Amyloid-β has a dose-response relationship with cognition in healthy adults. Additionally, the levels of functional connectivity within and between brain networks have been associated with cognitive performance in healthy adults. Aiming to explore potential synergistic effects, we investigated the relationship of inter-network functional connectivity, amyloid-β burden and memory decline among healthy individuals and individuals with preclinical, prodromal or clinical Alzheimer's disease.

Methods: In this longitudinal cohort study (ADNI2), participants (55-88 years) were followed for maximally 5 years. We included cognitively healthy participants and patients with mild cognitive impairment (with or without elevated amyloid-β) or Alzheimer's disease. Associations between memory decline, amyloid-β burden and connectivity between networks across the groups were investigated using linear and curvilinear mixed effects models.

Results: We found synergistic relationships between inter-network functional connectivity and amyloid-β burden on memory decline. Dose-response relationships between amyloid-β and memory decline varied as a function of directionality of inter-network connectivity across groups. When inter-network correlations are negative, the curvilinear mixed effects models revealed that higher amyloid-β burden is associated with greater memory decline in cognitively normal participants, but when inter-network correlations are positive, there was no association between the magnitude of amyloid-β burden and memory decline. Opposite patterns were observed in patients with mild cognitive impairment. Combining negative inter-network correlations with amyloid burden can reduce the required sample size for clinical trials aiming to slow down memory decline with 88%.

Conclusions: The direction of inter-network connectivity provides additional information to amyloid-β burden about the rate of expected memory decline, especially in the preclinical phase. These results may be valuable for optimizing patient selection and decreasing study time to assess efficacy in clinical trials.

Keywords: Alzheimer's disease; Amyloid-β; Cognitively normal; Inter-network functional connectivity; Longitudinal; Memory performance; Mild cognitive impairment; Preclinical; Prodromal; clinical trials

BACKGROUND

Elevated levels of amyloid-β (Aβ), a neuropathological hallmark of Alzheimer's disease (AD) [1-6], are crucial in identifying the earliest stages of AD. While Aβ does not relate well to cognition cross-sectionally, it has a dose-response relationship with cognition in healthy adults [7]. However, dementia-related pathologies, including Aβ, only explain 41% of variation in cognitive decline [8] and a low signal-to-noise ratio of biomarkers in the asymptomatic stages of the disease for entry criteria in clinical trials has been reported as a reason for trial failure [9].

Healthy aging has previously been associated with reduced activity within the default mode network (DMN), a network often associated with memory-related processes, such as thinking about the future, episodic memory and autobiographical memory [10]. Reduced connectivity within the DMN, as measured with resting-state functional magnetic resonance imaging, is also associated with impaired cognitive performance in old age [11]. Additionally, levels of functional connectivity within cognition-related intrinsic brain networks, such as the DMN, and Aβ burden have a synergistic effect on memory decline in clinically normal older individuals [12]. Various networks predict cognitive decline, which may indicate that Aβ burden impacts the interaction between networks. Negative correlations between the default mode network and task-positive networks has been positively associated with cognitive performance in young individuals [13, 14]. These negative correlation patterns are also referred to as "anti-correlations" in the literature and have been described as intrinsically organized antagonistic activation patterns between networks in the brain [15]. These patterns are reported to be part of a mechanism that facilitates cognition, possibly by reinforcing connections between two loci in the brain dedicated to cognitive functions [14, 16].

Previous studies reported attenuating effects of aging on negative correlations between resting-state networks, with negative correlations further decreasing in patients with mild cognitive impairment (MCI) and AD [17-19]. While detrimental effects of Aβ on cognition and on functional connectivity within networks have been shown [2, 20-22], it remains unknown whether Aβ modulates functional connectivity between networks. Given the close relationship between inter-network connectivity and cognitive decline and these first reported associations with Aβ, combining information from inter-network connectivity with Aβ may reduce noise when selecting asymptomatic individuals at risk for AD in clinical trials aimed at slowing down cognitive decline.

To that end, we investigated whether functional connectivity between the DMN and task-positive networks predicts memory decline differently among cognitively normal individuals, MCI patients with and without elevated Aβ or AD patients. Additionally, we investigated whether the relationship between inter-network connectivity and memory decline depends on Aβ levels in a dose-response type relationship. We expected that as the magnitude of negative correlations decreases, memory performance would be lower, and that the strength of these associations would show a dose-response relationship with Aβ burden. To investigate domain-specificity of our findings, we have also investigated our hypotheses using executive functions as a control outcome measure.

METHODS

Data used in this article were obtained from the ADNI database (adni.loni.usc.edu). ADNI was launched in 2003, led by Principal Investigator Michael W. Weiner, MD. The main goal of ADNI has been to test whether magnetic resonance imaging, positron emission tomography, other biological markers, and clinical and neuropsychological assessment can be combined to measure the progression of MCI and AD. For up-to-date information, see www.adni-info.org.

PARTICIPANTS

We included data from a total of 122 eligible participants from the ADNI2 study (per March 2017), of which seven were removed due to low imaging data quality, resulting in a total of 115 participants. Qualified clinicians working for ADNI categorized participants into four groups; cognitively normal, early MCI, late MCI or AD, based on diagnostic procedures from the ADNI protocol [23]. However, for the purposes of our study, we grouped all patients with MCI based on their Aβ levels being below or above a pathological cutoff point of 1.11 ^{18}F-AV-45 florbetapir positron emission tomography standardized uptake value ratio [24], respectively referred to as MCI- and MCI+ in this manuscript. MCI diagnoses were based on the Petersen criteria for MCI [25, 26], while patients with AD met the NINCDS-ADRDA criteria for probable Alzheimer's disease [27]. For a detailed overview of exclusion-, inclusion- and diagnostic criteria and procedures, please refer to the ADNI2 protocol (http://adni.loni.usc.edu/wp-content/uploads/2008/07/adni2-procedures-manual.pdf). Additionally, only participants with complete resting-state functional magnetic resonance imaging and

Aβ data at baseline were eligible for inclusion, and patients with AD were only eligible if their Aβ levels were above the cutoff point to ensure only AD-related pathology was represented in this group. A complete listing of all participant IDs that were included in the final analyses can be found in Supplementary Table 1.

MATERIALS AND EQUIPMENT

Test batteries

The main outcome measures we used are the composite memory score ADNI-Mem and the composite executive functions score ADNI-EF, which have a good validity and are ideally suited to track changes over time. These scores were derived by combining scores related to memory performance and executive functions. ADNI-Mem score is derived from several test batteries, including the Rey Auditory Verbal Learning Test, Alzheimer's Disease Assessment Schedule-Cognition, Mini-Mental State Examination, Wechsler Memory Scale-Revised [28]. ADNI-EF score is derived from tests including WAIS-R Digit Symbol Substitution, Digit Span Backwards, Trails A and B, Category Fluency and Clock Drawing [29].

Biomarker assessment

^{18}F-AV-45 Florbetapir positron emission tomography measures were used to quantify levels of neocortical Aβ at baseline. The duration of positron emission tomography imaging was 20 minutes and started 50 minutes after injection of tracer fluid. The neocortical standardized uptake value ratio is the mean uptake in an aggregate of the frontal lobe, cingulate cortex, lateral parietal, and lateral temporal regions relative to mean uptake in the whole cerebellum, including white and gray matter. Further processing of positron emission tomography images occurred as is described in a previous report [24]. Participants were characterized as Aβ-positive if they exceeded the cutoff value of 1.11 standardized uptake value ratio, as previously determined in ADNI cohorts [24].

Imaging equipment and acquisition

Imaging data were acquired using Philips Medical Systems 3.0 Tesla magnetic resonance systems. Structural T1-weighted gradient echo pulse sequence data with dimensions of 170*256*256 mm with a voxel resolution of 1.2*1*1 mm were acquired in sagittal orientation with a repetition time of 6.8 ms, echo time of 3.1 ms,

flip angle of 9° and slice thickness of 1.2 mm. Additionally, resting-state functional magnetic resonance imaging scans of 7 minutes were obtained, consisting of 140 volumes of T2*-weighted data with 48 slices per volume, dimensions of 64*64*48 mm and a voxel resolution of 3.3*3.3*3.3 mm. Functional images were acquired in transverse orientation with repetition time of 3000 ms, echo time of 30 ms, flip angle of 80° and a slice thickness of 3.3 mm.

Image preprocessing and denoising

For preprocessing we used the default preprocessing pipeline for volume-based analyses within the NITRC CONN toolbox (version 17.a) (http://www.nitrc.org/projects/conn/) [30]. Images were realigned and unwarped, centered, slice-time corrected, segmented (gray/white/CSF), normalized to MNI space and outliers were identified with the Artifact Detection Toolbox. Outliers were regressed out (scrubbing) using conservative settings (95^{th} percentile in normative sample, global signal Z value=2, motion =0.5 mm and we discarded the first three volumes). Functional data were smoothed with a Gaussian kernel of 6mm full width at half maximum. As the reliability and validity of negative correlation measures has been subject of debate [31], denoising of data involved regressing out principal components of the signal from white matter and cerebrospinal fluid following the CompCor method [32], which reduces the presence of artificial negative correlations. Additionally, linear detrending and an after-regression BOLD signal band-pass filter ($0.008<f<0.09$ Hz) were applied. Data quality was ensured by visual inspection of histograms of functional connectivity values before and after denoising for each participant. Histograms that did not show a normal distribution of functional connectivity values after denoising were indicative of a suboptimal denoising process and these participants were excluded from data analysis in order to preserve a high level of data quality (n=7). Motion parameters were entered as regressor in our analyses. Volumes with motion above 0.5mm were entered as regressor in our general linear models (“scrubbing”). Furthermore, all images were inspected for irregularities during the entire preprocessing and analysis process.

Functional connectivity analyses

A bivariate correlation, hemodynamic response function-weighted ROI-to-ROI analysis was performed within CONN, using 4 independent network regions of interest as sources, with a total of 19 structurally defined hub regions. The

regions of interest include the DMN and regions representing task-positive networks, including the dorsal attention network (DAN), salience network (SN) and frontoparietal network (FPN). These regions of interest, which are part of the CONN software package, were generated by an independent component analysis on 497 healthy control participants (293 females) part of the Human Connectome Project (http://www.humanconnectome.org) [30]. As a reference for future replication efforts, peak coordinates of the regions of interest used for this functional connectivity analysis are provided in Supplementary Table 2 and the networks used are visualized in Figure 1. To assess inter-network connectivity, the average time course signal from each network was extracted and Fisher r-to-z transformed inter-network correlation values were exported for statistical analyses.

Statistical analysis

All data were analyzed using R version 3.3.1 (https://www.r-project.org/) and MATLAB R2016a. Baseline participant characteristics were compared with analysis of variance for continuous variables and chi-squared for categorical variables. Linear regression analyses were used for cross-sectional data. Because of their ability to deal with missing data in longitudinal studies without being subject to complete-case bias [33, 34], longitudinal analyses were performed with linear and curvilinear mixed effect regression analyses using maximum likelihood, utilizing nlme version 3.1-128 [35]. Fixed effects were predictor of interest, a random intercept for each participant and random slope for time. Time was calculated as number of years since baseline assessment. During the construction of statistical models, we first investigated effects in the whole sample. In case of a significant effect, the sample was split based on clinical groups and the level of amyloid burden, for which interactive analyses were performed with the cognitively normal group as reference. We also performed within-group analyses to better understand the patterns. For all models, we compared the Akaike Information Criteria between models with a random intercept and random slope or a random intercept only using the Log-likelihood ratio test and selected the most parsimonious model. In all models, age, sex, education and their interaction with time were included as covariate if $p < 0.10$ (using the Wald t-statistic) [36]. To improve longitudinal data quality [37], variability in head size, intracranial volume, as measured with FreeSurfer version 5.1 [38], was added as a covariate [39]. Additionally, intracranial volume can be used as a measure of atrophy and atrophy can reduce blood flow [40]. AD patients may show more

atrophy than patients with MCI or healthy controls which is an important reason to control for intracranial volume. The most complex model constructed for analyses is described in detail in Supplementary Box 1. Residual plots and Q-Q-plots were examined for all models. Significance was set at $p < 0.050$ (two-sided) and results were corrected for multiple comparisons using the false-discovery rate (FDR). Power calculations were performed using MATLAB scripts for the mixed effects model using the slope of memory decline and residual variance [40] to estimate the number of participants a clinical trial would need to enroll to detect slowing of memory decline of 30% (two arms for four-year annual assessments, 80% power, alpha=0.05) using high amyloid levels as inclusion criteria. These mixed effects models included the covariates, random intercept and random slope.

RESULTS

Demographics

The total sample consisted of 115 participants, including 53 females (46%) with a mean age of 72.91 (SD = 6.68) at baseline. Of these participants, 28 were in the cognitively normal group, 27 were in the MCI- group, 36 were in the MCI+ group and 24 were in the AD group. Other participant characteristics are summarized in Table 1.

Table 1. Summary table of participant characteristics at baseline[a]

Variable	CN (n = 28)	MCI- (n = 27)	MCI+ (n = 36)	AD (n = 24)	*p* Value
AV45 SUVR	1.16 (0.21)	1.01 (0.05)	1.39 (0.17)	1.50 (0.15)	< 0.001
Age (years)	74 (5.71)	71.36 (8.03)	72.58 (5.79)	74 (7.32)	0.42
Education (years)	16.43 (1.93)	16.48 (2.68)	15.86 (2.46)	15.46 (2.50)	0.36
Females	15 (54%)	12 (44%)	14 (39%)	12 (50%)	0.67
ICV (mm^3)	1,572,034 (153,316.20)	1,545,103 (168,923.10)	1,568,839 (174,101.60)	1,574,218 (210,862)	0.94
APOE ε4	10 (36%)	4 (15%)	24 (66%)	20 (83%)	< 0.001[b]
ADNI-Mem	0.89 (0.52)	0.37 (0.49)	0.15 (0.60)	-1.10 (0.56)	< 0.001
ADNI-EF	0.80 (0.56)	0.25 (0.80)	0.34 (0.86)	-0.94 (0.62)	< 0.001
CDR-SB	0.05 (0.16)	1.26 (0.92)	1.90 (1.06)	4.41 (1.31)	< 0.001
FC DMN-DAN	-0.12 (0.28)	0.00 (0.33)	-0.03 (0.24)	-0.15 (0.30)	0.17
FC DMN-SN	-0.15 (0.29)	-0.11 (0.28)	-0.08 (0.28)	-0.18 (0.27)	0.56
FC DMN-FPN	0.31 (0.23)	0.20 (0.30)	0.26 (0.23)	0.17 (0.29)	0.24
Follow-up time (years)	1.63 (1.24)	1.30 (0.96)	1.46 (1.09)	0.90 (0.53)	0.001

► Abbreviations: APOE ε4, apolipoprotein ε4; AD, Alzheimer's Disease; ADNI-EF, ADNI executive functions score composite; ADNI-Mem, ADNI memory score composite; AV45, ^{18}F-AV-45 florbetapir; CDR-SB, Clinical Dementia Rating scale – Sum of Boxes; CN, Cognitively Normal; DAN, Dorsal Attention Network; DMN, Default Mode Network; FC, Functional Connectivity; FPN, Frontoparietal Network; ICV, Intracranial Volume; MCI, Mild Cognitive Impairment, - and + indicate amyloid-β negative- or positive grouping, respectively; SN, Salience Network; SUVR, Standardized Uptake Value Ratio.

[a]Groups are listed in the top row. Data is presented as Mean (standard deviation) for the continuous variables and as n (%) for the categorical variable. The APOE ε4 row gives the number of participants in this group with one or more APOE ε4 alleles. Statistical significance was tested with analysis of variance for continuous variables and chi-squared for the categorical variables.

[b]All groups were significantly different from each other, except CN versus MCI- and MCI+ versus AD.

Analyses of variance indicated group differences in ^{18}F-AV-45 florbetapir standardized uptake value ratio, ADNI-Mem, ADNI-EF, clinical dementia rating scale scores and follow-up times. Proportion of cases at each time point were as follows: baseline, 115 (100%); month 6, 110 (96%); month 12, 98 (85%); month 24, 74 (64%); month 36, 6 (5%); month 48, 29 (25%); month 60, 1 (<1%). Results of Tukey tests for post-hoc differences between group characteristics are available in Supplementary Table 3. Additionally, we found no differences in image preprocessing parameters between groups (Supplementary table 4).

Effects of functional connectivity and group on memory at baseline

There were no significant associations between functional connectivity between networks and memory performance at baseline across the entire sample or within the groups. An association was found between functional connectivity between the DMN and FPN and executive functions across the entire sample at baseline. Further analyses of the association between functional connectivity and executive functions within the diagnosis groups reveal an association in the amyloid negative MCI group (Supplementary Table 5).

Longitudinal linear effects of functional connectivity and group on memory

Linear mixed effect models were performed to investigate effects of functional connectivity and group on memory decline over time. The associations between functional connectivity between the networks and time for the whole sample

were not significant (Supplementary Table 6). Using the cognitively normal group as reference level, a significant three-way interaction effect of time, group and functional connectivity was found in comparison to the MCI+ group for the DMN-DAN and DMN-SN correlations, but not for the DMN-FPN correlations (Table 2). Adding inter-network functional connectivity to the models with the covariates contributed significantly to the explained variance of memory decline for the DMN-DAN (R^2 difference = 0.03, 95% CI: [0.01, 0.07], p = 0.04), but not for the DMN-SN (R^2 difference = 0.001, 95% CI: [-0.001, 0.01], p = 0.21) or the DMN-FPN (R^2 difference = < 0.001, 95% CI: [-0.001, 0.01], p = 0.48).

Table 2. Associations between group, inter-network functional connectivity and memory decline[a,b]

Fitted model	Est.	SE	95% CI	DF	T Value	*p* Value	*p* Value (FDR)
DMN-DAN (n = 115, number of observations = 433)							
Time*MCI-*DMN-DAN	-0.43	0.22	-0.68 to -0.01	310	-2.00	0.047	0.14
Time*MCI+*DMN-DAN	-0.79	0.23	-1.25 to -0.34	310	-3.43	0.001	0.001
Time*AD*DMN-DAN	-0.24	0.30	-0.84 to 0.36	310	-0.79	0.43	0.43
DMN-SN (n = 115, number of observations = 433)							
Time*MCI-*DMN-SN	-0.26	0.23	-0.71 to 0.19	310	-1.13	0.26	0.32
Time*MCI+*DMN-SN	-0.55	0.20	-0.93 to -0.16	310	-2.81	0.01	0.01
Time*AD*DMN-SN	-0.36	0.31	-0.98 to 0.25	310	-1.17	0.25	0.37
DMN-FPN (n = 115, number of observations = 433)							
Time*MCI-*DMN-FPN	-0.27	0.27	-0.81 to 0.26	310	-1.00	0.32	0.32
Time*MCI+*DMN-FPN	-0.21	0.26	-0.72 to 0.30	310	-0.81	0.42	0.42
Time*AD*DMN-FPN	-0.45	0.33	-1.09 to 0.19	310	-1.38	0.17	0.37

Abbreviations: AD, Alzheimer's Disease; CI, Confidence Interval; DAN, Dorsal Attention Network; DF, Degrees of Freedom; DMN, Default Mode Network; FDR, False Discovery Rate; FPN, Frontoparietal Network; MCI, Mild Cognitive Impairment, - and + indicate amyloid-β negative- or positive grouping, respectively; SE, Standard Error; SN, Salience Network.

[a]Results are acquired using the cognitively normal group as reference group.

[b]Regression models are adjusted for age, intracranial volume, sex and education. Beta coefficients are unstandardized.

Figure 1 and Table 2 show significant associations between DMN-DAN and DMN-SN functional connectivity and memory decline between the cognitively normal and MCI+ groups. Post hoc linear mixed models within each group confirmed that

for the cognitively normal group, positive correlations between these network pairs are positively associated with memory performance over time, whereas in the MCI+ group, positive correlations were negatively associated with memory performance (Supplementary Table 7). No significant associations were found for executive functions (Supplementary Table 8).

Figure 1. Linear effects of functional connectivity on memory decline over time per group.

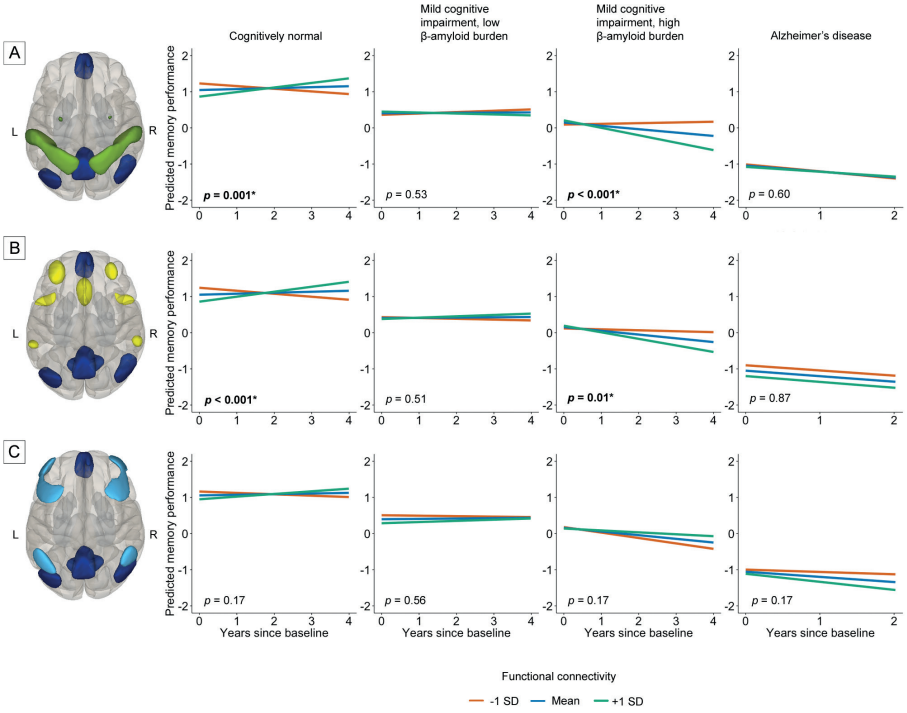

Note. The effect of baseline functional connectivity between networks on memory performance over time was investigated in three network pairs in all groups. Functional connectivity values were standardized to ensure that the mean reflects a z-value of 0. Red, green and blue lines indicate the estimated marginal means for the moderation by negative (-1SD)-, positive (+1SD)- and no (Mean) correlation between networks, respectively, but the analyses were done using functional connectivity measures continuously. Network combinations from top to bottom: DMN-DAN, DMN-SN and DMN-FPN. The DMN is shown in dark blue, the DAN in green, the SN in yellow and the FPN in light blue. The brain images give a superior viewpoint of the brain; top = anterior, left = left, right = right, bottom = posterior. The AD group only had a maximum follow-up time of 2 years (Table 1). All *p* values are corrected for multiple comparisons using FDR. Significant effects are indicated by an asterisk and bold font. Figure 1A: DMN-DAN: Significant effects were found in the cognitively normal and MCI+ groups. Figure 1B: DMN-SN: Significant effects were found in the cognitively normal and MCI+ groups. Figure 1C: DMN-FPN: No significant effects were found for this network pair.

As the cognitively normal group consisted of 11 individuals with Aβ levels above the threshold, we also examined associations between functional inter-network connectivity, Aβ as a continuous variable and memory decline in the cognitively normal group. These results showed that this interaction was significant for the DMN-DAN and the DMN-SN, but not the DMN-FPN. This shows that Aβ moderates the association between functional connectivity and memory decline also in the cognitively normal group, in such a way that negative correlations were associated with memory decline with elevated Aβ (Table 4). Similar findings are observed when grouping cognitively normal individuals based on the Aβ cut-off value (Supplementary Table 9).

Table 3. Three-way interaction of functional connectivity, amyloid-β and time in the cognitively normal group[a]

Fitted model	Est.	SE	95% CI	DF	T Value	*p* Value	*p* Value (FDR)
DMN-DAN (n = 28, number of observations = 118)							
DMN-DAN*Aβ*Time	1.97	0.48	1.03 to 2.92	86	4.14	< 0.001	< 0.001
DMN-SN (n = 28, number of observations = 118)							
DMN-SN*Aβ*Time	1.86	0.56	0.74 to 2.97	86	3.31	0.001	0.001
DMN-FPN (n = 28, number of observations = 118)							
DMN-FPN*Aβ*Time	-0.62	0.97	-2.55 to 1.30	86	-0.64	0.52	0.52

Abbreviations: Aβ, Amyloid-β; CI, Confidence Interval; DAN, Dorsal Attention Network; DF, Degrees of Freedom; DMN, Default Mode Network; FPN, Frontoparietal Network; SE, Standard Error; SN, Salience Network.

[a]Regression models are adjusted for age, intracranial volume, sex and education. Beta coefficients are unstandardized.

Table 4. Curvilinear associations between functional inter-network connectivity, amyloid-β burden and memory decline[a]

Fitted model	Est.	SE	95% CI	DF	T Value	*p* Value	*p* Value (FDR)
Whole sample, excluding AD group (n = 91, number of observations = 364)							
DMN-DAN (n = 91, number of observations = 364)							
DMN-DAN*Aβ*(Time^2)	0.42	0.16	0.10 to 0.74	266	2.60	0.01	0.02
DMN-SN (n = 91, number of observations = 364)							
DMN-SN*Aβ*(Time^2)	0.25	0.14	-0.02 to 0.52	266	1.84	0.07	0.07
Subset of participants with positive correlation between DMN and DAN[b]							
Whole sample, excluding AD group (n = 39, number of observations = 157)							
Aβ*Time	-0.43	0.15	-0.73 to -0.13	116	-2.83	0.01	0.01
CN (n = 10, number of observations = 43)							
Aβ*Time	0.22	0.20	-0.19 to 0.63	31	1.08	0.29	0.29
MCI (n = 29, number of observations = 114)							
Aβ*Time	-0.44	0.13	-0.69 to -0.18	83	-3.43	0.001	0.001
Subset of participants with negative correlation between DMN and DAN[b]							
Whole sample. excluding AD group (n = 52, number of observations = 207)							
Aβ*(Time^2)	-0.05	0.01	-0.07 to -0.03	152	-4.23	< 0.001	< 0.001
CN (n = 18, number of observations = 75)							
Aβ*(Time^2)	-0.25	0.08	-0.41 to -0.10	53	-3.33	0.001	0.001
MCI (n = 34, number of observations = 132)							
Aβ*Time	-0.26	0.15	-0.56 to 0.04	96	-1.73	0.09	0.09

Abbreviations: Aβ, Amyloid-β; AD, Alzheimer's Disease; CI, Confidence Interval; CN, Cognitively Normal; DAN, Dorsal Attention Network; DF, Degrees of Freedom; DMN, Default Mode Network; FDR, False Discovery Rate; MCI, Mild Cognitive Impairment; SE, Standard Error; SN, Salience Network.

[a]Regression models are adjusted for age, intracranial volume, sex and education. Beta coefficients are unstandardized.

[b]Models include a quadratic term only if it explained more variance than the linear model without quadratic term.

Longitudinal curvilinear effects of functional connectivity and amyloid-β on memory.

Since our linear mixed model results showed opposite moderations by Aβ on the association between functional connectivity and memory performance across the diagnostic groups, we examined curvilinear (quadratic) mixed effect models for these network interactions, using Aβ as a continuous variable to investigate a possible dose-response relationship with memory decline. To ensure that individuals with the highest Aβ levels would not drive associations, we excluded the AD group from these analyses. In the whole sample, excluding the AD group, a quadratic three-way interaction effect of functional connectivity, Aβ and time was

found for the DMN-DAN, but marginally, not for the DMN-SN correlations (Table 5). To visualize this interaction, we plotted simple slopes for different values of ^{18}F-AV-45 florbetapir standardized uptake value ratio in both groups; broken down by positive and negative inter-network correlations and holding all other fixed effects constant (Figure 2). Values for Aβ were chosen to reflect Aβ negativity (0.9), the cut-off (1.1), slightly elevated Aβ (1.3), moderately elevated Aβ (1.5) and high Aβ (1.7).

Figure 2. Curvilinear three-way interaction of functional connectivity, amyloid-β and time and its relation with memory performance.

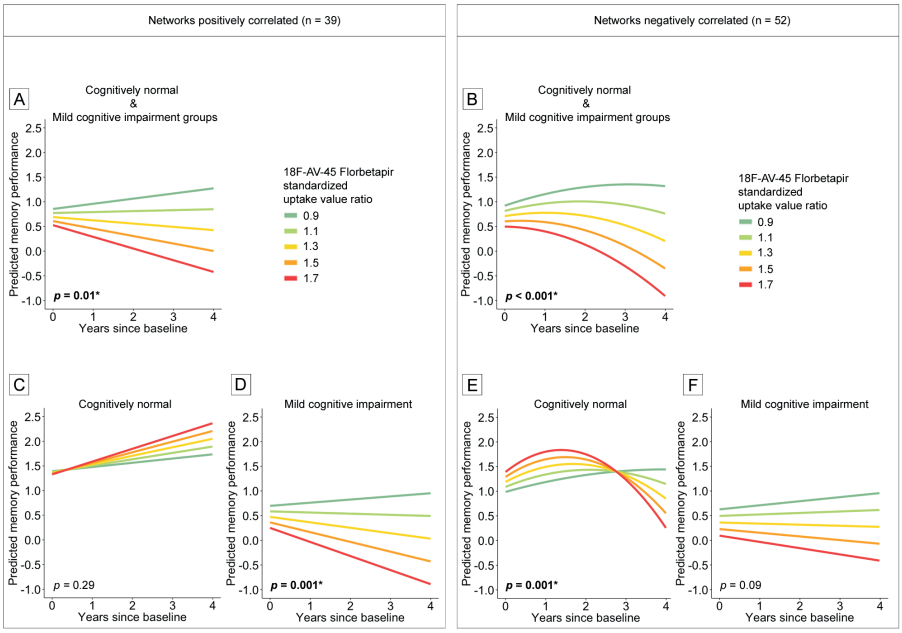

Note. To visualize the three-way interaction, the whole sample, excluding the AD group, was split based on whether functional connectivity between DMN-DAN was below or above zero, allowing us to visualize the dose-response relationship of amyloid-β burden (measured with ^{18}F-AV-45 florbetapir standardized uptake value ratio) on memory decline in both subgroups. ^{18}F-AV-45 florbetapir standardized uptake value ratio values over 1.11 indicate amyloid-β positivity. Linear or curvilinear graphs were drawn, based on which type of association showed the best fit for each model. All *p* values are FDR-corrected. Significant effects are indicated by an asterisk and bold font. Figure 2A: Effects within the subgroup of cognitively normal participants and MCI patients showing positive correlations between networks. Figure 2B: Curvilinear effects within the subgroup of cognitively normal participants and MCI patients showing negative correlations between networks. Figure 2C: Effects within the cognitively normal subgroup with positive correlations between networks: no significant dose-response relationship of Aβ on memory (practice effects). Figure 2D: Effects within the MCI subgroup with positive correlations between networks showing a dose-response relationship of Aβ on memory. Figure 2E: Effects within the cognitively normal subgroup with negative correlations between networks showing a curvilinear dose-response relationship of Aβ on memory. Figure 2F: Effects within the MCI subgroup with negative correlations between networks showing no (borderline) significant effect of Aβ burden on memory.

Figure 2 shows that the dose-response relationship between Aβ and memory decline is modulated by both diagnosis and the direction of DMN-DAN correlations. Within the cognitively normal group, negative DMN-DAN correlations have a curvilinear dose-response relationship with memory decline. However, when networks are positively correlated, we found no significant association between Aβ and memory decline. Conversely, in the MCI group, positive DMN-DAN correlations were associated with a linear dose-response relationship between Aβ and rate of memory. No moderation effects of Aβ were found for the MCI group with negative correlations, though linear effects approached significance (Table 4).

Power estimations were performed in the cognitively normal group to investigate the added value of adding functional inter-network connectivity to higher levels of Aβ burden as an inclusion criterium on the required sample size per arm in clinical trials (Figure 3).

Figure 3. Power analysis in the cognitively normal group.

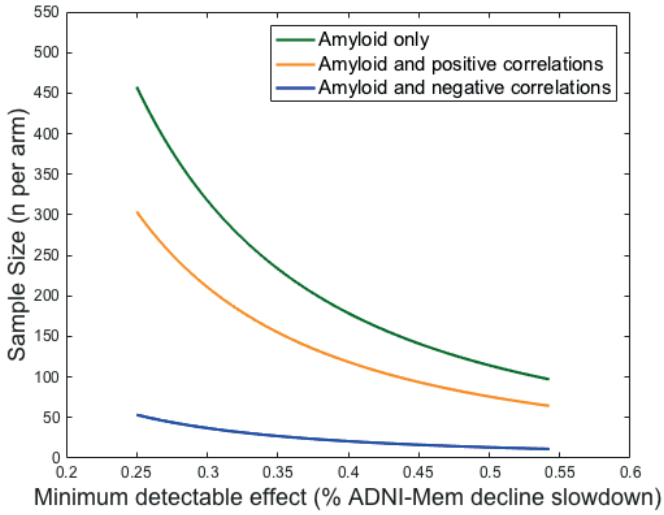

Note. To assess the effect of including inter-network connectivity as an inclusion criterium in clinical trials, we performed a power analysis in the cognitively normal group. The x-axis describes the memory slope reduction in percentages and the y-axis describes the number of participants needed per arm to detect this reduction with 80% power and α = 0.05 in a four-year trial with annual assessments. The red line shows the sample size needed when only amyloid is used as an inclusion criterium and inter-network connectivity between the DMN and DAN is not considered. The orange line shows the required sample size when positive inter-network correlations between the DMN and DAN and amyloid are used as inclusion criteria. The blue line shows the required sample size when negative inter-network correlations between the DMN and DAN and amyloid are used as inclusion criteria.

These results show that selecting cognitively normal participants with higher levels of Aβ burden and who also have a negative DMN-DAN correlation may greatly reduce the sample size needed to detect amyloid-related changes in memory decline in clinical trials, as compared to only including preclinical AD individuals or those with positive correlations. For instance, the required sample size per arm to detect an effect size of 0.3 (30%) can be reduced by 88% when using both amyloid and negative inter-network correlations (n=37) as inclusion criteria in clinical trials towards asymptomatic AD, as opposed to considering only amyloid (n=318) in the inclusion process.

While functional inter-network connectivity is a relatively affordable and easy measure to collect in participants, this additional requirement can increase the rate of screen failures at inclusion.

DISCUSSION

This study provides evidence for a dose-response relationship between Aβ burden and inter-network connectivity on memory decline over four years in both healthy and patient populations. Previous studies suggested that negative correlations between task-positive and task-negative networks might have a beneficial effect on memory in young individuals [13, 14]. We now showed that in older adults these associations depend on disease stage and the burden of Aβ. In cognitively normal older individuals, negative correlations were associated with memory decline and this association became stronger in individuals with higher levels of Aβ. Conversely, in patients with MCI, the magnitude of Aβ burden predicted the rate of memory decline associated with positive inter-network correlations.

These results suggest that the direction of baseline inter-network connectivity can provide additional information when combined with baseline Aβ burden about the rate of expected memory decline and can add important information to the complexity of factors contributing to cognitive decline. Additionally, these findings can have prognostic implications when using functional connectivity as a potential biomarker and show the importance of including both the direction of inter-network connectivity and Aβ burden for projecting cognitive trajectories as outcome especially in preclinical AD.

Interestingly, the associations we observed involved mainly the DMN-DAN correlations. The DMN is one of the most investigated networks and is among

the first networks where Aβ accumulates significantly early in the disease [41]. It is therefore likely that other functional networks, especially networks tightly coupled to the DMN, are indirectly susceptible to Aβ-related alterations. Animal and electrophysiological studies have provided evidence that Aβ burden leads to synaptic dysfunction and network disorganization [42].

Widespread inter-network reorganization under the influence of Aβ have indeed been reported for the coupling between DMN and DAN [43], DMN and SN [19] and DMN and FPN [43], suggesting topographical closeness to certain hubs, such as the association cortices of the DMN, may put networks at increased risk for Aβ-toxicity. Our findings now show that functional implications of the interactions between large-scale brain networks and amyloid in relation to memory decline were mainly observed for the DMN-DAN correlations, with borderline significant associations for the DMN-SN correlations. This is in line with previous research suggesting that an optimal interaction between these specific networks is important for cognitive functioning [13, 14, 44]. The fact that we observed associations between greater positive inter-network correlations and better memory performance over time in clinically normal individuals suggests the presence of compensation mechanisms involving possible reconfiguration of large-scale networks [46, 47]. In the context of preclinical AD, this compensation may provide the architectural basis for maintaining optimal memory performance in old age [45, 46]. These compensation mechanisms may be moderated by cognitive reserve [47]. Individuals with preclinical AD may be able to compensate for AD pathology in the form of positive inter-network correlations.

Furthermore, previous studies reported differential connectivity patterns for the anterior versus posterior DMN [48]. Increased within-network functional connectivity in the anterior DMN was associated with higher levels of amyloid pathology in preclinical AD [21], indicative of regional compensatory mechanisms. But as the disease progresses, compensatory mechanisms may be dependent on cognitive reserve to stave off memory decline. Attenuated negative correlations between the DMN-DAN may signal impending neuronal breakdown resulting from Aβ toxicity in the prodromal phase, a finding consistent with previous work [47].

The DMN and DAN may operate in a negative correlation pattern in order to facilitate attention-related processes during cognitive tasks. Especially during memory tasks the DAN is thought to coordinate cross-talk between brain networks. The coordination between brain networks may become especially important in

MCI, where medial temporal lobe structures become functionally isolated from other regions or networks. In MCI, a coordinated antiphase functional connection between the DMN and DAN may be fundamental in maintaining optimal levels of memory performance [47].

Finally, functional connectivity deteriorates as the disease progresses to more advanced stages [48]. This may partially explain the lack of connectivity-related findings in the AD group, as coherent connectivity patterns between networks may dissipate, leaving no association between inter-network connectivity and cognition.

Our dose-response findings relating Aβ burden to memory decline, depending on functional connectivity status showed different patterns between cognitively normal individuals and patients with MCI. This has important implications for early detection of individuals at-risk of cognitive decline and the selection of preclinical and prodromal AD individuals for trials using a combination of functional connectivity and Aβ. Patients with MCI showed a dose-response relationship between Aβ and memory decline for positive DMN-DAN correlations. In clinically normal individuals, Aβ has a dose-response relationship with memory decline when DMN-DAN correlations are negative. Selecting preclinical AD individuals with positive DMN-DAN correlations could lead to the selection of individuals where individuals with higher levels of Aβ have similar practice effects as individuals with lower levels of Aβ burden. Thus, the direction of inter-network connectivity in combination with Aβ burden can have important implications for participant selection in clinical trials. This notion is further outlined by the results from our power analysis showing that the selection of CN individuals with elevated Aβ levels and negative inter-network correlations reduced the required sample size with 88% to slow down memory decline with 30%..

Furthermore, we did not observe independent or synergistic effects of inter-network connectivity or Aβ on cognition in patients with AD in the 2-year follow-up period. This could be related to widespread deposits of both Aβ and tau that may have impacted the integrity of the entire brain. We also did not observe between group differences in inter-network connectivity of the DMN-DAN at baseline, which is in contrast to previous reports in similar populations [17-19]. These discrepancies may be related to sample size, methodological differences (regional versus network-based analyses) and the larger age range of the participants in our study.

Interestingly, the results found in our study seem to be domain-specific for memory. This may be explained by the DMN being specifically associated with memory functions [10, 47]. Since we found the most convincing results in the DMN-DAN correlation, this may emphasize the domain-specific nature of the interaction between DMN-DAN correlation, amyloid burden and memory decline in preclinical AD.

Limitations

Due to the observational nature of our study, our data does not allow for any causal inferences between changes in functional connectivity between networks or Aβ deposition. Determining the temporal direction of the three-way association between amyloid, memory decline and inter-network functional connectivity requires further experimental investigation. Furthermore, longitudinal data of the AD group is limited to a follow-up period of 2 years. This may partially explain the lack of significant results found in this group, although it is also possible that the disease process and associated pathological accumulations are too widespread and may have affected functional networks in multiple ways, all associated with cognitive decline.

Future directions

With the recent development of tau positron emission tomography tracers, future studies can investigate how tau pathology may impact inter-network connectivity, as research has suggested a dynamic influence of tau on connectivity within networks, depending on Aβ levels [49-51]. Results from such a study could ultimately culminate in clinical trials where participants can be chosen using multi-modal selective criteria for memory decline due to Alzheimer's disease.

Additionally, future studies should investigate whether carriers of the apolipoprotein ε4 allele show stinger synergistic effects between AD pathology [52, 53], and inter-network correlations on cognitive decline. Such investigations may further refine the selection criteria for trials and may have implications for determining response to treatment.

Finally, previous research has shown that AD variants, such as posterior cortical atrophy and early-onset AD, may have unique networks that are preferentially affected in the disease process [54]. Thus, future research may

want to investigate how Aβ, inter-network correlations and cognitive decline are associated in these different variants of AD and whether inter-network correlations may be associated with different cognitive domains in these variants.

Conclusions

In conclusion, our results show that the direction of inter-network connectivity provides additional information to baseline Aβ burden about the rate of expected memory decline. These findings add important information for the understanding of factors contributing to cognitive decline. These results also suggest that when using functional connectivity as biomarker or selection criteria for trials in preclinical populations, the directionality of inter-network connectivity might aid in selecting individuals that are more likely to be on an Aβ-related negative memory trajectory. Including information about both Aβ burden and inter-network functional connectivity can improve recruitment strategies and decrease the time to determine the efficacy of clinical trials in the asymptomatic phase of the disease.

REFERENCES:

1. McKhann, G., et al., *The diagnosis of dementia due to Alzheimer's disease: recommendations from the National Institute on Aging-Alzheimer's Association workgroups on diagnostic guidelines for Alzheimer's disease.* Alzheimers Dement, 2011. **7**(3): p. 263-9.
2. Jagust, W.J. and E.C. Mormino, *Lifespan brain activity, beta-amyloid, and Alzheimer's disease.* Trends Cogn Sci, 2011. **15**(11): p. 520-6.
3. Jack, C.R., et al., *Tracking pathophysiological processes in Alzheimer's disease: an updated hypothetical model of dynamic biomarkers.* The Lancet Neurology, 2013. **12**(2): p. 207-216.
4. Price, J.L., et al., *The distribution of tangles, plaques and related immunohistochemical markers in healthy aging and Alzheimer's disease.* Neurobiology of aging, 1991. **12**(4): p. 295-312.
5. Mulder, C., et al., *Amyloid-β (1–42), total tau, and phosphorylated tau as cerebrospinal fluid biomarkers for the diagnosis of Alzheimer disease.* Clinical chemistry, 2010. **56**(2): p. 248-253.
6. Braak, H. and E. Braak, *Neuropathological stageing of Alzheimer-related changes.* Acta neuropathologica, 1991. **82**(4): p. 239-259.
7. Farrell, M.E., et al., *Association of longitudinal cognitive decline with amyloid burden in middle-aged and older adults: Evidence for a dose-response relationship.* JAMA Neurology, 2017. **74**(7): p. 830-838.
8. Boyle, P.A., et al., *Much of late life cognitive decline is not due to common neurodegenerative pathologies.* Annals of neurology, 2013. **74**(3): p. 478-489.
9. Gauthier, S., et al., *Why has therapy development for dementia failed in the last two decades?* Alzheimer's & Dementia, 2016. **12**(1): p. 60-64.
10. Damoiseaux, J.S., et al., *Reduced resting-state brain activity in the "default network" in normal aging.* Cerebral Cortex, 2008. **18**(8): p. 1856-1864.
11. Andrews-Hanna, J.R., et al., *Disruption of Large-Scale Brain Systems in Advanced Aging.* Neuron, 2007. **56**(5): p. 924-935.
12. Buckley, R.F., et al., *Functional network integrity presages cognitive decline in preclinical Alzheimer disease.* Neurology, 2017.
13. Fornito, A., et al., *Competitive and cooperative dynamics of large-scale brain functional networks supporting recollection.* Proceedings of the National Academy of Sciences, 2012. **109**(31): p. 12788-12793.
14. Kelly, A.M., et al., *Competition between functional brain networks mediates behavioral variability.* Neuroimage, 2008. **39**(1): p. 527-37.
15. Fox, M.D., et al., *The human brain is intrinsically organized into dynamic, anticorrelated functional networks.* Proceedings of the National Academy of Sciences of the United States of America, 2005. **102**(27): p. 9673-9678.
16. Pinsk, M.A. and S. Kastner, *Unconscious networking.* Nature, 2007. **447**: p. 46.
17. Wang, K., et al., *Altered functional connectivity in early Alzheimer's disease: a resting-state fMRI study.* Human brain mapping, 2007. **28**(10): p. 967-978.
18. Esposito, R., et al., *Modifications in resting state functional anticorrelation between default mode network and dorsal attention network: comparison among young adults, healthy elders and mild cognitive impairment patients.* Brain Imaging and Behavior, 2017: p. 1-15.

19. Brier, M.R., et al., *Loss of intranetwork and internetwork resting state functional connections with Alzheimer's disease progression.* Journal of Neuroscience, 2012. **32**(26): p. 8890-8899.
20. Mormino, E.C., et al., *Synergistic effect of beta-amyloid and neurodegeneration on cognitive decline in clinically normal individuals.* JAMA Neurol, 2014. **71**(11): p. 1379-85.
21. Mormino, E.C., et al., *Relationships between beta-amyloid and functional connectivity in different components of the default mode network in aging.* Cereb Cortex, 2011. **21**(10): p. 2399-407.
22. Sheline, Y.I., et al., *Amyloid plaques disrupt resting state default mode network connectivity in cognitively normal elderly.* Biological Psychiatry, 2010. **67**(6): p. 584-587.
23. Mueller, S.G., et al., *The Alzheimer's disease neuroimaging initiative.* Neuroimaging Clinics of North America, 2005. **15**(4): p. 869-877.
24. Landau, S.M., et al., *Amyloid deposition, hypometabolism, and longitudinal cognitive decline.* Annals of neurology, 2012. **72**(4): p. 578-586.
25. Petersen, R.C., *Mild cognitive impairment as a diagnostic entity.* Journal of internal medicine, 2004. **256**(3): p. 183-194.
26. Petersen, R.C., et al., *Alzheimer's disease Neuroimaging Initiative (ADNI) clinical characterization.* Neurology, 2010. **74**(3): p. 201-209.
27. McKhann, G., et al., *Clinical diagnosis of Alzheimer's disease Report of the NINCDS-ADRDA Work Group* under the auspices of Department of Health and Human Services Task Force on Alzheimer's Disease.* Neurology, 1984. **34**(7): p. 939-939.
28. Crane, P.K., et al., *Development and assessment of a composite score for memory in the Alzheimer's Disease Neuroimaging Initiative (ADNI).* Brain imaging and behavior, 2012. **6**(4): p. 502-516.
29. Gibbons, L.E., et al., *A composite score for executive functioning, validated in Alzheimer's Disease Neuroimaging Initiative (ADNI) participants with baseline mild cognitive impairment.* Brain imaging and behavior, 2012. **6**(4): p. 517-527.
30. Whitfield-Gabrieli, S. and A. Nieto-Castanon, *Conn: a functional connectivity toolbox for correlated and anticorrelated brain networks.* Brain connectivity, 2012. **2**(3): p. 125-141.
31. Murphy, K., et al., *The impact of global signal regression on resting state correlations: are anti-correlated networks introduced?* Neuroimage, 2009. **44**(3): p. 893-905.
32. Behzadi, Y., et al., *A component based noise correction method (CompCor) for BOLD and perfusion based fMRI.* Neuroimage, 2007. **37**(1): p. 90-101.
33. Field, A., *Discovering statistics using IBM SPSS statistics*. 2013: sage.
34. Ibrahim, J.G. and G. Molenberghs, *Missing data methods in longitudinal studies: a review.* Test (Madrid, Spain), 2009. **18**(1): p. 1-43.
35. *Pinheiro J, Bates D, DebRoy S, Sarkar D, R Core Team. nlme: Linear and Nonlinear Mixed Effects Models. R package version 3.1-128, URL: http://CRAN.R-project.org/package=nlme.* 2016.
36. Bischof, G.N., et al., *Amyloid deposition in younger adults is linked to episodic memory performance.* Neurology, 2016. **87**(24): p. 2562-2566.
37. Whitwell, J.L., et al., *Normalization of cerebral volumes by use of intracranial volume: implications for longitudinal quantitative MR imaging.* American Journal of Neuroradiology, 2001. **22**(8): p. 1483-1489.

38. Fischl, B., *FreeSurfer.* Neuroimage, 2012. **62**(2): p. 774-781.
39. Buckner, R.L., et al., *A unified approach for morphometric and functional data analysis in young, old, and demented adults using automated atlas-based head size normalization: reliability and validation against manual measurement of total intracranial volume.* Neuroimage, 2004. **23**(2): p. 724-738.
40. Hanseeuw, B.J., et al., *PET staging of amyloidosis using striatum.* Alzheimer's & Dementia, 2018.
41. Elman, J.A., et al., *Effects of Beta-Amyloid on Resting State Functional Connectivity Within and Between Networks Reflect Known Patterns of Regional Vulnerability.* Cerebral Cortex, 2016. **26**(2): p. 695-707.
42. Mucke, L. and D.J. Selkoe, *Neurotoxicity of amyloid β-protein: synaptic and network dysfunction.* Cold Spring Harbor perspectives in medicine, 2012. **2**(7): p. a006338.
43. Grothe, M.J. and S.J. Teipel, *Spatial patterns of atrophy, hypometabolism, and amyloid deposition in Alzheimer's disease correspond to dissociable functional brain networks.* Human brain mapping, 2016. **37**(1): p. 35-53.
44. Keller, J.B., et al., *Resting-state anticorrelations between medial and lateral prefrontal cortex: association with working memory, aging, and individual differences.* Cortex, 2015. **64**: p. 271-80.
45. Spreng, R.N., et al., *Attenuated anticorrelation between the default and dorsal attention networks with aging: evidence from task and rest.* Neurobiology of Aging, 2016. **45**(Supplement C): p. 149-160.
46. Cabeza, R., et al., *Aging gracefully: compensatory brain activity in high-performing older adults.* Neuroimage, 2002. **17**(3): p. 1394-1402.
47. Franzmeier, N., et al., *Cognitive reserve moderates the association between functional network anti-correlations and memory in MCI.* Neurobiology of Aging, 2017. **50**: p. 152-162.
48. Damoiseaux, J.S., et al., *Functional connectivity tracks clinical deterioration in Alzheimer's disease.* Neurobiology of Aging, 2012. **33**(4): p. 828.e19-828.e30.
49. Schultz, A.P., et al., *Phases of Hyperconnectivity and Hypoconnectivity in the Default Mode and Salience Networks Track with Amyloid and Tau in Clinically Normal Individuals.* The Journal of Neuroscience, 2017. **37**(16): p. 4323-4331.
50. Sepulcre, J., et al., *Tau and amyloid β proteins distinctively associate to functional network changes in the aging brain.* Alzheimer's & Dementia, 2017. **13**(11): p. 1261-1269.
51. Jacobs, H.I., et al., *Structural tract alterations predict downstream tau accumulation in amyloid-positive older individuals.* Nature neuroscience, 2018. **21**(3): p. 424.
52. Corder, E.H., et al., *Gene dose of apolipoprotein E type 4 allele and the risk of Alzheimer's disease in late onset families.* Science, 1993. **261**(5123): p. 921-923.
53. Strittmatter, W.J., et al., *Apolipoprotein E: high-avidity binding to beta-amyloid and increased frequency of type 4 allele in late-onset familial Alzheimer disease.* Proceedings of the National Academy of Sciences, 1993. **90**(5): p. 1977-1981.
54. Lehmann, M., et al., *Intrinsic connectivity networks in healthy subjects explain clinical variability in Alzheimer's disease.* Proceedings of the National Academy of Sciences, 2013. **110**(28): p. 11606-11611.

SUPPLEMENTARY MATERIAL

Supplementary Table 1. List of participant IDs included in final analyses.

031_S_4005	018_S_4349	013_S_4595	002_S_4251	006_S_4515	006_S_4867
031_S_4024	130_S_4352	018_S_4597	019_S_4252	136_S_4517	018_S_4868
012_S_4026	006_S_4357	130_S_4605	002_S_4262	002_S_4521	130_S_4883
031_S_4029	006_S_4363	013_S_4616	013_S_4268	130_S_4542	018_S_4889
031_S_4032	019_S_4367	130_S_4641	002_S_4270	006_S_4546	013_S_4917
031_S_4042	013_S_4395	012_S_4643	019_S_4285	019_S_4548	130_S_4925
012_S_4094	018_S_4399	002_S_4654	019_S_4293	019_S_4549	031_S_4947
012_S_4128	018_S_4400	130_S_4660	130_S_4294	100_S_4556	006_S_4960
031_S_4149	130_S_4405	053_S_4661	018_S_4313	053_S_4557	130_S_4971
006_S_4150	130_S_4415	006_S_4679	130_S_4343	053_S_4578	130_S_4982
006_S_4153	130_S_4417	019_S_4680	010_S_4345	013_S_4580	130_S_4984
002_S_4171	136_S_4433	018_S_4696	006_S_4346	031_S_4590	013_S_4985
012_S_4188	002_S_4447	006_S_4713	130_S_5059	019_S_5012	012_S_4987
006_S_4192	006_S_4449	031_S_4721	053_S_5070	002_S_5018	130_S_4990
031_S_4194	130_S_4468	130_S_4730	013_S_5071	130_S_5006	053_S_4813
031_S_4203	100_S_4469	002_S_4746	100_S_5106	130_S_4997	
002_S_4213	002_S_4473	013_S_4791	002_S_4229	006_S_4485	
031_S_4218	031_S_4474	002_S_4799	002_S_4237	031_S_4496	
002_S_4219	031_S_4476	018_S_4809	130_S_4250	100_S_4512	
002_S_4225	012_S_4849	019_S_4835	130_S_4817	019_S_4477	

Supplementary Table 2. Peak coordinates of regions of interest in MNI space.

Region[a]	X	Y	Z
DMN			
MPFC	1	55	-3
LP (L)	-39	-77	33
LP (R)	47	-67	29
PCC	1	-61	38
DAN			
FEF (L)	-27	-9	64
FEF (R)	30	-6	64
IPS (L)	-39	-43	52
IPS (R)	39	-42	54
SN			
ACC	0	22	35
Insula (L)	-44	13	1
Insula (R)	47	14	0
RPFC (L)	-32	45	27
RPFC (R)	32	46	27
SMG (L)	-60	-39	31
SMG (R)	62	-35	32
FPN			
LPFC (L)	-43	33	28
LPFC (R)	41	38	49
PPC (L)	-46	-58	30
PPC (R)	52	-52	45

Abbreviations: ACC, Anterior Cingulate Cortex; DAN, Dorsal Attention Network; DMN, Default Mode Network; FEF, Frontal Eye Fields; FPN, Frontoparietal Network; IPS, Intraparietal Sulcus; LP, Lateral Parietal region; LPFC, Lateral Prefrontal Cortex; MPFC, Medial Prefrontal Cortex; PCC, Posterior Cingulate Cortex; PPC, Posterior Parietal Cortex; RPFC, Rostral Prefrontal Cortex; SMG, Supramarginal Gyrus; SN, Salience Network.

[a]Hemisphere of nodes is indicated between brackets; L = left hemisphere, R = right hemisphere.

Supplementary Box 1. Regression model construction.

$$Outcome_{ij} = \beta_1 + \beta_2 Age_i + \beta_3 Education_i + \beta_4 Sex_i + \beta_5 ICV_i + \beta_6 PredictorA_i + \beta_7 PredictorB_i + \beta_8 Time_{ij} + [\beta_9 PredictorA_i * Timeij] + [\beta_{10} PredictorB_i * Time_{ij}] +$$

$$[\beta_{11} PredictorA_i * PredictorB_i * Time_{ij}] + [\beta_{12} PredictorA_i * (Time_{ij}^2)] +$$

$$[\beta_{13} PredictorB_i * (Time_{ij}^2)] + [\beta_{14} PredictorA_i * PredictorB_i * (Time_{ij}^2)] + b_{si} Time_{ij} + b_{1i} + \varepsilon_i$$

Outcome: outcome variable measured over time (ADNI Memory composite);

Age_i, $Education_i$, Sex_i, ICV_i: age, education, sex or intracranial volume (ICV) for each participant;

Predictor A/B: independent variables of interest for the investigated model;

$Time_{ij}$: time at testing session, relative to baseline testing session;

b_{1i}: random intercept for each participant;

b_{si}: random slope for each participant

ε_i: error term for each participant

Supplementary Table 3. Tukey tests for differences of baseline characteristics[a]

Groups	Difference	95% CI Lower bound	95% CI Upper bound	Adjusted *p* value[b]
AV45				
MCI- v CN	-0.14	-0.25	-0.03	< 0.001
MCI+ v CN	0.24	0.13	0.34	< 0.001
AD v CN	0.34	0.23	0.46	< 0.001
MCI+ v MCI-	0.38	0.27	0.48	< 0.001
AD v MCI-	0.49	0.37	0.60	< 0.001
AD v MCI+	0.11	0.00	0.21	0.05
ADNI-EF				
MCI- v CN	-0.55	-1.07	-0.03	0.03
MCI+ v CN	-0.46	-0.94	0.02	0.07
AD v CN	-1.74	-2.27	-1.20	< 0.001
MCI+ v MCI-	0.09	-0.40	0.58	0.96
AD v MCI-	-1.19	-1.72	-0.65	< 0.001
AD v MCI+	-1.28	-1.78	-0.77	< 0.001
ADNI-Mem				
MCI- v CN	-0.14	-0.25	-0.03	0.01
MCI+ v CN	0.24	0.13	0.34	< 0.001
AD v CN	0.34	0.23	0.46	< 0.001
MCI+ v MCI-	0.38	0.27	0.48	< 0.001
AD- v MCI-	0.49	0.37	0.60	< 0.001
AD- v MCI+	0.11	0.00	0.21	0.05
CDR-SB				
MCI- v CN	1.21	0.53	1.88	< 0.001
MCI+ v CN	1.85	1.22	2.48	< 0.001
AD v CN	4.36	3.67	5.06	< 0.001
MCI+ v MCI-	0.64	0.01	1.28	0.046
AD v MCI-	3.16	2.46	3.86	< 0.001
AD v MCI+	2.51	1.86	3.17	< 0.001
Follow-up time				
MCI- v CN	-0.33	-0.76	0.10	0.19
MCI+ v CN	-0.16	-0.55	0.22	0.69
AD v CN	-0.73	-1.22	-0.23	0.001
MCI+ v MCI-	0.17	-0.24	0.58	0.72
AD v MCI-	-0.39	-0.91	0.12	0.20
AD v MCI+	-0.56	-1.04	-0.08	0.01

Abbreviations: AD: Alzheimer's Disease; ADNI-EF: ADNI executive functions score composite; ADNI-Mem: ADNI memory score composite; APOE ε4, apolipoprotein ε4; AV45: ^{18}F-AV-45 florbetapir; CDR-SB: Clinical Dementia Rating scale – Sum of Boxes; CI: Confidence interval; CN: Cognitively Normal; MCI: Mild Cognitive Impairment, - and + indicate amyloid negative- or positive grouping, respectively.

[a]Only characteristics showing a significant difference at baseline between any of the groups are listed here.

[b]*p* Values are adjusted with family-wise correction.

Supplementary table 4. Summary of maximum motion parameter values and scrubbed volumes across groups.

Parameter	CN	MCI-	MCI+	AD	*p* Value[a]
Motion 1[b]	0.14 (0.08)	0.18 (0.12)	0.14 (0.09)	0.13 (0.09)	0.31
Motion 2[b]	0.35 (0.29)	0.34 (0.26)	0.26 (0.13)	0.31 (0.23)	0.37
Motion 3[b]	0.41 (0.65)	0.32 (0.21)	0.36 (0.48)	0.39 (0.24)	0.90
Motion 4[b]	0.01 (< 0.01)	0.01 (0.01)	< 0.01 (< 0.01)	< 0.01 (0.01)	0.18
Motion 5[b]	< 0.01 (< 0.01)	< 0.01 (0.01)	< 0.01 (< 0.01)	< 0.01 (< 0.01)	0.12
Motion 6[b]	< 0.01 (< 0.01)	< 0.01 (< 0.01)	< 0.01 (< 0.01)	< 0.01 (< 0.01)	0.19
Scrubbed volumes[c]	26.71 (23.70)	27.37 (20.48)	25.11 (20.30)	24.30 (15.70)	0.94

ap Values were calculated using ANOVA.

bThe maximum displacement of each motion parameter was calculated for each participant. Group averages were calculated from these numbers and standard deviations are shown in brackets behind the average values. Motion parameter values are given in millimeters.

cScrubbed volumes values are given in the average number of scrubbed volumes per perticipant in each group. Standard deviations are shown in brackets behind the averages. Scrubbed volumes are volumes that were regressed out due to a total displacement larger than 0.5mm.

Supplementary Table 5. Baseline results.

Associations between baseline inter-network functional connectivity and baseline memory performance and executive functions in the whole sample[a,b]

Network	Estimate	SE	T Value	*p* Value
Memory				
DMN-DAN (n=115, number of observations = 115)				
DMN-DAN	0.13	0.29	0.47	0.64
DMN-SN (n=115, number of observations = 115)				
DMN-SN	-0.16	0.30	-0.54	0.59
DMN-FPN (n=115, number of observations = 115)				
DMN-FPN	0.22	0.30	0.73	0.47
Executive functions				
DMN-DAN (n=115, number of observations = 115)				
DMN-DAN	-0.08	0.30	-0.28	0.78
DMN-SN (n=115, number of observations = 115)				
DMN-SN	2.53	0.31	-0.81	0.42
DMN-FPN (n=115, number of observations = 115)				
DMN-FPN	0.67	0.31	2.15	0.03

Associations between inter-network functional connectivity on baseline memory and executive functions performance for each group separately[a]

Network	Estimate	SE	T Value	*p* Value
Memory				
CN (n=28, number of observations = 28)				
DMN-DAN	-0.39	0.33	-1.21	0.24
DMN-SN	-0.48	0.32	-1.51	0.15
DMN-FPN	-0.37	0.41	-0.92	0.37
MCI- (n=27, number of observations = 27)				
DMN-DAN	0.04	0.33	0.12	0.90
DMN-SN	-0.10	0.41	-0.24	0.81
DMN-FPN	-0.44	0.35	-1.27	0.22
MCI+ (n=36, number of observations = 36)				
DMN-DAN	0.07	0.39	0.18	0.86
DMN-SN	-0.07	0.34	-0.20	0.84
DMN-FPN	-0.13	0.42	-0.30	0.77
AD (n=24, number of observations = 24)				
DMN-DAN	-0.18	0.47	-0.39	0.70
DMN-SN	-0.59	0.47	-1.26	0.22
DMN-FPN	-0.31	0.43	-0.71	0.49
Executive functions				
CN (n=28, number of observations = 28)				
DMN-DAN	-0.48	0.43	-1.13	0.27
DMN-SN	0.08	0.44	0.18	0.86
DMN-FPN	0.37	0.54	0.70	0.49
MCI- (n=27, number of observations = 27)				
DMN-DAN	-0.05	0.47	-0.12	0.91
DMN-SN	-0.31	0.58	-0.54	0.60
DMN-FPN	1.25	0.44	2.83	0.01
MCI+ (n=36, number of observations = 36)				
DMN-DAN	-0.37	0.52	-0.71	0.48
DMN-SN	0.23	0.47	0.48	0.63
DMN-FPN	-0.49	0.57	-0.85	0.40
AD (n=24, number of observations = 24)				
DMN-DAN	-0.20	0.51	-0.39	0.70
DMN-SN	0.18	0.53	0.34	0.74
DMN-FPN	0.11	0.48	0.23	0.82

Abbreviations: AD: Alzheimer's Disease; DAN: Dorsal Attention Network; DMN: Default Mode Network; FPN: Frontoparietal Network; MCI: Mild Cognitive Impairment, - and + indicate amyloid negative- or positive grouping, respectively; SE: Standard Error; SN: Salience Network.

[a] Regression models are adjusted for age, intracranial volume, sex and years of education. Beta coefficients are unstandardized.

[b] Results are obtained using CN as the reference group.

Supplementary table 6. Associations between functional inter-network connectivity and memory decline in the whole sample.

Fitted model	Est.	SE	95% CI	DF	T Value	*p* Value
Whole sample (n = 115, number of observations = 433)						
Time*DMN-DAN	-0.04	0.09	-0.22 to 0.15	316	-0.40	0.69
Time*DMN-SN	0.06	0.09	-0.12 to 0.23	316	0.65	0.52
Time*DMN-FPN	0.04	0.10	-0.16 to 0.24	316	0.39	0.70

Abbreviations: CI: Confidence interval; DAN: Dorsal Attention Network; DF, Degrees of Freedom; DMN: Default Mode Network; FPN: Frontoparietal Network; SE: Standard Error; SN: Salience Network.

Supplementary Table 7. Longitudinal linear effects of inter-network functional connectivity between each network pair on memory, per group[a]

Fitted model	Estimate	SE	95 % CI	DF	T Value	*p* Value
CN (n=28, number of observations = 118)						
DMN-DAN*Time	0.37	0.11	0.16 to 0.58	88	3.49	0.001
DMN-SN*Time	0.39	0.10	0.20 to 0.59	88	4.06	< 0.001
DMN-FPN*Time	0.25	0.14	-0.02 to 0.52	88	1.87	0.06
MCI- (n=27, number of observations = 100)						
DMN-DAN*Time	-0.10	0.12	-0.33 to 0.13	71	-0.85	0.40
DMN-SN*Time	0.11	0.12	-0.13 to 0.35	71	0.88	0.38
DMN-FPN*Time	0.08	0.14	-0.19 to 0.35	71	0.58	0.56
MCI+ (n=36, number of observations = 146)						
DMN-DAN*Time	-0.49	0.11	-0.72 to -0.26	108	-4.27	< 0.001
DMN-SN*Time	-0.28	0.09	-0.46 to -0.10	108	-3.09	0.001
DMN-FPN*Time	0.21	0.13	-0.04 to 0.46	108	1.66	0.10
AD (n=24, number of observations = 69)						
DMN-DAN*Time	0.10	0.19	-0.28 to 0.49	43	0.53	0.60
DMN-SN*Time	-0.03	0.20	-0.44 to 0.37	43	-0.16	0.87
DMN-FPN*Time	-0.27	0.18	-0.63 to 0.08	43	-1.54	0.13

Abbreviations: AD: Alzheimer's Disease; CN: Cognitively Normal; DAN: Dorsal Attention Network; DF: Degrees of Freedom; DMN: Default Mode Network; FPN: Frontoparietal Network; MCI: Mild Cognitive Impairment, - and + indicate amyloid negative- or positive state, respectively; SE: Standard Error; SN: Salience Network.

[a] Regression models are adjusted for age, intracranial volume, sex and education. Beta coefficients are unstandardized.

Supplementary Table 8. Associations between group, inter-network functional connectivity and decline in executive functions[a,b]

Fitted model	Est.	SE	95% CI	DF	T Value	*p* Value
DMN-DAN (n = 115, number of observations = 433)						
Time*MCI-*DMN-DAN	0.17	0.26	-0.35 to 0.69	310	0.64	0.52
Time*MCI+*DMN-DAN	-0.18	0.28	-0.73 to 0.38	310	-0.63	0.53
Time*AD*DMN-DAN	-0.02	0.36	-0.74 to 0.70	310	-0.05	0.96
DMN-SN (n = 115, number of observations = 433)						
Time*MCI-*DMN-SN	0.16	0.28	-0.38 to 0.71	310	0.59	0.55
Time*MCI+*DMN-SN	0.03	0.24	-0.44 to 0.50	310	0.11	0.91
Time*AD*DMN-SN	-0.19	0.37	-0.92 to 0.54	310	-0.52	0.61
DMN-FPN (n = 115, number of observations = 433)						
Time*MCI-*DMN-FPN	310	0.69	-0.39 to 0.82	310	0.69	0.49
Time*MCI+*DMN-FPN	310	0.23	-0.51 to 0.65	310	0.23	0.82
Time*AD*DMN-FPN	310	-1.14	-1.15 to 0.31	310	-1.14	0.26

Abbreviations: AD, Alzheimer's Disease; CI, Confidence Interval; DAN, Dorsal Attention Network; DF, Degrees of Freedom; DMN, Default Mode Network; FDR, False Discovery Rate; FPN, Frontoparietal Network; MCI, Mild Cognitive Impairment, - and + indicate amyloid-β negative- or positive grouping, respectively; SE, Standard Error; SN, Salience Network.

[a]Results are acquired using the cognitively normal group as reference group.

[b]Regression models are adjusted for age, intracranial volume, sex and education. Beta coefficients are unstandardized.

Supplementary Table 9. Associations between functional connectivity, time, amyloid status, memory and executive functioning in the cognitively normal group.

Fitted model	Est.	SE	95% CI	DF	T Value	*p* Value
Memory (n=28, number of observations = 118)						
Time*Amyloid status*DMN-DAN	0.61	0.30	0.01 to 1.20	86	2.02	0.046
Time*Amyloid status*DMN-SN	0.53	0.31	-0.10 to 1.15	86	1.68	0.10
Time*Amyloid status*DMN-FPN	0.29	0.53	-0.76 to 1.34	86	0.55	0.58
Executive functioning (n=28, number of observations = 118)						
Time*Amyloid status*DMN-DAN	0.38	0.37	-0.35 to 1.11	86	1.03	0.31
Time*Amyloid status*DMN-SN	-0.09	0.38	-0.85 to 0.68	86	-0.22	0.82
Time*Amyloid status*DMN-FPN	-0.81	0.56	-1.92 to 0.30	86	-1.45	0.15

Abbreviations: CI: Confidence interval; DAN: Dorsal Attention Network; DF, Degrees of Freedom; DMN: Default Mode Network; FPN: Frontoparietal Network; SE: Standard Error; SN: Salience Network.

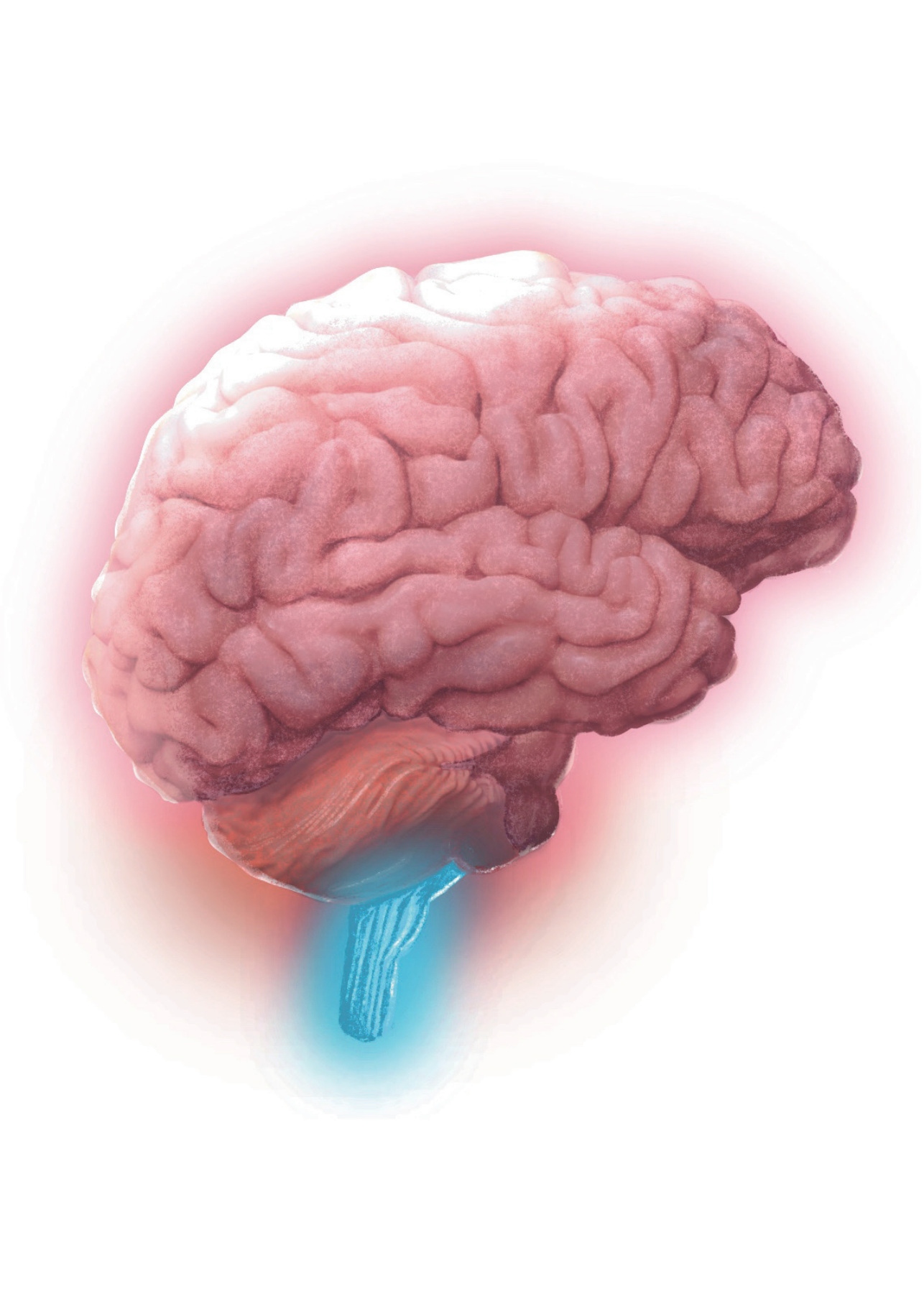

ELEVATED NOREPINEPHRINE METABOLISM IS LINKED TO CORTICAL THICKNESS IN THE CONTEXT OF ALZHEIMER'S DISEASE PATHOLOGY

CHAPTER 3

Published in Neurobiology of Aging (2021)

Roy W.E. van Hooren
Frans R.J. Verhey
Inez H.G.B. Ramakers
Willemijn J. Jansen
Heidi I.L. Jacobs

ABSTRACT

Background: Advanced Alzheimer's disease (AD) is characterized by higher noradrenaline metabolite levels that may be associated with AD pathology. The locus coeruleus (LC) is the main site for cerebral noradrenaline synthesis and LC volume loss occurs as early as Braak stage 1. This study investigates the association between noradrenergic turnover and brain morphology, and the modifying effect of AD pathology.

Method: The study sample included 77 memory clinic patients (37 cognitively unimpaired and 40 cognitively impaired (mild cognitive impairment or AD dementia)). Cortical thickness and volumetric analyses were performed using FreeSurfer. Cerebrospinal fluid was analyzed for noradrenergic metabolite 3-methoxy-4-hydroxyphenylethyleneglycol (MHPG), Aβ42 and phosphorylated tau.

Results: Higher MHPG was associated with lower cortical thickness and hippocampal volume at lower, but subthreshold, levels of Aβ42 and at higher p-tau levels. These associations remained significant after adding APOE-E4 or cognitive status as covariates.

Discussion: Our results suggest that greater MHPG together with worse AD pathology contributes to neurodegeneration, possibly before significant amyloidosis. The noradrenergic system may play an important role in early detection of AD-related processes.

Keywords: Alzheimer's disease; Locus coeruleus; Noradrenaline; Amyloid-beta; Tau; Brain morphology

INTRODUCTION

Alzheimer's disease (AD) is a progressive neurodegenerative disease characterized by its hallmark pathologies, accumulations of tau and amyloid-beta (Aβ) misfolded proteins, resulting in significant loss of cognitive functions [1-4]. The earliest signs of tau aggregates have been traced back to the locus coeruleus (LC) [5], which is the primary site for the synthesis of noradrenaline (NA) in the brain. Volume loss of the LC occurs as early as in Braak stage 1, a stage when cortical tauopathy is still restricted to the entorhinal cortex and the cortex is not yet affected by amyloidosis [5-7]. Thus, investigating the LC-noradrenergic system may facilitate detection of AD in its earliest stages.

Apart from its structure, the function of the noradrenergic (NA) system is also affected in AD. Studies analyzing the NA metabolite 3-methoxy-4-hydroxyphenylglycol (MHPG) in cerebrospinal fluid (CSF) reported higher MHPG levels in patients with advanced AD [8, 9]. It has been suggested that these higher levels may reflect a compensatory mechanism in response to cell loss in the LC, whereby surviving LC neurons exhibit increased activity and NA turnover [8, 10-13]. However, elevated MHPG levels may be detrimental rather than compensatory, as they have been associated with cognitive impairment, suggesting that higher MHPG levels presage neuronal changes such as unavailing sprouting [9]. Furthermore, MHPG may be associated with AD pathology, as previous CSF work and animal studies showed associations between higher NA-metabolites and worse AD-pathology, aggrevated tau and beta-amyloid pathology [14-16]. It is conceivable that the combination of greater metabolism of NA neurons in the LC and rising levels of AD pathology put a strain on and predispose cortical target regions of the LC [17, 18] to neurodegeneration.

We set out to investigate the relationship between metabolism of the noradrenergic system and brain structure as well as the modifying effect of hallmark AD pathologies on this relationship in a convenience memory clinic sample. Given the involvement of the LC-NA system in AD, CSF MHPG measures may have potential as an early marker of AD-related brain disintegrity.

METHODS

Participants

The study comprised a convenience sample of 77 patients from the memory clinic of the Maastricht University Medical Center (MUMC). Of this sample, 37 (48%) patients were diagnosed with subjective cognitive decline (SCD) (cognitively unimpaired) and 40 (52%) patients were cognitively impaired (MCI or AD dementia). Diagnoses were made by experienced clinicians in accordance with clinical criteria for MCI and AD dementia [19-21]. Presence of SCD was assessed with self-reported cognitive complaints and affirmative response to the question "Do you think your memory is becoming worse?" [22]. Patients with SCD did not show impairment on cognitive tests, defined by scores lower than 1.5 SD below the age-,sex- and education-adjusted mean. Exclusion criteria were major neurological disease, clinical diagnoses of other neurodegenerative disorders, transient ischemic attack or stroke that occurred less than two years before testing, history of severe psychiatric disorders and alcohol or drug abuse. All patients had complete cerebrospinal fluid (CSF) measures of MHPG, Aβ42 and p-tau, provided informed consent and protocols were approved by the local Medical Ethics Committee of the MUMC.

CSF and blood analyses

CSF was collected via a lumbar puncture in the L3-4 or L4-5 vertebral interspaces, centrifuged, aliquoted, and stored at −80 °C in polypropylene tubes. Biochemical analysis of CSF Aβ42 and p-tau181p (Innotest ELISA, Innogenetics, Ghent, Belgium) was performed blind to diagnostic information and following a standardized biobanking protocol [23]. We chose to focus on p-tau as it is more closely correlated to AD pathology than t-tau [24] and p-tau correlated strongly with t-tau in our data (r = 0.90). CSF MHPG levels were determined using high-performance liquid chromatography [25]. AD pathology measures are treated as continuous variables, given evidence that even subthreshold levels of pathology can predict clinical progression [26]. Apolipoprotein E4 (APOE) genotyping was performed using polymerase chain reaction .

Imaging equipment and acquisition

Imaging data were acquired using using a 3.0T whole-body MR system release 2.0 (Philips Achieva, Philips Medical Systems, Best, The Netherlands). Structural T1-

weighted data with dimensions of 240 × 240 × 180 mm with a voxel resolution of 1 mm isotropic were acquired in sagittal orientation with a repetition time of 8.2 ms, echo time of 3.8 ms and flip angle of 8°.

Image analysis and statistical analysis

Imaging data was processed with FreeSurfer version 6.0 [27] (http://surfer.nmr.mgh.harvard.edu/) using the software package's default, automated reconstruction protocol as described previously [28]. We visually inspected and, if necessary, edited for over- or under-estimation of gray/white matter boundaries and to identify brain areas erroneously excluded during skull stripping (data was edited for 10 participants in the cognitively unimpaired group and 9 participants in the cognitively impaired group). Additionally, given the innervation of the amygdala and hippocampus by the LC-NA system [29], we also included hippocampal and amygdala volumes derived from the default FreeSurfer segmentation and adjusted for intracranial volume.

For group analysis, cortical thickness maps were spatially smoothed using a gaussian kernel at 15mm full width at half maximum and subsequently averaged across participants using a spherical averaging method which aligned cortical folds. For the vertex-based analysis, general linear models were set up to predict cortical thickness at each vertex across the cortical mantle. Predictor of interest was levels of CSF MHPG. In a second step, we tested interactions between MHPG and Aβ42 or p-tau. All models were corrected for age, sex and education. Additionally, Mini-Mental State Examination (MMSE) score was added as a covariate to account for the range in disease severity. In a third step, we added APOE status, a known genetic risk factor for AD, as a covariate. Critical p-values were adjusted for multiple comparisons by running a Monte Carlo simulation with 10,000 iterations using a vertex-based cluster-forming threshold of $p < 0.05$ [30]. For each cluster, cortical thickness values per participant were exported to R version 3.3.1 (https://www.r-project.org/) for further visualization. Finally, a floodlight approach using aforementioned regression models with FDR-adjustment for multiple comparisons determined the region of significance for the biomarkers regarding the slope between MHPG and cortical thickness. This technique probes the entire range of AD pathology values and avoids having to pick predetermined and arbitrary values for AD pathology at which to investigate the slope between MHPG and cortical thickness [31].

RESULTS

Demographics

The study sample included a total of 77 participants with a mean age of 63 years (standard deviation (SD) = 8.62, range 46-80), of which 49 (64%) were male. Median education level was 4 (IQR = 2 , range 1-8), whereby 4 indicates an average education level, equating to approximately 10 years of education. The average MMSE score was 27.39 (SD = 2.65, range 16-30). CSF value means were 38.68 nM/L (SD = 9.73, range = 21-63) for MHPG, 928.01 pg/mL (SD = 394.49, range = 140-1898) for Aβ42 and 65.31 pg/mL (SD = 34.93, range = 22 -188) for p-tau. Finally, 39 (51%) participants carried at least one APOE E4-allele. Participant demographics per diagnostic group can be found in Supplementary table 1.

Interaction between levels of CSF MHPG and AD biomarkers on cortical thickness

There were no associations between MHPG and cortical thickness in the entire sample and weak, non-significant, correlations were found between MHPG and AD pathology (Supplementary table 2, Supplementary figure 1). However, after including CSF biomarkers in the models we found interaction effects between MHPG and CSF biomarkers (Figure 1, Supplementary table 3). For all analyses, we observed that worse pathology (lower CSF Aβ or higher CSF p-tau) [32, 33] and higher levels of MHPG were associated with lower cortical thickness. These effects were observed in the insula, middle temporal regions such as the parahippocampal gyrus and entorhinal cortex, multiple parts of the prefrontal cortex, including the pars opercularis and frontal gyri as well as parietal areas like the precuneus. These results remained significant after covarying for APOE status (Supplementary table 4). Posthoc, we investigated whether these effects were driven by the cognitively impaired participants (MCI and AD patients) by constructing three-way interaction models between MHPG, AD biomarker levels and a dichotomous group variable based on diagnosis (SCD versus MCI/AD). Here, MMSE score was not included as covariate. No significant three-way interactions were observed in these models for any of the biomarkers (Supplementary table 4).

We also investigated associations between MHPG and hippocampal and amygdala volumes. Similarly, we observed no direct association between MHPG and these volumes (Supplementary table 5). We found a significant interaction between Aβ42 and MHPG on right hippocampal volume (Standardized β=1.160, t=2.696, p(FDR)=0.003) but no interaction for the left hippocampal volume (Standardized

β=0.883, t=1.870, p(FDR)=0.132) (Figure 1, Supplementary table 4). No interactions were found for CSF p-tau or with amygdala volume as outcome variable and hippocampal associations remained significant after APOE-E4 adjustment (Supplementary table 4).

Figure 1. Association between MHPG and cortical thickness or hippocampal volume at varying levels of AD biomarkers

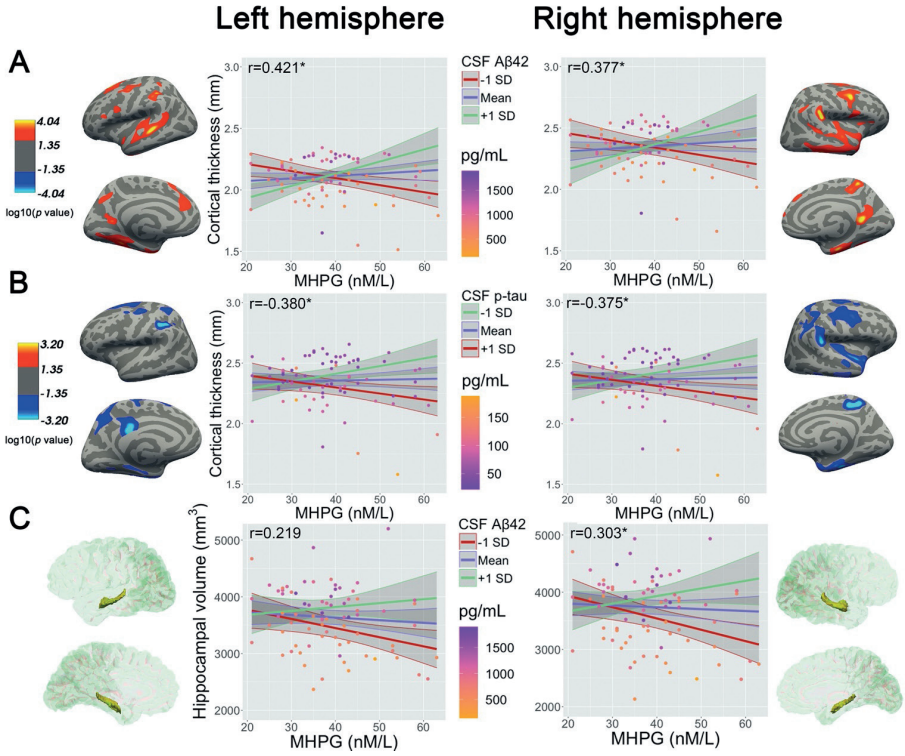

Note. Results of vertex-based cortical thickness analyses and ROI-based volumetric analyses in the hippocampus. All general linear models were constructed with the predictors of interest, age, sex, education and Mini-Mental State Examination score as covariates, as well as total intracranial volume for volumetric models. Results were adjusted for multiple comparisons using cluster-based correction at $p < 0.050$. The p-values are expressed as -log(p value). Predicted simple slopes for the aggregated significant vertices of the hemisphere or hippocampal volume, including 95% confidence interval, are plotted for the mean biomarker values and 1 SD below and above the mean (for visualization purposes only, analyses were done with continuous data). Correlation coefficients for the interactions are shown in the top left corner of each graph. Significant interactions are indicated with an asterisk. CSF marker levels for each data point are visualized using an orange-to-purple gradient, expressed in pg/mL. For a detailed description of all clusters, please see Supplementary table 3. Bilateral hemisphere-averaged data can be found in Supplementary figure 2. A: Interaction between MHPG and Aβ42 levels on cortical thickness. B: Interaction between MHPG and p-tau levels on cortical thickness. C: Interaction between MHPG and Aβ42 levels on hippocampal volume. Abbreviations: Aβ42; Amyloid-Beta 42, CSF; Cerebrospinal Fluid, MHPG; 3-methoxy-4-hydroxyphenylglycol.

Finally, FDR-corrected floodlight analyses revealed that the effects of MHPG are twofold. When AD pathology was worse, we observed a negative relationship between MHPG and cortical thickness (all clusters concatenated). These negative associations were significant when p-tau was higher than ~102 pg/mL or Aβ was lower than 634 (left hemisphere) or 584 (right hemisphere) pg/mL (Figure 2). This p-tau lower range value lies above our clinical threshold (85 pg/mL), but for Aβ these values are slightly above the clinical threshold (500 pg/mL) [34]. Conversely, when AD pathology was less present, we observed a positive relationship between MHPG and cortical thickness.

Figure 2. Ranges of AD biomarker levels at which the association between MHPG and cortical thickness was statistically significant.

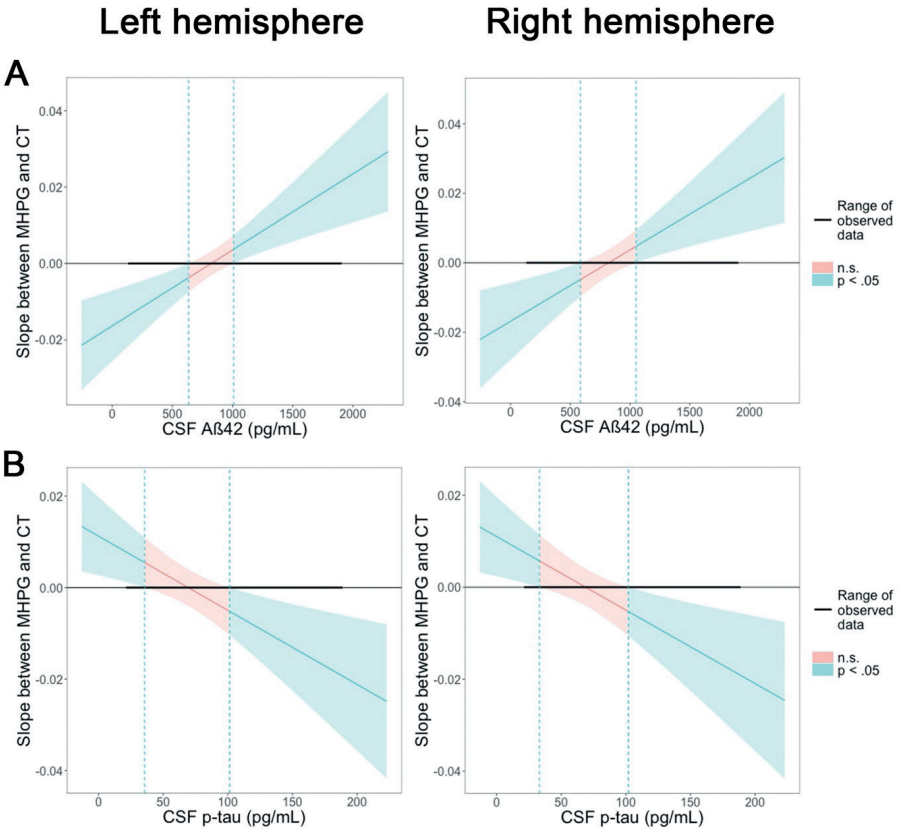

Note. Floodlight analyses demonstrating at which ranges of biomarkers (A and B) the association between MHPG and cortical thickness was statistically significant. Results are FDR-corrected. Please note that interpretations of these associations are limited to the range of observed data. Visualization for the average of both hemispheres can be found in Supplementary figure 3. A: Association between MHPG and Aβ42 levels. B: Association between MHPG and p-tau levels. Abbreviations: Aβ42; Amyloid-Beta 42, CSF; Cerebrospinal fluid, CT; Cortical Thickness, MHPG; 3-methoxy-4-hydroxyphenylglycol, n.s; Not Significant.

DISCUSSION

The current study provides evidence for synergistic associations between CSF MHPG and AD biomarkers on cortical thickness. High turnover of NA has previously been linked to advanced AD [8, 9], and though we did not find a difference in MHPG levels between healthy controls and patients with AD, likely due to the mild disease severity of patients in our sample (Supplementary table 1), we now show that worse pathology in tandem with higher levels of MHPG is associated with lower cortical thickness in widespread cortical regions, including a large number of LC target sites. These associations remained significant after adding APOE-status or the level of cognitive impairment as covariates, suggesting that MHPG and AD-pathology act on brain morphology throughout the entire disease continuum.

However, the role of MHPG in brain morphology may be twofold. When AD-pathology markers are within the normal range, elevated MHPG, a reflection of NA metabolism, may be a compensatory factor, as we observed associations with higher cortical thickness. Such a compensatory role of MHPG on brain integrity is consistent with previous literature demonstrating that via its anti-inflammatory actions NA promotes Aβ clearance, and thus can possibly preserve cortical integrity [14, 35-37]. In contrast, when AD-pathology is worse, this compensatory action of MHPG may put a high demand on the system, as reflected in our negative associations with cortical thickness. This is consistent with animal research showing that LC lesions in the presence of tau pathology promote neuronal loss in the hippocampus [37]. In addition, increased turnover of the DOPEGAL metabolite –situated on the NA biosynthesis pathway upstream to MHPG - has been shown to induce tau aggregation and spreading [16]. We speculate that in later stages of the AD pathological process, MHPG levels may be increased disproportionately to NA levels because its turnover outpaces NA release possibly due to decreased presynaptic a1-adrenergic reuptake ability [10, 14, 38]. As such, the compensatory role of NA diminishes, possibly contributing to a neurodegenerative cascade. Unfortunately, we had no information available on NA levels, but future work may test the hypothesis that the MHPG to NA ratio increases as a function of disease progression [10], suggesting that the availability of NA may hold the key in understanding the role of elevated MHPG. Additionally, structural integrity of the LC may be associated with cortical thickness [39] and future research investigating the interplay between LC integrity, CSF levels of MHPG and AD pathology and cortical thickness may provide more insight into the role of the noradrenergic system in the

disease process. Future studies should also include information about the intake of drugs that may affect the noradrenergic system. Additionally, the diffusion of MHPG into spinal cord tissue has challenged its interpretation as a pure indicator of NE metabolism [40]. Future studies should consider including plasma MHPG as an additional measure, but similar associations can be expected given that CSF MHPG measures correlate very highly with plasma measures [8, 25, 41, 42].

Finally, while our data is cross-sectional and does not allow us to infer temporal relationships, we do note that the negative relationship between MHPG and cortical thickness occurred above the clinical threshold for tau pathology, but at a subthreshold level for Aβ42 [23]. Given that tau pathology in the LC and entorhinal cortex precedes amyloid deposition [5-7], it is likely that the function of the noradrenergic system is also affected early on in the disease process. Longitudinal studies are required to confirm this premise, but MHPG in combination with p-tau measures may have the potential to predict worsening AD-related brain integrity, possibly prior to significant amyloidosis. These findings contribute to a better understanding of the contribution of the NA-system to brain integrity in the context of AD-pathology. More research on the interactions between NA measures and AD pathology is warranted, especially in a longitudinal framework, given that the LC-NA system is involved early in the disease and may facilitate early detection of AD-related processes, possibly even prior to subjective report of cognitive decline.

REFERENCES:

1. McKhann, G., et al., *Clinical diagnosis of Alzheimer's disease Report of the NINCDS-ADRDA Work Group* under the auspices of Department of Health and Human Services Task Force on Alzheimer's Disease.* Neurology, 1984. **34**(7): p. 939-939.
2. Jagust, W.J. and E.C. Mormino, *Lifespan brain activity, beta-amyloid, and Alzheimer's disease.* Trends Cogn Sci, 2011. **15**(11): p. 520-6.
3. Mulder, C., et al., *Amyloid-β (1–42), total tau, and phosphorylated tau as cerebrospinal fluid biomarkers for the diagnosis of Alzheimer disease.* Clinical chemistry, 2010. **56**(2): p. 248-253.
4. Braak, H. and E. Braak, *Neuropathological stageing of Alzheimer-related changes.* Acta neuropathologica, 1991. **82**(4): p. 239-259.
5. Braak, H., et al., *Stages of the Pathologic Process in Alzheimer Disease: Age Categories From 1 to 100 Years.* Journal of Neuropathology & Experimental Neurology, 2011. **70**(11): p. 960-969.
6. Tomlinson, B., D. Irving, and G. Blessed, *Cell loss in the locus coeruleus in senile dementia of Alzheimer type.* Journal of the neurological sciences, 1981. **49**(3): p. 419-428.
7. Theofilas, P., et al., *Locus coeruleus volume and cell population changes during Alzheimer's disease progression: A stereological study in human postmortem brains with potential implication for early-stage biomarker discovery.* Alzheimer's & Dementia, 2017. **13**(3): p. 236-246.
8. Raskind, M.A., et al., *Norepinephrine and mhpg levels in csf and plasma in alzheimer's disease.* Archives of General Psychiatry, 1984. **41**(4): p. 343-346.
9. Sheline, Y.I., et al., *Higher Cerebrospinal Fluid MHPG in Subjects With Dementia of the Alzheimer Type: Relationship With Cognitive Dysfunction.* The American Journal of Geriatric Psychiatry, 1998. **6**(2): p. 155-161.
10. Hoogendijk, W.J., et al., *Increased activity of surviving locus ceruleus neurons in Alzheimer's disease.* Annals of Neurology: Official Journal of the American Neurological Association and the Child Neurology Society, 1999. **45**(1): p. 82-91.
11. Chalermpalanupap, T., et al., *Targeting norepinephrine in mild cognitive impairment and Alzheimer's disease.* Alzheimer's Research & Therapy, 2013. **5**(2): p. 21.
12. Lawlor, B.A., et al., *Plasma 3-methoxy-4-hydroxyphenylglycol (MHPG) and clinical symptoms in Alzheimer's disease.* Biological psychiatry, 1995. **38**(3): p. 185-188.
13. Peskind, E.R., et al., *Effects of Alzheimer's Disease and Normal Aging on Cerebrospinal Fluid Norepinephrine Responses to Yohimbine and Clonidine.* Archives of General Psychiatry, 1995. **52**(9): p. 774-782.
14. Jacobs, H.I.L., et al., *Alzheimer's disease pathology: pathways between central norepinephrine activity, memory, and neuropsychiatric symptoms.* Mol Psychiatry, 2019.
15. Weinshenker, D., *Long Road to Ruin: Noradrenergic Dysfunction in Neurodegenerative Disease.* Trends in Neurosciences, 2018. **41**(4): p. 211-223.
16. Kang, S.S., et al., *Norepinephrine metabolite DOPEGAL activates AEP and pathological Tau aggregation in locus coeruleus.* The Journal of Clinical Investigation, 2020. **130**(1): p. 422-437.
17. Schwarz, L.A. and L. Luo, *Organization of the Locus Coeruleus-Norepinephrine System.* Current Biology, 2015. **25**(21): p. R1051-R1056.

18. Bari, B., V. Chokshi, and K. Schmidt, *Locus coeruleus-norepinephrine: basic functions and insights into Parkinson’s disease.* Neural Regeneration Research, 2020. **15**(6): p. 1006-1013.
19. Albert, M.S., et al., *The diagnosis of mild cognitive impairment due to Alzheimer's disease: Recommendations from the National Institute on Aging-Alzheimer's Association workgroups on diagnostic guidelines for Alzheimer's disease.* Alzheimer's & Dementia, 2011. **7**(3): p. 270-279.
20. McKhann, G.M., et al., *The diagnosis of dementia due to Alzheimer's disease: Recommendations from the National Institute on Aging-Alzheimer's Association workgroups on diagnostic guidelines for Alzheimer's disease.* Alzheimer's & Dementia, 2011. **7**(3): p. 263-269.
21. Petersen, R.C., *Mild cognitive impairment as a diagnostic entity.* Journal of Internal Medicine, 2004. **256**(3): p. 183-194.
22. Jessen, F., et al., *Prediction of dementia by subjective memory impairment: effects of severity and temporal association with cognitive impairment.* Archives of general psychiatry, 2010. **67**(4): p. 414-422.
23. de Jong, D., et al., *Current state and future directions of neurochemical biomarkers for Alzheimer's disease.* Clinical chemistry and laboratory medicine, 2007. **45**(11): p. 1421.
24. Blennow, K., et al., *Cerebrospinal fluid and plasma biomarkers in Alzheimer disease.* Nature Reviews Neurology, 2010. **6**(3): p. 131.
25. Janssens, J., et al., *Cerebrospinal fluid and serum MHPG improve Alzheimer's disease versus dementia with Lewy bodies differential diagnosis.* Alzheimer's & dementia (Amsterdam, Netherlands), 2018. **10**: p. 172-181.
26. Tijms, B.M., et al., *Low normal cerebrospinal fluid Aβ42 levels predict clinical progression in nondemented subjects.* Annals of neurology, 2017. **81**(5): p. 749-753.
27. Fischl, B., *FreeSurfer.* Neuroimage, 2012. **62**(2): p. 774-781.
28. Dale, A.M., B. Fischl, and M.I. Sereno, *Cortical surface-based analysis. I. Segmentation and surface reconstruction.* Neuroimage, 1999. **9**(2): p. 179-94.
29. Samuels, E.R. and E. Szabadi, *Functional neuroanatomy of the noradrenergic locus coeruleus: its roles in the regulation of arousal and autonomic function part I: principles of functional organisation.* Current neuropharmacology, 2008. **6**(3): p. 235-253.
30. Hagler, D.J., A.P. Saygin, and M.I. Sereno, *Smoothing and cluster thresholding for cortical surface-based group analysis of fMRI data.* NeuroImage, 2006. **33**(4): p. 1093-1103.
31. Spiller, S.A., et al., *Spotlights, Floodlights, and the Magic Number Zero: Simple Effects Tests in Moderated Regression.* Journal of Marketing Research, 2013. **50**(2): p. 277-288.
32. Buerger, K., et al., *CSF phosphorylated tau protein correlates with neocortical neurofibrillary pathology in Alzheimer's disease.* Brain, 2006. **129**(11): p. 3035-3041.
33. Herukka, S.-K., et al., *CSF Aβ42 and tau or phosphorylated tau and prediction of progressive mild cognitive impairment.* Neurology, 2005. **64**(7): p. 1294-1297.
34. Jong, D.d., et al., *Current state and future directions of neurochemical biomarkers for Alzheimer's disease.* 2007. **45**(11): p. 1421.
35. Counts, S.E. and E.J. Mufson, *Noradrenaline activation of neurotrophic pathways protects against neuronal amyloid toxicity.* Journal of Neurochemistry, 2010. **113**(3): p. 649-660.

36. Kalinin, S., et al., *Noradrenaline deficiency in brain increases β-amyloid plaque burden in an animal model of Alzheimer's disease.* Neurobiology of Aging, 2007. **28**(8): p. 1206-1214.
37. Chalermpalanupap, T., et al., *Locus Coeruleus Ablation Exacerbates Cognitive Deficits, Neuropathology, and Lethality in P301S Tau Transgenic Mice.* The Journal of Neuroscience, 2018. **38**(1): p. 74-92.
38. Raskind, M.A., et al., *Patterns of cerebrospinal fluid catechols support increased central noradrenergic responsiveness in aging and Alzheimer's disease.* Biological Psychiatry, 1999. **46**(6): p. 756-765.
39. Bachman, S.L., et al., *Locus coeruleus MRI contrast is associated with cortical thickness in older adults.* 2020.
40. Eisenhofer, G., I.J. Kopin, and D.S. Goldstein, *Catecholamine Metabolism: A Contemporary View with Implications for Physiology and Medicine.* Pharmacological Reviews, 2004. **56**(3): p. 331-349.
41. Kopin, I., et al., *Relation between plasma and cerebrospinal fluid levels of 3-methoxy-4-hydroxyphenylglycol.* Science, 1983. **219**(4580): p. 73-75.
42. Elsworth, J.D., D.E. Redmond, and R.H. Roth, *Plasma and cerebrospinal fluid 3-methoxy-4-hydroxyphenylethylene glycol (MHPG) as indices of brain norepinephrine metabolism in primates.* Brain Research, 1982. **235**(1): p. 115-124.

SUPPLEMENTARY MATERIAL

Supplementary table 1. Participant demographics per diagnostic group.

	SCD (N=37)	MCI (N=22)	AD (N=18)	*p*-Value
Age in years	59.27 (8.22) Range: 46-78	65.64 (8.01) Range: 50-80	69.06 (5.67) Range: 61-79	< 0.001[a]
Males	27 (73%)	13 (59%)	9 (50%)	0.219
Education	4 (2) Range: 1-8	4 (4) Range: 1-8	3.5 (2) Range: 1-8	0.819
MMSE	28.84 (1.17) Range: 26-30	27.27 (2.19) Range: 22-30	24.56 (3.09) Range: 16-29	< 0.001[b]
MHPG (nM/L)	38.32 (7.93) Range: 25-58	37.64 (10.45) Range: 21-58	40.67 (12.19) Range: 21-63	0.597
CSF Aβ42 (pg/mL)	1131.16 (330.44) Range: 448-1898	852.95 (424.01) Range: 315-1852	602.17 (181.28) Range: 140-873	< 0.001[a]
CSF p-tau (pg/mL)	47.14 (26.62) Range: 22-185	70.14 (34.08) Range: 32-188	96.78 (26.88) Range: 68-151	< 0.001[b]
APOE E4 carriers	16 (43%)	9 (41%)	14 (78%)	0.031[c]

Note. Data are presented as the mean (standard deviation) for the continuous variables and as n (%) for the categorical variable. Ranges are also presented for the continuous variables.

The education row gives the median education level and interquartile range between brackets.

The APOE ε4 row gives the number of participants in this group with one or more APOE ε4 alleles.

Statistical significance was tested with analysis of variance for continuous variables and chi-squared test for the categorical variables

[a] All groups were significantly different from each other, except MCI versus AD

[b] All groups were significantly different from each other

[c] Only the AD group showed a significantly larger amount of APOE E4 carriers than would be expected under equal distribution of E4 carriers across groups ($p < 0.03$)

Abbreviations: AD; Alzheimer's Disease, APOE E4; Apolipoprotein E4, Aβ42; Amyloid-Beta 42, CSF; Cerebrospinal Fluid, MCI; mild cognitive impairment, MHPG; 3-methoxy-4-hydroxyphenylglycol, MMSE; Mini-Mental State Examination, SCD; Subjective Cognitive Decline.

Supplementary table 2. Correlation matrix for the main predictors of interest and age.

	MHPG	CSF Aβ42	CSF p-tau
CSF Aβ42	-0.086 (0.456)		
CSF p-tau	0.128 (0.269)	-0.543 (<0.001)	
Age	0.259 (0.023)	-0.450 (<0.001)	0.477 (<0.001)

Note. Correlation table detailing the correlations between the main predictors of interest and age. *p*-Values are given between brackets.

Abbreviations: Aβ42; Amyloid-Beta 42, CSF; Cerebrospinal Fluid, MHPG; 3-methoxy-4-hydroxyphenylglycol.

Supplementary figure 1. Associations between CSF AD biomarkers and MHPG levels.

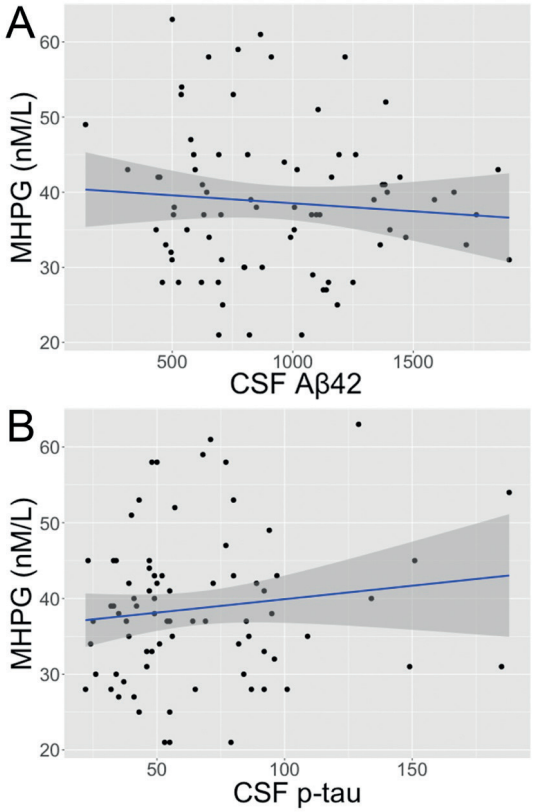

Note. Associations between CSF AD biomarkers and MHPG levels. A: Associations between CSF Aβ42 and MHPG levels (r=-0.086, *p*=0.456). B: Associations between CSF p-tau and MHPG levels (r=0.128, *p*=0.269). Abbreviations: Aβ42; Amyloid-Beta 42, CSF; Cerebrospinal Fluid, MHPG; 3-methoxy-4-hydroxyphenylglycol.

Supplementary table 3. Clusters from vertex-based cortical thickness analyses after cluster-wise corrected whole brain analysis, with and without APOE covariate[a]

Cluster number	*Regions (% of the cluster)*	*Cluster size (mm^2)*	*Peak -log(p) value of cluster*
Without APOE covariate			
Left hemisphere			
MHPG*Aβ42			
Cluster 1	Superior parietal lobule (100%)	494	1.728
Cluster 2	Precuneus (50.56%) Isthmus cingulate cortex (28.41%) Lingual gyrus (19.16%) Cuneus (1.33%) Pericalcarine gyrus (0.53%)	2249	3.250
Cluster 3	Superior temporal gyrus (50.66%) Bank superior temporal sulcus (19.76%) Transverse temporal gyrus (11.36%) Middle temporal gyrus (10.42%) Supramarginal gyrus (5.53%) Inferior parietal lobule (2.26%)	7878	4.283
Cluster 4	Superior frontal gyrus (54.33%) Precentral Gyrus (20.79%) Caudal middle frontal gyrus (17.53%) Caudal anterior cingulate gyrus (3.41%) Rostral anterior cingulate gyrus (3.14%) Postcentral gyrus (0.65%) Rostral middle frontal gyrus (0.16%)	9557	4.230
Cluster 5	Precuneus (87.97%) Superior parietal gyrus (12.03%)	2195	2.571
Cluster 6	Fusiform gyrus (32.83%) Inferior temporal gyrus (21.83%) Lingual gyrus (20.42%) Parahippocampal gyrus (12.61%) Entorhinal cortex (10.27%)	8999	3.870
Cluster 7	Superior temporal gyrus (100%)	587	2.237
Cluster 8	Precentral gyrus (54.27%) Pars opercularis (33.33%) Caudal middle frontal gyrus (12.40%)	1089	2.494
Cluster 9	Supramarginal gyrus (66.56%) Superior parietal lobule (30.63%) Postcentral gyrus (2.81%)	3882	3.842
Cluster 10	Pars opercularis (92.88%) Rostral middle frontal gyrus (6.98%) Pars triangularis (0.14%)	702	2.118
Cluster 11	Rostral middle frontal gyrus (53.68%) Caudal middle frontal Gyrus (46.32%)	272	1.646
Cluster 12	Postcentral gyrus (84.72%) Supramarginal gyrus (15.28%)	72	1.448
Cluster 13	Precentral gyrus (100%)	32	1.347

Cluster number	***Regions (% of the cluster)***	***Cluster size (mm^2)***	***Peak -log(p) value of cluster***
MHPG*p-tau			
Cluster 1	Superior frontal gyrus (92.35%) Paracentral gyrus (4.71%) Precentral gyrus (2.27%) Caudal middle frontal gyrus (0.67%)	3568	2.520
Cluster 2	Precuneus (66.74%) Superior parietal lobule (13.67%) Postcentral gyrus (11.44%) Paracentral gyrus (8.14%)	2640	2.365
Cluster 3	Posterior cingulate cortex (75.77%) Isthmus cingulate cortex (21.50%) Precuneus (2.73%)	1977	3.612
Cluster 4	Precentral gyrus (100%)	844	2.584
Cluster 5	Superior parietal lobule (58.43%) Postcentral gyrus (41.56%)	1044	2.531
Cluster6	Supramarginal gyrus (92.42%) Postcentral gyrus (7.58%)	2151	3.836
Cluster 7	Fusiform gyrus (57.92%) Inferior temporal gyrus (38.71%) Entorhinal cortex (2.55%)	1723	3.648
Cluster 8	Parahippocampal gyrus (90.65%) Entorhinal cortex (9.35%)	738	1.935
Cluster 9	Caudal middle frontal gyrus (100%)	122	1.505
Cluster 10	Superior parietal lobule (100%)	43	1.354
Cluster 11	Lingual gyrus (100%)	108	1.432
Cluster 12	Superior parietal lobule (100%)	35	1.341
Right hemisphere			
MHPG*Aβ42			
Cluster 1	Superior parietal lobule (100%)	497	1.726
Cluster 2	Superior temporal gyrus (22.61%) Fusiform gyrus (16.68%) Middle temporal gyrus (15.77%) Inferior temporal gyrus (14.19%) Insula (6.80%) Bank superior temporal sulcus (6.14%) Parahippocampal gyrus (4.76%) Entorhinal cortex (3.61%) Transverse temporal gyrus (3.47%) Inferior parietal lobule (2.76%) Lingual gyrus (0.89%)	19578	3.865
Cluster 3	Precuneus (52.78%) Isthmus cingulate cortex (36.86%) Lingual gyrus (9.91%) Pericalcarine gyrus (0.29%) Parahippocampal gyrus (0.17%)	3492	4.388

Cluster number	***Regions (% of the cluster)***	***Cluster size (mm^2)***	***Peak -log(p) value of cluster***
Cluster 4	Precentral gyrus (36.30%) Caudal middle frontal gyrus (30.72%) Superior frontal gyrus (18.65%) Pars opercularis (12.89%) Rostral middle frontal gyrus (1.39%) Postcentral gyrus (0.05%)	9565	4.225
Cluster 5	Supramarginal gyrus (48.66%) Inferior parietal lobule (36.24%) Superior parietal lobule (15.10%)	2205	2.567
Cluster 6	Supramarginal gyrus (90.85%) Superior temporal gyrus (9.15%)	2153	4.645
Cluster 7	Superior frontal gyrus (100%)	1088	2.491
Cluster 8	Precuneus (42.70%) Superior parietal lobule (25.22%) Paracentral gyrus (24.09%) Posterior cingulate cortex (6.43%) Postcentral gyrus (1.57%)	3890	3.840
Cluster 9	Pars triangularis (39.74%) Insula (32.47%) Pars orbitalis (21.71%) Lateral orbitofrontal gyrus (6.08%)	1004	2.329
Cluster 10	Superior frontal gyrus (97.57%) Medial orbitofrontal gyrus (2.43%)	700	2.115
Cluster 11	Parahippocampal gyrus (73.36%) Lingual gyrus (26.64%)	304	1.663
Cluster 12	Superior frontal gyrus (83.82%) Rostral middle frontal gyrus (16.18%)	272	1.642
Cluster 13	Paracentral gyrus (97.18%) Superior frontal gyrus (2.82%)	71	1.444
Cluster 14	Superior frontal gyrus (100%)	32	1.345
MHPG*p-tau			
Cluster 1	Precentral gyrus(57.71%) Caudal middle frontal gyrus (39.88%) Postcentral gyrus (2.41%)	3573	2.523
Cluster 2	Supramarginal gyrus (41.29%) Postcentral gyrus (33.90%) Inferior parietal lobule (21.12%) Superior parietal lobule (3.70%)	2652	2.361
Cluster 3	Supramarginal gyrus (93.01%) Superior temporal gyrus (6.99%)	2004	3.473
Cluster 4	Superior frontal gyrus (85.09%) Precentral gyrus(14.91%)	845	2.582
Cluster 5	Postcentral gyrus (62.93%) Superior parietal lobule (37.07%)	1044	2.526
Cluster 6	Superior temporal gyrus (55.52%) Insula (22.41%) Transverse temporal gyrus (20.41%) Middle temporal gyrus (0.77%) Supramarginal gyrus (0.60%)	3494	2.875

Cluster number	***Regions (% of the cluster)***	***Cluster size (mm^2)***	***Peak -log(p) value of cluster***
Cluster 7	Precuneus (51.42%) Paracentral gyrus (45.75%) Posterior cingulate cortex (2.83%)	2153	3.834
Cluster 8	Fusiform gyrus (53.56%) Parahippocampal gyrus (28.19%) Entorhinal cortex (18.25%)	1852	3.641
Cluster 9	Superior frontal gyrus (75.21%) Caudal middle frontal gyrus (24.79%)	121	1.501
Cluster 10	Middle temporal gyrus (71.60%) Inferior temporal gyrus (28.40%)	426	1.774
Cluster 11	Superior parietal lobule (100%)	42	1.352
Cluster 12	Entorhinal cortex (43.12%) Fusiform gyrus (11.13%) Insula (2.83%)	494	1.725
Cluster 13	Inferior temporal gyrus (100%)	149	1.406
Cluster 14	Inferior temporal gyrus (100%)	105	1.430
Cluster 15	Superior parietal lobule (100%)	31	1.339
Cluster 16	Superior temporal gyrus (100%)	205	1.489
With APOE E4 covariate			
Left hemisphere			
Aβ42			
Cluster 1	Superior parietal lobule (100%)	433	1.685
Cluster 2	Precuneus (51.97%) Isthmus cingulate cortex (27.93%) Lingual gyrus (18.40%) Cuneus (1.16%) Pericalcarine gyrus (0.54%)	2234	3.206
Cluster 3	Superior temporal gyrus (50.89%) Bank superior temporal sulcus (20.04%) Transverse temporal gyrus (11.43%) Middle temporal gyrus (9.84%) Supramarginal gyrus (5.59%) Inferior parietal lobule (2.20%)	7714	4.198
Cluster 4	Superior frontal gyrus (54.01%) Precentral gyrus(21.14%) Caudal middle frontal gyrus (17.77%) Rostral anterior cingulate gyrus (3.18%) Caudal anterior cingulate gyrus (3.15%) Postcentral gyrus (0.51%) Rostral middle frontal gyrus (0.23%)	9294	4.154
Cluster 5	Precuneus (88.58%) Superior parietal lobule (11.42%)	2190	2.683
Cluster 6	Fusiform gyrus (33.31%) Lingual gyrus (20.71%) Inferior temporal gyrus (20.29%) Parahippocampal gyrus (12.49%) Entorhinal cortex (10.56%)	8681	3.841

Cluster number	***Regions (% of the cluster)***	***Cluster size (mm^2)***	***Peak -log(p) value of cluster***
Cluster 7	Superior temporal gyrus (100%)	601	2.252
Cluster 8	Precentral gyrus(55.79%) Pars opercularis (32.84%) Caudal middle frontal gyrus (11.47%)	1011	2.429
Cluster 9	Supramarginal gyrus (66.71%) Superior parietal lobule (30.77%) Postcentral gyrus (2.52%)	3770	3.759
Cluster 10	Pars opercularis (92.42%) Rostral middle frontal gyrus (7.43%) Pars triangularis (0.15%)	686	2.078
Cluster 11	Rostral middle frontal gyrus (55.91%) Caudal middle frontal gyrus (44.09%)	254	1.628
Cluster 12	Precentral gyrus(100%)	20	1.330
Cluster 13	Postcentral gyrus (90.57%) Supramarginal gyrus (9.43%)	53	1.407
MHPG*p-tau			
Cluster 1	Precuneus (64.93%) Superior parietal lobule (19.31%) Postcentral gyrus (10.42%) Paracentral gyrus (5.35%)	3216	2.439
Cluster 2	Posterior cingulate cortex (75.48%) Isthmus cingulate cortex (23.50%) Precuneus (1.02%)	1970	3.629
Cluster 3	Superior parietal lobule (60.95%) Postcentral gyrus (39.05%)	922	2.442
Cluster 4	Precuneus (100%)	88	1.498
Right hemisphere			
MHPG*Aβ42			
Cluster 1	Superior parietal lobule (100%)	436	1.683
Cluster 2	Superior temporal gyrus (22.66%) Fusiform gyrus (16.45%) Middle temporal gyrus (15.71%) Inferior temporal gyrus (14.21%) Insula (6.88%) Bank superior temporal sulcus (6.29%) Parahippocampal gyrus (4.67%) Entorhinal cortex (3.79%) Transverse temporal gyrus (3.55%) Inferior parietal lobule (2.95%) Lingual gyrus (0.71%)	19089	3.836
Cluster 3	Precuneus (52.72%) Isthmus cingulate cortex (37.49%) Lingual gyrus (9.41%) Pericalcarine gyrus (0.20%) Parahippocampal gyrus (0.17%)	3452	4.309

Cluster number	***Regions (% of the cluster)***	***Cluster size (mm^2)***	***Peak -log(p) value of cluster***
Cluster 4	Precentral gyrus(35.38%) Caudal middle frontal gyrus (31.18%) Superior frontal gyrus (18.90%) Pars opercularis (12.97%) Rostral middle frontal gyrus (1.56%)	9294	4.150
Cluster 5	Supramarginal gyrus (48.32%) Inferior parietal lobule (37.31%) Superior parietal lobule (14.38%)	2198	2.678
Cluster 6	Supramarginal gyrus (91.19%) Superior temporal gyrus (8.81%)	2133	4.559
Cluster 7	Superior frontal gyrus (100%)	1010	2.427
Cluster 8	Pars triangularis (40.77%) Insula (32.93%) Pars orbitalis (20.18%) Lateral orbitofrontal gyrus (6.12%)	981	2.321
Cluster 9	Superior frontal gyrus (96.63%) Medial orbitofrontal gyrus (3.37%)	683	2.075
Cluster 10	Parahippocampal gyrus (75%) Lingual gyrus (25%)	248	1.604
Cluster 11	Superior frontal gyrus (84.13%) Rostral middle frontal gyrus (15.87%)	252	1.624
MHPG*p-tau			
Cluster 1	Supramarginal gyrus (32.74%) Postcentral gyrus (30.74%) Inferior parietal lobule (25.01%) Superior parietal lobule (9.51%)	3227	2.435
Cluster 2	Supramarginal gyrus (92.97%) Superior temporal gyrus (7.03%)	1992	3.451
Cluster 3	Superior temporal gyrus (52.26%) Insula (26.19%) Transverse temporal gyrus (20.12%) Supramarginal gyrus (0.76%)	3291	3.041
Cluster 4	Fusiform gyrus (36.33%) Entorhinal cortex (33.93%) Parahippocampal gyrus (19.38%) Insula (1.32%)	2502	3.257
Cluster 5	Postcentral gyrus (61.54%) Superior parietal lobule (38.46%)	923	2.438
Cluster 6	Middle temporal gyrus (72.32%) Inferior temporal gyrus (27.68%)	354	1.717
Cluster 7	Superior parietal lobule (100%)	85	1.493

Note. Overview of clusters shown in the significance maps (Figure 1) for the association between MHPG and biomarkers on cortical thickness. Localization of regions corresponding to cluster location are based on the Desikan-Killiany atlas provided by FreeSurfer [27]. Clusters < 20mm^2 in size were not included in this table.

[a] Regression models are adjusted for age, sex, education and MSSE score.

Abbreviations: APOE; Apolipoprotein E4, Aβ42; Amyloid-Beta 42, MHPG; 3-methoxy-4-hydroxyphenylglycol, MMSE; Mini-Mental State Examination.

Supplementary table 4. Posthoc associations between biomarkers, MHPG, APOE and cognitive status in relation to cortical thickness and subcortical volumes, including three-way interaction models[a]

Predictor	Left hemisphere				Right hemisphere			
	Estimate	SE	*t* Value	*p* Value (FDR)	Estimate	SE	t Value	*p* Value (FDR)
Interaction MHPG*Aβ42								
Cortical thickness								
MHPG*Aβ42	1.920	0.481	3.999	**0.001**	1.810	0.517	3.495	**0.003**
MHPG*Aβ42(+APOE)	1.910	0.484	3.947	**0.001**	1.790	0.520	3.446	**0.006**
MHPG*Aβ42*group	-0.847	1.910	-0.444	0.793	-0.967	2.060	-0.469	0.815
Hippocampal volume								
MHPG*Aβ42	0.883	0.472	1.870	0.132	1.160	0.430	2.696	**0.003**
MHPG*Aβ42(+APOE)	0.926	0.468	1.978	0.104	1.200	0.425	2.830	**0.012**
MHPG*Aβ42*group	3.920	1.800	2.172	0.100	1.080	1.720	0.629	0.815
Amygdala volume								
MHPG*Aβ42	0.610	0.482	1.264	0.252	0.641	0.462	1.389	0.203
MHPG*Aβ42(+APOE)	0.617	0.487	1.267	0.251	0.600	0.458	1.310	0.234
MHPG*Aβ42*group	5.570	1.760	3.162	**0.014**	3.890	1.730	2.248	0.168
Interaction MHPG*p-tau								
Cortical thickness								
MHPG*p-tau	-1.330	0.399	-3.346	**0.004**	-1.320	0.402	-3.285	**0.003**
MHPG*p-tau(+APOE)	-1.290	0.408	-3.169	**0.007**	-1.280	0.411	-3.119	**0.008**
MHPG*p-tau*group	1.350	1.280	1.057	0.589	1.130	1.290	0.880	0.815
Hippocampal volume								
MHPG*p-tau	0.002	0.416	0.006	0.996	-0.272	0.385	-0.706	0.482
MHPG*p-tau(+APOE)	-0.178	0.408	-0.435	0.665	-0.450	0.375	-1.199	0.235
MHPG*p-tau*group	-0.564	1.280	-0.441	0.793	0.029	1.210	0.024	0.815
Amygdala volume								
MHPG*p-tau	0.433	0.420	1.029	0.252	0.094	0.420	0.234	0.203
MHPG*p-tau(+APOE)	0.341	0.426	0.801	0.251	0.119	0.409	0.290	0.234
MHPG*p-tau*group	-0.209	1.310	-0.159	0.874	0.420	1.240	0.338	0.815

Note. Associations between biomarkers, MHPG and cognitive group on cortical thickness and hippocampal volume, including three-way interaction models. Only predictors of interest are listed. +APOE indicates that the model included APOE status as a covariate.

[a] Regression models are adjusted for age, sex, education and MMSE score. Hippocampal volume models were also adjusted for intracranial volume. Predictors with the group (cognitively unimpaired versus impaired) variable were not corrected for MMSE. Beta coefficients are standardized.

[b] The interaction effect of MHPG and Aβ42 on left amygdala volume was driven by outliers and is no longer significant when a bootstrapped model (2000 iterations, 95% confidence interval of β= [-0.017 to 0.089]) is used and is therefore not further interpreted.

Abbreviations: APOE: apolipoprotein E4, Aβ42; Amyloid-Beta 42, MHPG; 3-methoxy-4-hydroxyphenylglycol, SE; Standard Error.

Supplementary table 5. Associations between MHPG levels and bilateral hippocampal and amygdala volumes[a].

Predictor	Left hemisphere				Right hemisphere			
	Estimate	**SE**	***t* Value**	***p* Value (FDR)**	**Estimate**	**SE**	**t Value**	***p* Value (FDR)**
Hippocampal volume								
MHPG	-0.119	0.090	-1.331	0.375	-0.107	0.084	-1.270	0.354
Amygdala volume								
MHPG	-0.038	0.091	-0.416	0.679	-0.081	0.087	-0.933	0.354

Note. Associations between MHPG levels and hippocampal and amygdala volumes.

[a] Regression models are adjusted for age, sex, education, MMSE score and intracranial volume. Beta coefficients are standardized.

Abbreviations: MHPG; 3-methoxy-4-hydroxyphenylglycol, SE; Standard Error.

Supplementary figure 2. Association between MHPG and cortical thickness or hippocampal volume at varying levels of AD biomarkers (thickness or volume averaged across hemispheres).

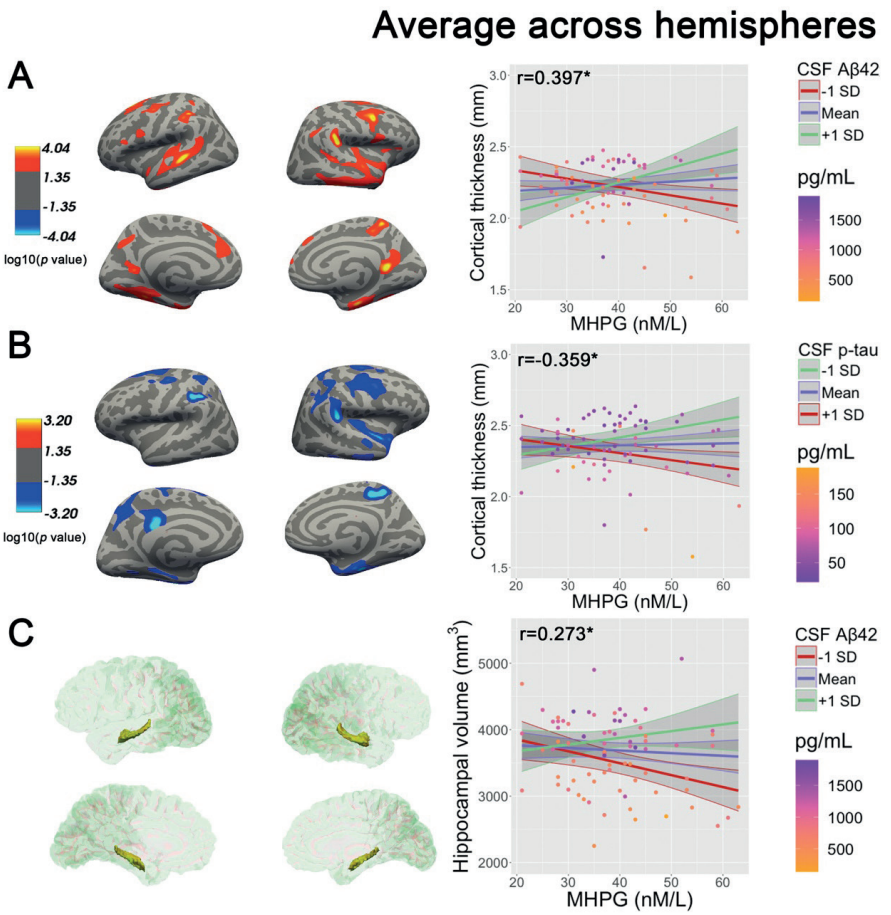

Note. Results of vertex-based cortical thickness analyses and ROI-based volumetric analyses in the hippocampus. All general linear models were constructed with the predictors of interest, age, sex, education and Mini-Mental State Examination score as covariates, as well as total intracranial volume for volumetric models. Results were adjusted for multiple comparisons using cluster-based correction at $p < 0.050$. The p-values are expressed as -log(*p* value). Predicted simple slopes for the aggregated significant vertices of the hemisphere or hippocampal volume, including 95% confidence interval, are plotted for the mean biomarker values and 1 SD below and above the mean (for visualization purposes only, analyses were done with continuous data). Correlation coefficients for the interactions are shown in the top left corner of each graph. Significant interactions are indicated with an asterisk. CSF marker levels for each data point are visualized using an orange-to-purple gradient, expressed in pg/mL. For a detailed description of all clusters, please see Supplementary table 3. A: Interaction between MHPG and Aβ42 levels on cortical thickness. B: Interaction between MHPG and p-tau levels on cortical thickness. C: Interaction between MHPG and Aβ42 levels on hippocampal volume. Abbreviations: Aβ42; Amyloid-Beta 42, CSF; Cerebrospinal Fluid, MHPG; 3-methoxy-4-hydroxyphenylglycol.

Supplementary figure 3. Ranges of AD biomarker levels at which the association between MHPG and cortical thickness was statistically significant (cortical thickness averaged across hemispheres).

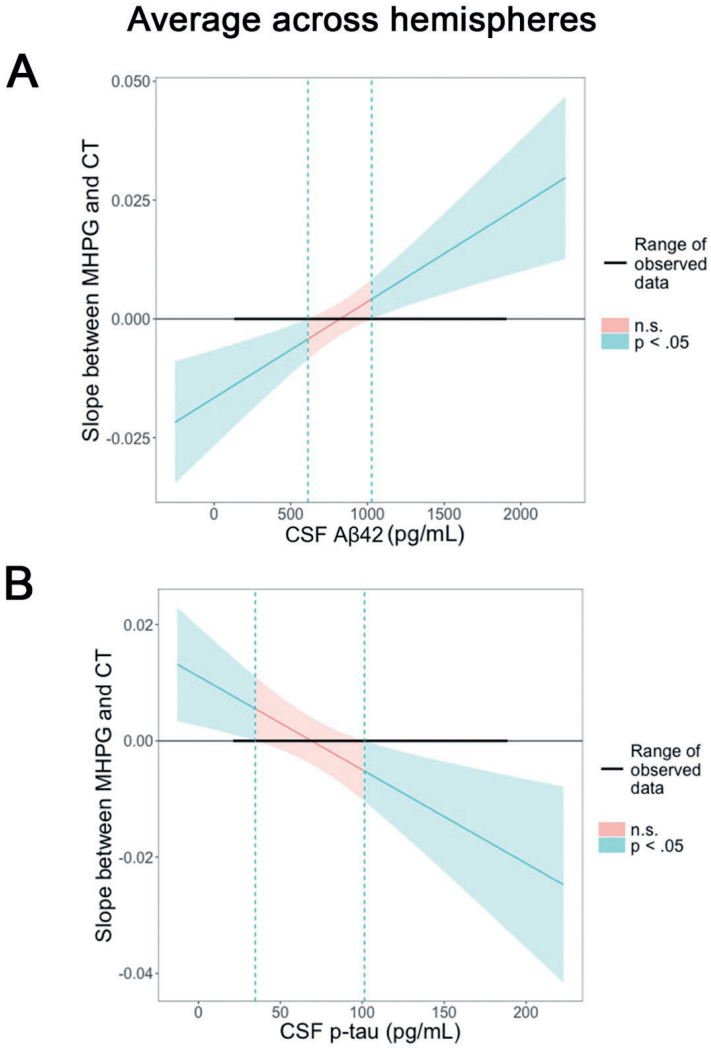

Note. Floodlight analyses demonstrating at which ranges of biomarkers (A and B) the association between MHPG and cortical thickness was statistically significant. Results are FDR-corrected. Please note that interpretations of these associations are limited to the range of observed data. A: Association between MHPG and Aβ42 levels (significant when Aβ levels were below 612.23 or above 1028.13 pg/mL) B: Association between MHPG and p-tau levels (significant when p-tau was below 34.76 or above 101.48 pg/mL). Abbreviations: Aβ42; Amyloid-Beta 42, CSF; Cerebrospinal fluid, CT; Cortical Thickness, MHPG; 3-methoxy-4-hydroxyphenylglycol, n.s; Not Significant.

ASSOCIATIONS BETWEEN THE MAGNETIZATION TRANSFER-WEIGHTED MRI SIGNAL AT 7T AND MICROSTRUCTURAL CHARACTERISTICS OF THE LOCUS COERULEUS AND ITS PROJECTIONS

CHAPTER 4

In prep

Roy W.E. van Hooren
Maxime van Egroo
Frans R.J. Verhey
Heidi I.L. Jacobs

ABSTRACT

Background: The brainstem locus coeruleus (LC) is one of the earliest brain regions affected by Alzheimer's disease (AD) pathology. While volume loss in the LC is reported as early as Braak stage a-c, frank cell death of LC neurons, however, is not reported until Braak stage IV. In vivo measures of LC structural integrity have been linked to Braak staging but the biological correlates underlying the loss of LC integrity remain unclear. In this study, we investigated microstructural correlates of LC structural integrity using diffusion-weighted imaging (DWI)-based tractography and Neurite Orientation Dispersion and Density Imaging (NODDI).

Methods: Fifty-eight cognitively unimpaired participants underwent magnetic resonance imaging including DWI and LC-sensitive magnetization transfer (MT)-weighted scans at 7 Tesla. Microstructural DWI metrics, including neurite density and dispersion orientation in the LC and quantitative anisotropy in its projections, were correlated to magnetization transfer-based LC signal intensity. LC projections were generated using a LC seed-based approach with a minimum tract length of 20 voxels with whole brain and cerebellum endpoints.

Results: Within the LC itself, there was no association between MT signal intensity and neurite density or orientation dispersion. However, we found a positive association between MT signal intensity and quantitative anisotropy in tracts originating from the right LC. These tracts included the right reticular tract, left and right dentatorubrothalamic tracts, as well as the superior cerebellar peduncles.

Conclusions: These results suggest that the integrity of LC projections is affected in the presence of early LC integrity changes in asymptomatic individuals, in whom LC cell death is unlikely. This information helps us identify microstructural characteristics associated with LC integrity in aging and in neurodegenerative diseases, potentially before irreversible cell death.

INTRODUCTION

The brainstem locus coeruleus (LC) is the main source of brain noradrenaline and has numerous connections to cortical and subcortical regions supporting its modulatory role in cognition and arousal [1, 2]. It is one of the first brain regions accumulating Alzheimer's disease (AD)-related hyperphosphorylated tau [3, 4], and post-mortem studies have revealed that neuron loss in the LC is associated with tau pathology levels and antemortem cognitive performance in prodromal stages of AD [5]. Interestingly, volume loss in the LC has been reported as early as Braak stage a-c (also referred to as Braak stage 0), with approximately 8% of LC volume lost per Braak stage; however, loss of LC cells is not reported until Braak stage IV [6].

Multiple explanations have been proposed regarding the neurobiological correlates of LC volume loss in AD that do not involve immediate cell death. One animal study modelled early AD pathophysiological processes using TgF344-AD rats, which express elevated hyperphosphorylated tau in the LC compared to wild type rodents but without frank noradrenergic cell loss. They found that hyperphosphorylated tau in the LC is associated with reduced innervation of the medial temporal region, even in the absence of loss of noradrenergic cells in the LC [7]. These results suggest that the axonal integrity of LC projections is compromised in the presence of emerging AD pathology before LC cell death. Additionally, autopsy studies have revealed reduced dendritic arborization of LC neurons in more advanced AD [8], presenting another potential substrate of LC volume loss without explicit cell death. These early processes of LC deterioration remain poorly investigated in humans in vivo.

To investigate the LC in vivo, LC-sensitive magnetic resonance (MRI) sequences, such as magnetization transfer (MT) and turbo spin echo scans, have been developed, and these have proven to be successful at imaging the LC at ultra-high resolution in humans [9, 10]. The LC-related signal intensity in these scans is generally regarded as an informative proxy for LC integrity [9, 11, 12]; however, it is unclear to what degree the LC signal reflects specific microstructural properties of the LC. One of the leading theories is that the signal is related to neuromelanin, a compound that is abundantly deposited in the LC as a byproduct of elevated noradrenalin metabolism [11-13]. This hypothesis was supported by the fact that the substantia nigra also show as hyperintense regions on MT-weighted scans, and also contain neuromelanin cells [12, 14]. However, recent animal work and MRI-modeling studies indicated that the underlying biological source may be more complex and may be related to neuronal density [15], lipids, iron and tau depositions [16, 17].

Given the early changes to the neuropil of LC neurons, we aimed to examine correlations between LC integrity and microstructural characteristics of the LC and

its projections as measured by neurite orientation dispersion and density imaging (NODDI) and diffusion imaging. NODDI is able to quantify the microstructural characteristics of dendrites and axons, utilizing information about neurite density and the variation in neurite orientation as a measure of neurite complexity and the degree of neuronal arborization [18]. This information will facilitate our interpretation of the LC signal in aging and in neurodegenerative diseases, potentially before irreversible cell death.

METHODS

Participants

We included 58 cognitively unimpaired participants across the adult lifespan recruited in the South-East region of the Netherlands (age range: 30-85). Exclusion criteria were MRI contraindications, major neurological disease, clinical diagnoses of neurodegenerative disorders or abnormal cognitive scores deviating ±2 standard deviations from the norm, transient ischemic attack or stroke, current or past presence of severe psychiatric disorders and alcohol or drug abuse. All participants provided informed consent and protocols were approved by the local Medical Ethics Committee of the Maastricht University Medical Center.

Imaging equipment and acquisition

Imaging data were acquired using a MAGNETOM 7.0T whole-body MR system release 2.0 (Siemen Healthineers, Erlangen, Germany) with a 32-channel head coil (Nova Medical, Wilmington, MA, USA). Dielectric pads were placed at the temples during scanning to improve signal around the temporal areas. Whole-brain structural T1-weighted data were acquired in sagittal orientation using a Magnetization Prepared 2 Rapid Acquisition Gradient Echoes (MP2RAGE) sequence [19] for whole brain imaging (TR = 5000 ms, TE = 2.47 ms, flip angle = 5°/3°, voxel size = 0.7mm isotropic, number of slices = 280). An in-house developed magnetization transfer turbo flash (MT-TFL) sequence sensitive to LC contrast [9] was performed to image the LC at high resolution. The sequence consisted of a multi-shot 3D readout (TR = 538 ms, TE = 4.08, flip angle = 8°, voxel size = 0.4×0.4×0.5 mm^3, number of slices = 60) with center-out k-space sampling, preceded by 20 long off-resonant Gaussian sinc pulses. The field of view for the MT-TFL sequence was placed perpendicular to the pons, between the inferior colliculus and the caudal border of the pons. High angular resolution diffusion data were acquired (TR = 5000 ms, TE = 60.8 ms, flip angle = 90°, voxel size = 1.25mm

isotropic, number of slices = 72) at b=2000 s/mm^2 (66 gradient directions), b=700 s/mm^2 (35 gradient directions) and b=0 s/mm^2 (6 gradient directions). The diffusion-weighted sequence was a near whole-brain acquisition whereby only the most dorsal section of the parietal lobe was excluded from the field of view.

Image pre-processing

Using FSL's TOPUP and EDDY functions, diffusion-weighted images were corrected for susceptibility- and eddy current-induced distortions, subject movement, and gradient nonlinearities [20-23].

NODDI analysis (local LC microstructure)

Intensity-normalized MT-TFL images were obtained by dividing individual images by the subject-specific mean intensity of a 10 by 10 voxel region-of-interest located in the pontine tegmentum. A study-specific template was built based on all individual intensity-normalized MT-TFL images as described in detail in our previous work [24]. The LC was manually delineated on the resulting template in the common space, based on voxel intensities and the known LC anatomy. The individual MP2RAGE image was registered to the corresponding mean diffusion-weighted b0 volume using Statistical Parametric Mapping 12 (SPM12, http://www.fil.ion.ucl.ac.uk/spm/). The resulting transformation matrices were subsequently applied to the MT-TFL image, resliced to MP2RAGE resolution using *bbregister* from FreeSurfer v6.0 [25]. This allowed us to align the MT-TFL data, along with the previously created LC mask, to each individual diffusion space. Whole-brain NODDI parameter maps containing the neurite density index (NDI) and orientation dispersion index (ODI) were then computed using the Microstructure Diffusion Toolbox [26] (v1.2.6, https://github.com/robbert-harms/MDT). Both NDI and ODI are expressed as a value between 0 (NDI: mostly extracellular diffusion, e.g. low neurite density; ODI: parallel neurites, e.g. low arborization) and 1 (NDI: mostly intracellular diffusion, e.g. high neurite density; ODI: highly dispersed neurites, e.g. high arborization) [27]. To obtain local LC microstructure and MT signal data, we extracted the median NDI, ODI and MT-TFL intensity values from each slice of the LC mask using MATLAB and these were subsequently exported to R version 4.0.4. (https://www.r-project.org/).

Correlational tractography (LC projection microstructure)

For group-level correlational tractography of the LC projections, an LC mask in the MNI space was created using the following pipeline: for each individual in the

sample, we first retrieved the affine and non-linear registration matrices linking the template MT-TFL space to the native MT-TFL image, based on the study-specific LC mask creation procedure as described above. Next, for each participant, the individual MP2RAGE image was first denoised using the MP2RAGE toolbox (https://github.com/benoitberanger/mp2rage/, regularization factor = 5) implemented in SPM in MATLAB R2021b, and bias-field corrected using the *N4BiasFieldCorrection* function in ANTs. The denoised and bias-field corrected MP2RAGE image was then segmented using the Computational Anatomy Toolbox 12 (https://neuro-jena.github.io/cat/, expert-mode segmentation) in SPM12 to extract the brain while minimizing the potential presence of residual skull/meninges. The brain-extracted, denoised, and bias-field corrected MP2RAGE images were subsequently registered to the standard MNI152 brain (1mm) through a combination of linear and non-linear warping using the *AntsRegistration* function in ANTs. For each participant, all the transformation matrices generated across the different registrations described above were applied to our study-specific LC mask in a unified step using the *AntsApplyTransforms* function in ANTs. Finally, the individual LC masks in the MNI space were averaged, and the resulting average LC mask in the MNI space was thresholded at 0.20 and binarized to be used in the tractography analyses.

Correlation tractography was performed in DSI studio software [28] (Version 2021.12.03 "Chen"). Using DSI studio built-in functions, pre-processed diffusion-weighted images were co-registered into a connectometry database in the MNI space to enable tractography using standardized anatomical coordinates, Quantitative anisotropy (QA) was extracted and used as the outcome variable in the correlational tractography analysis. QA is a measure of the density of anisotropic diffusing water and reduced QA is thought to reflect axonal injury and degeneration [29, 30]. QA takes into account the amount of anisotropic spins that diffuse along each principal diffusion direction and is therefore less sensitive to partial volume effects introduced by crossing fibers than fractional anisotropy [31]. The seeding regions used for the tractography analysis were the separate left and right MT-TFL-based LC masks, registered to MNI space. The LC seed region? had a volume size of 25mm cubic for the right LC and 29mm cubic for the left LC (supplementary Figure 1B). The default T-score threshold of 2.5 was used for the deterministic fiber tracking algorithm [32] and tracts with a false discovery rate (FDR) value below 0.20 are reported as recommended by DSI studio guidelines (https://dsi-studio.labsolver.org/doc/gui_cx.html). The QA values were normalized so that the maximum QA of a subject is 1 and the tracts were filtered by topology-informed pruning [33] with 4 iterations, with a minimum length threshold of 20 voxels. To estimate the FDR, a total of 4000 randomized permutations were applied.

Statistical analyses

For the NODDI data, multiple linear regression models were constructed in R after extraction of NDI, ODI and MT-TFL intensity values. LC intensity was entered as the dependent variable, while age, sex, years of education, and apolipoprotein (APOE) ε4 allele presence were included as covariates with either NDI or ODI values as the independent variable of interest. These analyses were carried out bilaterally in the entire LC, as well as in three equidistant subsections of the LC along the rostrocaudal axis, as previously suggested [24]. These sections were created by dividing all slices both left and right LC into three contiguous parts and averaging the MT-TFL, NDI and ODI values obtained from the slices in these sections.

During correlational tractography, QA was correlated with an average of the median normalized LC intensity values in MT-TFL data, using a nonparametric Spearman partial correlation including age, years of education, APOE ε4 allele presence and sex as covariates.

RESULTS

Demographics

From the full dataset described in table 1, 11 participants were excluded from the final ROI-based analyses due to low quality of the LC mask registrations, resulting in a final sample size of 47. In DSI studio, 3 participants were removed due to corrupted data and/or poor registration to the standard space, resulting in a final set of 55 participants included for the correlational tractography analyses.

NODDI results

Figure 1 displays the LC mask used in the NODDI analyses and 3D surface renders of the LC mask can be found in Supplementary Figure 1. We found no associations between MT-weighted signal and NDI (standardized β = -0.040, t(37)= -0.255, p = 0.800) or ODI (standardized β = -0.140, t(37) = -0.932, p = 0.357) in the entire LC. Similarly, no associations were found for the left (NDI: standardized β = 0.010, t(37) = 0.100, p = 0.921; ODI: standardized β = 0.030, t(37) = 0.176, p = 0.861) and right (NDI: standardized β = 0.030, t(37) = 0.147, p = 0.884; ODI: standardized β = -0.180, t(37) = -1.168, p = 0.250) LC. While investigating three equidistant subsections of the left and right LC we again did not find any significant associations (Figure 2).

Table 1. Sample demographics.

	Whole sample	NODDI sample	Tractography sample
N	58	48	55
Age	59.52 ± 14.30 years	60.17 ± 13.70 years	59.40 ± 14.45 years
Sex	27 males (47%)	20 males (42%)	25 males (45%)
Education	14.43 ± 2.23 years	14.40 ± 2.17 years	14.38 ± 2.28 years
APOE ε4	12 (21%)	8 (17%)	11 (20%)
MT-TFL	0.15 ± 0.05	0.15 ± 0.03	0.15 ± 0.05
NDI	0.64 ± 0.09	0.63 ± 0.06	0.65 ± 0.09
ODI	0.09 ± 0.06	0.08 ± 0.03	0.09 ± 0.06

Note. Demographic details of the study sample. Numeric variables are expressed as mean ± standard deviation, while categorical variables are expressed as frequency (percentage of N). The APOE ε4 variable represents the number of subjects with at least one APOE ε4 allele, while MT-TFL, NDI and ODI values represent the average of the median intensity values in the entire bilateral LC. Using student's T-test for numeric variables and chi-squared test for categorical variables, we found no significant differences between the NODDI and tractography samples for any of the variables (age: p = 0.784; sex: p = 0.925; education: p = 0.960; APOE ε4 allele: p = 0.897, MT-TFL: p = 0.374; NDI: p = 0.337; ODI: p = 0.200)

Figure 1. Locus coeruleus mask used in NODDI analyses.

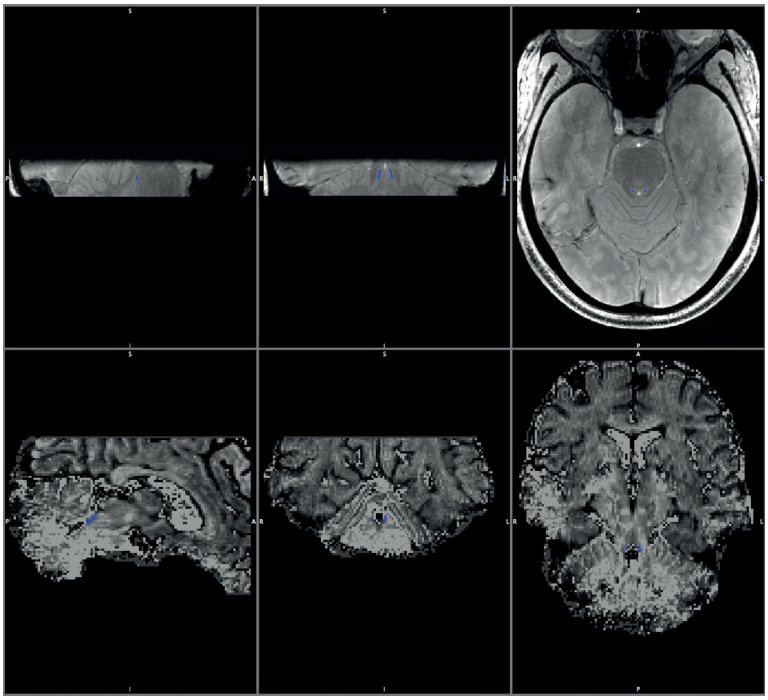

Note. Locus Coeruleus Mask is visualized in the blue ROI in the individual MT-TFL (top) and NDI map (bottom) images. Orientations are given on the edges of the images (A=anterior; I=inferior; L=left; P=posterior; R=right, S=superior).

Figure 2. Associations between magnetization transfer-weighted signal intensity and neurite density index values.

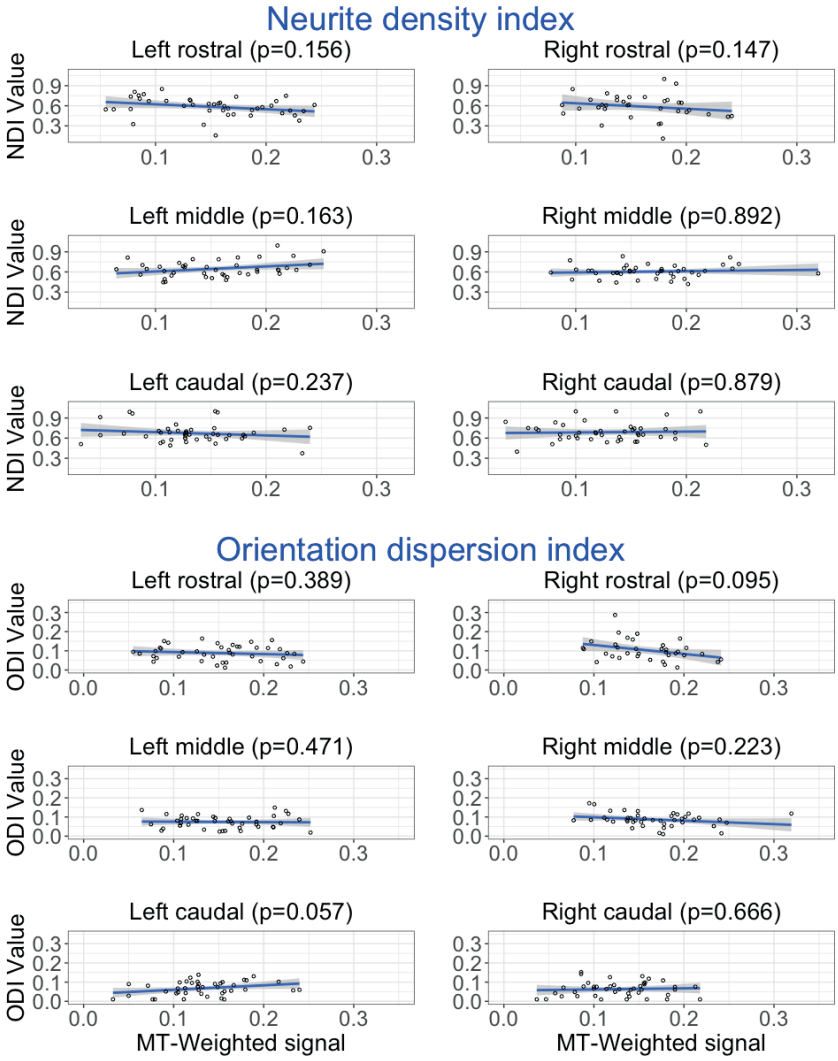

Note. Interpretation of y-axes: NDI (0 = mostly extracellular diffusion, 1 = mostly intracellular diffusion; ODI (0 = strongly aligned neurites, 1 = highly dispersed neurites).

Tractography results

Tractography results are visualized in Figure 3. For the left LC we found no associations between mean MT-TFL intensity and QA. For the right LC we found positive associations for the left and right dentatorubrothalamic tract, the superior cerebellar peduncle and the right reticular tract (FDR=0.167).

Figure 3. Associations between MT-weighted LC signal and QA in tracts originating from the LC.

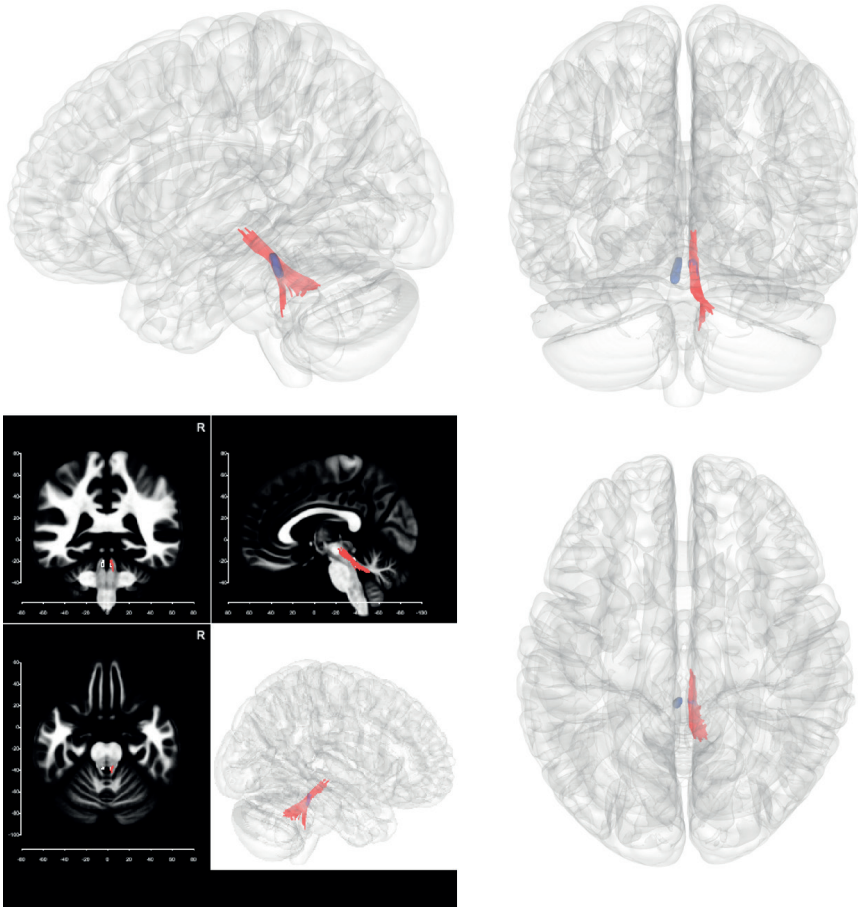

Note. Tracts where quantitative anisotropy was associated with MT-weighted LC signal are visualized in 3D surfaces based on the MNI ICBM-152 brain template. Tracts showing a positive association between MT-weighted LC signal and QA are visualized in red and the left and right LC seeding regions are visualized in blue.

DISCUSSION

The LC is one of the first brain regions involved in the early stages of the AD pathophysiological process and is characterized by volume loss as early as Braak stage a-c [3, 4, 6, 16, 34, 35]. While the MT-weighted LC signal has been established as a proxy for LC integrity [9, 11, 12], the microstructural correlates of the LC signal remain a topic of debate. Thus, in the present study, we aimed to elucidate the microstructural correlates of LC integrity measured in vivo, by probing the association between LC integrity and local measures of neurite density and arborization, while also investigating its association with axonal integrity of the LC projections. Here, we provide in vivo evidence suggesting that LC integrity is associated with the axonal integrity of LC projections, while local measures of neurite density and arborization in the LC itself do not appear to be associated. These results contribute to our understanding of the MT-TFL signal and associated microstructural characteristics of the LC, which may ultimately aid in developing intervention strategies in the earliest stages of LC deterioration.

We found no evidence for an association between LC integrity and NDI and ODI in the LC and its subsections in our cognitively normal subjects. This suggests that early LC degeneration may not be associated with reduced neurite density or arborization within the LC. Rather, our correlational tractography results suggest that the projections from the LC are affected in the early process of LC degeneration. Specifically, the loss of QA in these tracts indicates that lower LC integrity is associated with reduced axonal integrity in projections from the LC. These findings support previous evidence suggesting reduced integrity of tracts originating from the LC in early AD, during a time in life where LC cell death is less likely [7, 36]. This is in line with the previously reported selective vulnerability of LC axons to neurodegeneration. These axons are long, thin and poorly myelinated [37, 38], and may therefore be the first component of the LC system to falter in the presence of neuronal challenges, such as AD pathology. Finally, previous findings from our group report that elevated noradrenaline metabolites are associated with neurodegeneration in target sites of the LC at subthreshold levels of AD pathology, further suggesting an important role for LC projections in the early neurodegenerative processes of AD [39].

In particular, QA in the right reticular tract, left and right dentatorubrothalamic tracts as well as the superior cerebellar peduncles (SCP) show positive correlations with MT-weighted LC signal intensity. These tracts project not only from the

LC towards the thalamus, but also towards the cerebellum. They are part of a feedback-feedforward loop connecting the pons (including the locus coeruleus) to the cerebellum and from the cerebellum to the thalamus and cortex, from which connections return to the pons. Moreover, this cortico-ponto-cerebellar link serves a modulating role in cognition [40-44].

Specifically, the SCP are part of the principal white matter tracts that connect the cerebellum to the rest of the central nervous system. Moreover, they receive afferent noradrenergic projections from the LC and carry them towards the cerebellum [41]. Our finding showing that reduced LC integrity is associated with reduced structural integrity of the SCP is supported by previous work reporting reduced fractional anisotropy and increased mean diffusivity in the SCP in AD compared to healthy controls [45]. Additionally, the dentatorubrothalamic tract is a long tract connecting the cerebellar dentate nucleus to the thalamus [46]. The dentate nucleus is involved in memory processes, and altered functional connectivity between the dentate nucleus and cerebral regions has been reported in AD compared to healthy controls [47]. Finally, the reticular tract is part of the reticular activating system (RAS), which the LC also belongs to. The RAS has projections to the thalamus and cortex and is crucial in arousal and attention functions [48]. Indeed, arousal dysregulation and sleep-wake disturbances have been widely reported in the early phases of AD [49, 50], and LC integrity has previously been shown to be associated with nocturnal awakenings [24], suggesting that axonal degeneration of the reticular system may be involved in these behavioral symptoms.

Limitations and future directions

Our sample size in the NODDI analyses was reduced due to sub-par registrations of the LC mask in 11 participants. The LC is a small and difficult to image region, and to ensure robust analyses, we opted for strict quality assessments. Our sample size was moderate, which could account for some of the null-findings between neurite density and arborization and MT signal at the local LC level. Future research with larger cohorts is needed to replicate these analyses and provide more definitive information.

Furthermore, DWI is inherently limited by its spatial resolution, warranting careful interpretation of this data. We do want to emphasize that we acquired

the data at 7T, allowing us to push the resolution to 1.25mm up from the typical 2-3mm. Moreover, anatomical identification of the LC was facilitated by our unique dataset containing ultra-high-resolution MT-weighted data.

Finally, our sample only included healthy individuals and no impaired individuals. The inclusion of patients with varying degrees of AD would give us valuable insights into the microstructural properties of the LC in the different phases of AD, and may answer questions about how microstructural properties of the LC and its projections are affected in more severe stages of the disease.

Conclusions

In conclusion, in vivo MRI measures of LC integrity appear to be associated with integrity of LC projections, rather than local measures of arborization or neurite density in a cognitively normal population. These findings are important for early detection of changes in the LC and understanding the microstructural processes associated with these changes. Longitudinal research may investigate microstructural changes of the LC and its projections alongside changes in function and metabolism in order to gain a deeper understanding of the temporal ordering of these processes. In addition, future research will need to investigate whether these findings can be extended to patient populations with varying degrees of AD pathology.

REFERENCES:

1. Samuels, E.R. and E. Szabadi, *Functional neuroanatomy of the noradrenergic locus coeruleus: its roles in the regulation of arousal and autonomic function part I: principles of functional organisation.* Current neuropharmacology, 2008. **6**(3): p. 235-253.
2. Holland, N., T.W. Robbins, and J.B. Rowe, *The role of noradrenaline in cognition and cognitive disorders.* Brain, 2021. **144**(8): p. 2243-2256.
3. Braak, H. and E. Braak, *Neuropathological stageing of Alzheimer-related changes.* Acta Neuropathologica, 1991. **82**(4): p. 239-259.
4. Braak, H., et al., *Stages of the Pathologic Process in Alzheimer Disease: Age Categories From 1 to 100 Years.* Journal of Neuropathology & Experimental Neurology, 2011. **70**(11): p. 960-969.
5. Kelly, S.C., et al., *Locus coeruleus cellular and molecular pathology during the progression of Alzheimer's disease.* Acta Neuropathologica Communications, 2017. **5**(1): p. 8.
6. Theofilas, P., et al., *Locus coeruleus volume and cell population changes during Alzheimer's disease progression: A stereological study in human postmortem brains with potential implication for early-stage biomarker discovery.* Alzheimer's & Dementia, 2017. **13**(3): p. 236-246.
7. Rorabaugh, J.M., et al., *Chemogenetic locus coeruleus activation restores reversal learning in a rat model of Alzheimer's disease.* Brain, 2017. **140**(11): p. 3023-3038.
8. Chan-Palay, V. and E. Asan, *Alterations in catecholamine neurons of the locus coeruleus in senile dementia of the Alzheimer type and in Parkinson's disease with and without dementia and depression.* Journal of Comparative Neurology, 1989. **287**(3): p. 373-392.
9. Priovoulos, N., et al., *High-resolution in vivo imaging of human locus coeruleus by magnetization transfer MRI at 3T and 7T.* NeuroImage, 2018. **168**: p. 427-436.
10. Betts, M.J., et al., *Locus coeruleus imaging as a biomarker for noradrenergic dysfunction in neurodegenerative diseases.* Brain, 2019. **142**(9): p. 2558-2571.
11. Keren, N.I., et al., *Histologic validation of locus coeruleus MRI contrast in post-mortem tissue.* NeuroImage, 2015. **113**: p. 235-245.
12. Sasaki, M., et al., *Neuromelanin magnetic resonance imaging of locus ceruleus and substantia nigra in Parkinson's disease.* NeuroReport, 2006. **17**(11).
13. Trujillo, P., et al., *Quantitative magnetization transfer imaging of the human locus coeruleus.* NeuroImage, 2019. **200**: p. 191-198.
14. Kitao, S., et al., *Correlation between pathology and neuromelanin MR imaging in Parkinson's disease and dementia with Lewy bodies.* Neuroradiology, 2013. **55**(8): p. 947-953.
15. Watanabe, T., et al., *Magnetic resonance imaging of brain cell water.* Scientific Reports, 2019. **9**(1): p. 5084.
16. Jacobs, H.I.L., et al., *In vivo and neuropathology data support locus coeruleus integrity as indicator of Alzheimer's disease pathology and cognitive decline.* Science Translational Medicine, 2021. **13**(612): p. eabj2511.
17. Priovoulos, N., et al., *Unraveling the contributions to the neuromelanin-MRI contrast.* Brain Structure and Function, 2020. **225**(9): p. 2757-2774.
18. Zhang, H., et al., *NODDI: practical in vivo neurite orientation dispersion and density imaging of the human brain.* Neuroimage, 2012. **61**(4): p. 1000-1016.

19. Marques, J.P., et al., *MP2RAGE, a self bias-field corrected sequence for improved segmentation and T1-mapping at high field.* NeuroImage, 2010. **49**(2): p. 1271-1281.
20. Andersson, J.L.R. and S.N. Sotiropoulos, *An integrated approach to correction for off-resonance effects and subject movement in diffusion MR imaging.* Neuroimage, 2016. **125**: p. 1063-1078.
21. Andersson, J.L., S. Skare, and J. Ashburner, *How to correct susceptibility distortions in spin-echo echo-planar images: application to diffusion tensor imaging.* Neuroimage, 2003. **20**(2): p. 870-88.
22. Smith, S.M., et al., *Advances in functional and structural MR image analysis and implementation as FSL.* Neuroimage, 2004. **23 Suppl 1**: p. S208-19.
23. Jenkinson, M., et al., *FSL.* NeuroImage, 2012. **62**(2): p. 782-790.
24. Van Egroo, M., R.W.E. van Hooren, and H.I.L. Jacobs, *Associations between locus coeruleus integrity and nocturnal awakenings in the context of Alzheimer's disease plasma biomarkers: a 7T MRI study.* Alzheimer's Research & Therapy, 2021. **13**(1): p. 159.
25. Fischl, B., *FreeSurfer.* Neuroimage, 2012. **62**(2): p. 774-781.
26. Harms, R.L., et al., *Robust and fast nonlinear optimization of diffusion MRI microstructure models.* NeuroImage, 2017. **155**: p. 82-96.
27. Gatto, R.G., et al., *Neurite orientation dispersion and density imaging can detect presymptomatic axonal degeneration in the spinal cord of ALS mice.* Funct Neurol, 2018. **33**(3): p. 155-163.
28. Yeh, F.-C., D. Badre, and T. Verstynen, *Connectometry: A statistical approach harnessing the analytical potential of the local connectome.* NeuroImage, 2016. **125**: p. 162-171.
29. Shen, C.-Y., et al., *Quantitative Evaluation of Rabbit Brain Injury after Cerebral Hemisphere Radiation Exposure Using Generalized q-Sampling Imaging.* PLOS ONE, 2015. **10**(7): p. e0133001.
30. Yeh, F.-C., et al., *Differential tractography as a track-based biomarker for neuronal injury.* NeuroImage, 2019. **202**: p. 116131.
31. Yeh, F.-C., et al., *Deterministic Diffusion Fiber Tracking Improved by Quantitative Anisotropy.* PLOS ONE, 2013. **8**(11): p. e80713.
32. Yeh, F.C., et al., *Deterministic diffusion fiber tracking improved by quantitative anisotropy.* PLoS One, 2013. **8**(11): p. e80713.
33. Yeh, F.-C., et al., *Automatic Removal of False Connections in Diffusion MRI Tractography Using Topology-Informed Pruning (TIP).* Neurotherapeutics, 2019. **16**(1): p. 52-58.
34. Hämmerer, D., et al., *Locus coeruleus integrity in old age is selectively related to memories linked with salient negative events.* Proceedings of the National Academy of Sciences, 2018. **115**(9): p. 2228-2233.
35. Jacobs, H.I.L., et al., *Relevance of parahippocampal-locus coeruleus connectivity to memory in early dementia.* Neurobiology of Aging, 2015. **36**(2): p. 618-626.
36. Chu, W.T., et al., *Association of Cognitive Impairment With Free Water in the Nucleus Basalis of Meynert and Locus Coeruleus to Transentorhinal Cortex Tract.* Neurology, 2022. **98**(7): p. e700-e710.
37. Theofilas, P., et al., *Turning on the Light Within: Subcortical Nuclei of the Isodentritic Core and their Role in Alzheimer's Disease Pathogenesis.* Journal of Alzheimer's Disease, 2015. **46**: p. 17-34.

38. Matchett, B.J., et al., *The mechanistic link between selective vulnerability of the locus coeruleus and neurodegeneration in Alzheimer's disease.* Acta Neuropathologica, 2021. **141**(5): p. 631-650.
39. van Hooren, R.W.E., et al., *Elevated norepinephrine metabolism is linked to cortical thickness in the context of Alzheimer's disease pathology.* Neurobiology of Aging, 2021. **102**: p. 17-22.
40. Schmahmann, J.D., *From movement to thought: Anatomic substrates of the cerebellar contribution to cognitive processing.* Human Brain Mapping, 1996. **4**(3): p. 174-198.
41. Goodlett, C.R. and G. Mittleman, *Chapter 9 - The Cerebellum*, in *Conn's Translational Neuroscience*, P.M. Conn, Editor. 2017, Academic Press: San Diego. p. 191-212.
42. Berridge, C.W. and B.D. Waterhouse, *The locus coeruleus–noradrenergic system: modulation of behavioral state and state-dependent cognitive processes.* Brain Research Reviews, 2003. **42**(1): p. 33-84.
43. Jacobs, H.I.L., et al., *The cerebellum in Alzheimer's disease: evaluating its role in cognitive decline.* Brain, 2017. **141**(1): p. 37-47.
44. Sara, S.J., *The locus coeruleus and noradrenergic modulation of cognition.* Nature Reviews Neuroscience, 2009. **10**(3): p. 211-223.
45. Toniolo, S., et al., *Cerebellar White Matter Disruption in Alzheimer's Disease Patients: A Diffusion Tensor Imaging Study.* Journal of Alzheimer's Disease, 2020. **74**: p. 615-624.
46. Ou, S.-Q., et al., *Delineating the Decussating Dentato-rubro-thalamic Tract and Its Connections in Humans Using Diffusion Spectrum Imaging Techniques.* The Cerebellum, 2022. **21**(1): p. 101-115.
47. Olivito, G., et al., *Cerebellar dentate nucleus functional connectivity with cerebral cortex in Alzheimer's disease and memory: a seed-based approach.* Neurobiology of Aging, 2020. **89**: p. 32-40.
48. Giorgi, F.S., et al., *The Neuroanatomy of the Reticular Nucleus Locus Coeruleus in Alzheimer's Disease.* Frontiers in Neuroanatomy, 2017. **11**.
49. Lim, M.M., J.R. Gerstner, and D.M. Holtzman, *The sleep–wake cycle and Alzheimer's disease: what do we know?* Neurodegenerative Disease Management, 2014. **4**(5): p. 351-362.
50. Bubu, O.M., et al., *Sleep, Cognitive impairment, and Alzheimer's disease: A Systematic Review and Meta-Analysis.* Sleep, 2016. **40**(1).

SUPPLEMENTARY MATERIAL

Supplementary Figure 1. 3D Surface render of the LC mask used in NODDI analyses.

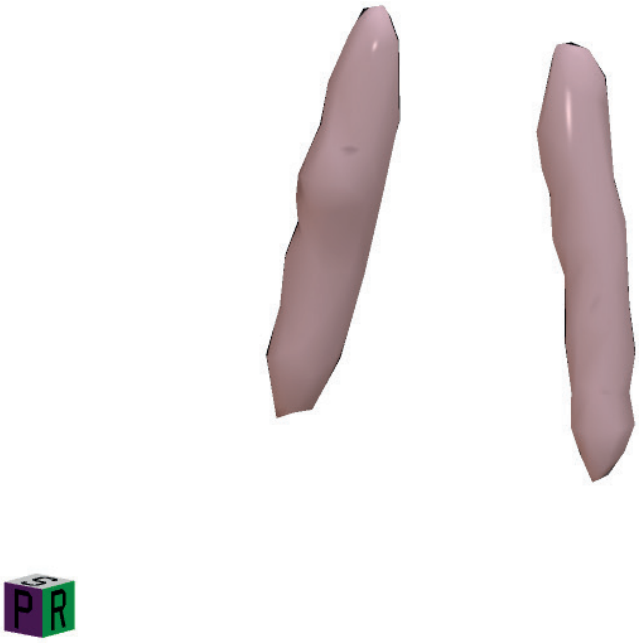

Note. The bilateral LC mask used in the NODDI analyses is displayed with the orientation visualized by the cube in the bottom left (S=superior (rostral); P=posterior (caudal); R=right). This 3D surface render was created with surfice software (https://www.nitrc.org/projects/surfice/).

VALIDITY AND RELIABILITY OF TEMPLATE-BASED AND MANUAL SEGMENTATION APPROACHES OF THE LOCUS COERULEUS IN VIVO AT 7T

CHAPTER 5

In prep

Roy W.E. van Hooren
Maxime van Egroo
Joost M. Riphagen
Frans R.J. Verhey
Heidi I.L. Jacobs

ABSTRACT

Introduction: The brainstem locus coeruleus (LC) is one of the first brain regions to accumulate Alzheimer's disease-related hyperphosphorylated tau pathology, making the integrity of the LC a promising early marker for Alzheimer's disease. However, imaging the structural properties of the locus coeruleus in vivo is challenging, therefore we aim to compare three different approaches for delineating the LC in vivo.

Methods: The study sample consisted of 144 cognitively healthy participants ranging from 30-87 years old who underwent ultra high-resolution MRI scanning at 7T. T1-Weighted data were obtained along with a magnetization transfer turbo flash sequence sensitive to locus coeruleus-related contrast. We compared bilateral univariate- and multivariate-guided template-based segmentations as well as manual segmentations of the locus coeruleus.

Results: We found excellent reliability metrics for the univariate template approach, mixed reliability measures for the multivariate template, and notably worse reliability statistics for the manual approach. Using nonlinear mixed-effects models, we found higher LC intensity in the caudal part of the LC compared to the more rostral sections in the left univariate template approach and the bilateral manual approach, whereas we found the higher LC intensity towards the rostral sections in the multivariate approach. Finally, we found that in the left univariate template more rostral sections displayed lower intensity with higher age compared to other sections. Both the right univariate and right manual delineations show an inverted U-curve pattern for LC intensity with age for the caudal section compared to other sections.

Discussion: We conclude that univariate, study-specific template approaches are likely an accurate tool for in vivo LC delineation. A complete manual approach is the less desired method if refined and accurate template approaches are an available alternative.

INTRODUCTION

The brainstem locus coeruleus (LC) has widespread noradrenergic connections to the entire brain, supporting its modulating role in cognition and arousal [1, 2]. It is one of the first brain regions to accumulate Alzheimer's disease (AD)-related hyperphosphorylated tau early in life [3, 4], and although this tau accumulation does not necessarily lead to LC cell death in the initial stages of the disease, post-mortem studies have shown that tau buildup is associated with morphological changes that manifest as LC volume loss as early as Braak stage 0 [5]. These observations have inspired a push for in vivo MRI studies of the LC to obtain an early marker of AD-related processes.

Investigating the LC in vivo is challenging due to its size and location. The LC is a small nucleus in the brainstem consisting of approximately 75,000 neurons in healthy individuals, a large portion of which are noradrenergic neuromelanin cells [6, 7]. It is bilaterally positioned along the length of the pons, bordering the medial edge of the fourth ventricle, and is on average approximately 2.5mm thick and 14.5mm in length [8]. Recent developments in ultra-high field MRI by our group now provide detailed structural images of the LC in vivo using the contrast provided by the magnetization transfer turbo flash (MT-TFL) sequence [9, 10]. The biological source driving this contrast is still unclear, but is thought to be related, directly or indirectly, to neuromelanin cell density. Indirect contributions may be related to iron or possibly also tau-related inclusion [11].

Varying biological contributions to this contrast during life may explain the different age-relationships with MRI signal intensity reported in various in vivo MRI LC studies. Using 7T MRI and following a template-based approach, Jacobs and colleagues reported an age-related inverted-U curve with LC intensity across the entire LC [11]. Furthermore, using a template-based approach at 3T, Liu and colleagues reported an age-related inverted-U curve with rostral LC intensity, and an overall larger variance of LC signal intensity in older compared to younger adults (N=708, age range: 18-88) [12]. However, using the 7T MT-TFL sequence and a template-based method to identify the LC, Ye et al. (2021) reported the highest signal intensity in the rostral and middle sections of the LC, but they did not detect an association between age and signal intensity (n=56, age range: 52-84) [13]. Similarly, Betts et al. (2017) also observed the highest LC signal intensity in the rostral section of the LC but, contradictory to Liu and colleagues, they found an age-related LC signal increase when investigating maximum, but not median LC signal intensity

[14]. Finally, a manual LC delineation approach was applied to 3T MRI data by Shibata and colleagues (2006), who reported age-related inverted-U curve patterns with intensity in the entire LC [15]. Altogether, these findings highlight the heterogenous and region-specific nature of age-related changes in the LC. It remains unknown, however, to what extent these discrepancies may be due to different segmentation methods of the LC, restricted age-ranges, and/or sample sizes.

To better understand the impact of various methodologies in defining the LC and its age-relationships, we compared three different methods of delineating the LC in vivo across the entire adult lifespan using dedicated high-resolution 7T imaging. We compared manual bilateral delineation of the LC, 2univariate-, and multivariate-guided template-based segmentations of the LC.

METHODS

Participants

We included 144 cognitively unimpaired participants across the adult lifespan recruited in the South-East region of the Netherlands (age range: 30-87). Exclusion criteria were MRI contraindications, major neurological disease, clinical diagnoses of neurodegenerative disorders, transient ischemic attack or stroke, current or past presence of severe psychiatric disorders, and alcohol or drug abuse. All participants provided informed consent and protocols were approved by the local Medical Ethics Committee of the Maastricht University Medical Center.

Imaging equipment and acquisition

Imaging data were acquired using a MAGNETOM 7.0T whole-body MR system release 2.0 (Siemens Healthineers, Erlangen, Germany) with a 32-channel head coil (Nova Medical, Wilmington, MA, USA). Dielectric pads were positioned at the temples during scanning to improve signal around the temporal areas. Whole-brain structural T1-weighted data were acquired in sagittal orientation using a Magnetization Prepared 2 Rapid Acquisition Gradient Echoes (MP2RAGE) sequence [16] for whole brain imaging (TR=5000 ms, TE=2.47 ms, flip angle=5°/3°, voxel size=0.7mm isotropic, number of slices=280).

An in-house developed MT-TFL sequence sensitive to LC contrast [9] was performed to image the LC at high resolution. The sequence consisted of a multi-shot 3D readout (TR=538 ms, TE=4.08, flip angle=8°, voxel size=0.4×0.4×0.5 mm^3,

number of slices=60) with center-out k-space sampling, preceded by 20 long off-resonant Gaussian sinc pulses. The field of view for the MT-TFL sequence was placed approximately perpendicular to the pons, covering an area between the inferior colliculus and the caudal border of the pons. A matched TFL sequence but with the MT pulses turned off (MT-off) was also acquired.

Template construction and other LC delineation methods

Univariate template

A univariate method for constructing an MT-weighted template was created using the *buildtemplateparallel* function from the ANTs software package [17]. This method minimizes the number of interpolations performed during template construction and builds the template in a single step using only the MT-TFL images. Processing steps include the creation of an initial template built using a single rigid registration which forms the reference template for a more advanced diffeomorphic template creation process using the greedy SyN method with 30,000 iterations (30 coarse x 50 middle x 20 fine). This univariate template exists in a template-specific space, and data were N4 bias-corrected using the *N4BiasFieldCorrection* function.

Multivariate template

The multivariate template approach involves a series of registrations using the *antsRegistration* and *antsApplyTransforms* functions. In the following order, the template construction steps consisted of an initial rigid alignment of the individual MT-TFL images, followed by N4 bias correction of all images using the *N4BiasFieldCorrection* function. Subsequently, a linear registration of the individual MT-off images to the corresponding aligned MT-TFL images was performed. This was followed by a linear registration of the MT-off image to the corresponding skull-stripped T1 image (FreeSurfer V6.0) [18]. Next, a diffeomorphic T1-based template was created with the *antsMultivariateTemplateConstruction2* function using the greedy SyN method with 7 million iterations (100x70 coarse x 50 middle x 20 fine), and the resulting template was then registered to the MNI152 space using a greedy SyN transformation. All warp files created during this entire process were then used to warp the individual MT-TFL images into MNI152 space in one unified step. An average of these images was then generated using the FSL 6.0 [19] *fslmaths* function to obtain the final template. This approach is similar to the

method described by Ye et al. (2021) [13]. On both the multivariate and univariate templates, four independent LC raters outlined the LC manually (RWEvH, MVE, JMR & HILJ) and all voxels that showed unanimous overlap comprised the final bilateral LC mask for each respective template.

Validation of univariate and multivariate templates

For the purpose of validating the template methods, our data was separated into a training and validation set, and a participant could only be present in one set. The split was set 70% for the training set and 30% for the validation set with similar age distributions across both sets. Our final template from the training data was warped to the individual MT-weighted images by using an affine registration, and we then applied the resulting transform file to warp the template LC mask to the individual native space for each subject in the validation training set. Subsequently, we extracted the intensity values of the left and right LC and compared the patterns of the intensity values across age and across the length of the LC with those obtained in our training data.

Manual delineation

We also performed manual delineation of the LC in all individual MT-TFL images. Using fslview software, all MT-TFL data were examined and the left and right LC were outlined for each participant (RWEvH). Delineations were based on image intensity and previously established anatomy of the LC [14]. Brightness and contrast settings in fslview were set for each individual image to obtain the optimal identification of the LC. This process was done twice in random order with 4 weeks in between delineations to reduce temporal effects and obtain an unbiased identification of the LC. The average intensity between the two rating sessions was used for further analyses.

LC intensity extraction

Using MATLAB R2017b software [20], we extracted median MT-TFL intensity values from each slice of the LC mask and these were subsequently exported to R version 4.0.4. (https://www.r-project.org/). Using the FSL 6.0 *fslstats* function, we also extracted the mean intensity of 10x10 voxel reference regions in the left and right side of the pontine tegmentum (PT) from each participant to normalize the intensity values. Final LC intensity was calculated in R for each hemisphere by dividing the LC intensity by the PT intensity, using the PT reference region matching the hemisphere of the

respective LC. For the template approaches, we visually evaluated the accuracy of the template-based LC mask at the individual level. The mask placement was visually compared to where the LC was visible in the individual MT-TFL scan and overlap was rated on a 1 (no overlap) to 5 (perfect overlap) scale (RWEvH). In addition, for visualization purposes in the template methodologies, we performed vertex-wise analyses associating age to LC intensity adjusting for sex, using R and FSL.

Statistical analyses

Linear and nonlinear mixed-effects models were constructed in R after extraction of intensity values. Linear and nonlinear model fits were compared, such that only the model with the best (lowest) Akaike information criterion is reported. In these models, LC intensity was entered as the dependent variable, quadratic fixed effects were age, slice number, and the interaction between age and slice number, while sex was included as a linear fixed effect. Additionally, we included a random intercept and slope (slice number) for each participant. Inter-rater reliability of the different approaches was calculated using a two-way agreement intraclass correlation coefficient (ICC) in R. In addition to the ICC, an in-house shell script was used to calculate the Dice similarity coefficient (DSC) as a measure of spatial overlap between delineations.

RESULTS

Demographics

One participant was excluded due to misplacement of the multivariate mask resulting in zero-value voxels, resulting in a sample of n=99 for the training set. There was no age difference between the training (mean=62, range 30-87 years) and validation sets (mean=62, range 31-82 years) sets (Student's t=-0.304, p=0.761) (Supplementary Figure 1). Additionally, no sex differences were found between the training set (50 men and 49 women) and validation set (22 men and 22 women) (χ^2=0.003, p=0.956).

Reliability

Template mask accuracy

For a visualization of the LC delineations in the univariate and multivariate template space, see Figure 1. Additionally, 3D surface renders of all methodologies are provided in Supplementary Figure 2. In the univariate template, 16 LC masks were

not aligned with the visible location of the LC (rating of 1), while 13 masks (including the aforementioned exclusion) did not align in the multivariate template. We found that lower accuracy ratings were related with older age in the multivariate template (unstandardized β=-0.022, t=-2.283, p=0.025), and a trend-level age-relationship for accuracy of the univariate template method (unstandardized β=-0.020, t=-1.934, p=0.056). Note that the manual approach covers more slices than the template methodologies. This is because the LC delineation in the template methodologies represents a template-based "common" morphology of the LC across all scans (based on unanimous agreement between 4 raters), while the manual delineation reflects the entire span of individual variations in observed LC morphology. The univariate template covers up to 11 slices (5.5mm), and the multivariate template covers up to 9 slices(4.5mm), while the longest manual delineation covers 27 slices (13.5mm).

Figure 1. Univariate and multivariate templates.

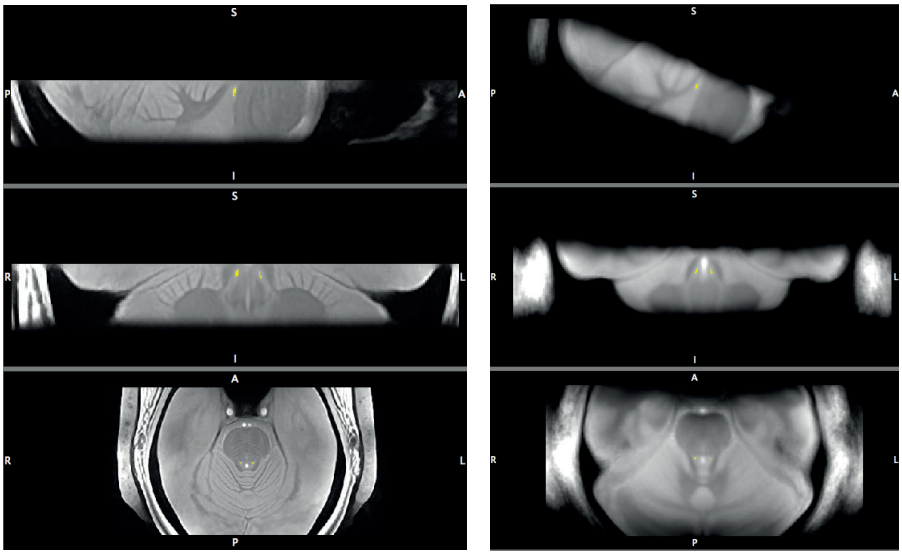

Note. The univariate (left) and multivariate (right) templates based on the MT-TFL images in. The bilateral locus coeruleus mask is marked in yellow in the sagittal (top), coronal (middle) and axial (bottom) views. Note that the slices displayed in this figure do not capture the entirety of the locus coeruleus mask. Orientation markers are A: Anterior; I: Inferior; L: Left; R: Right; P: Posterior; S: Superior.

ICC

Agreement between different raters in the univariate and multivariate template delineations, as measured by ICC, is 0.963 for the left univariate template, 0.972 for the right univariate template, 0.949 for the left multivariate template and 0.926 for the right multivariate template, all of which can be considered an excellent agreement [21]. For the manual method, the ICC between the two rating sessions was 0.781 for the left delineation and 0.847 for the right delineation, both of which can be considered a good agreement (Figure 2).

Dice similarity coefficient

The average DSC measuring the voxel-wise overlap between LC masks of different raters for the univariate method was 0.691 for the left univariate delineation and 0.658 for the right univariate delineation, signaling a substantial agreement for both delineations [22]. For the multivariate method, the average DSC was 0.329 for the left multivariate delineation and 0.410 for the right multivariate delineation which represents a fair agreement for the left delineation and a moderate agreement for the right delineation. Matrices describing the DSC between all raters can be found in supplementary table 1. The DSC for the two manual delineation sessions of the LC was 0.341 for the left LC and 0.371 for the right LC, signaling fair agreement in both cases (Figure 2).

Figure 2. Distributions of mean LC intensities for each of the different delineation methods.

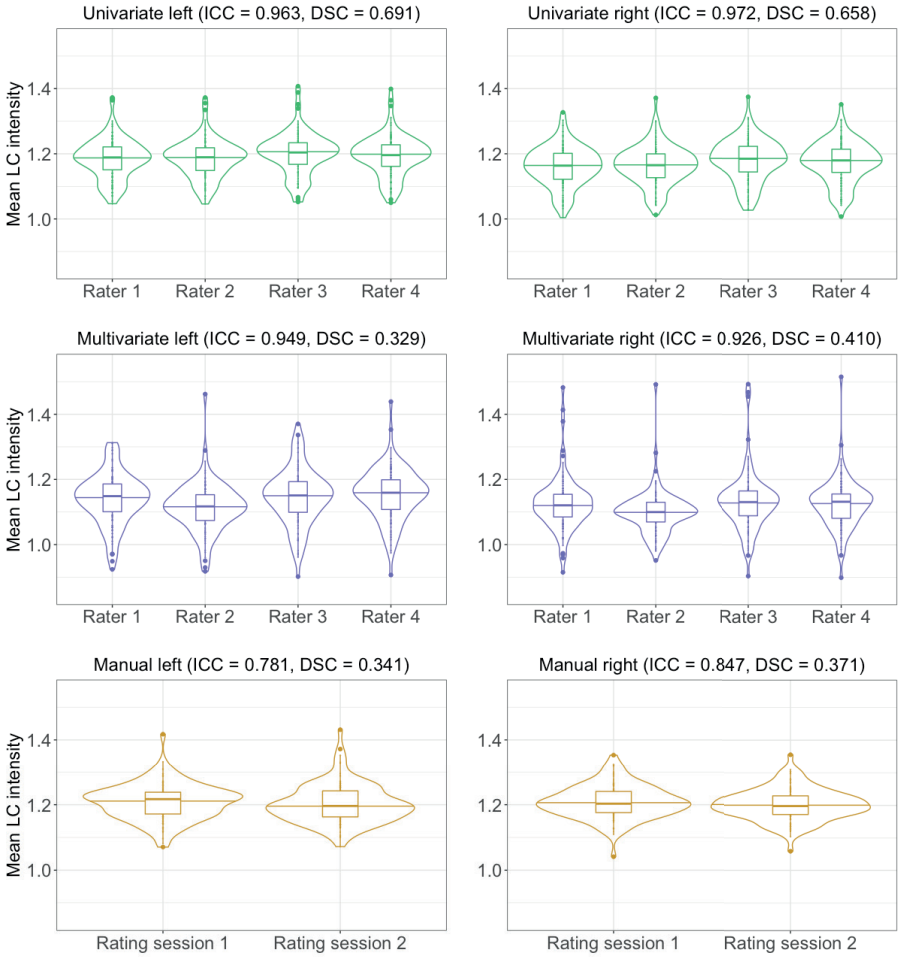

Note. Violin plots displaying the distributions of mean LC intensities for each of the different delineation methods. The intensity-normalized LC values are displayed on the y-axis, while different raters or rating sessions are displayed on the x-axes. Abbreviations: DSC: Dice Similarity Coefficient; ICC: Intraclass Correlation Coefficient; LC: Locus Coeruleus.

Intensity across slices

In all cases, nonlinear models provided a better fit and therefore only nonlinear models are presented. The association between LC slice number (higher number means a more rostral-directed position) and intensity is visualized for each of the delineation methods in Figure 3. Higher LC intensity was associated with a more caudal slice position in the left univariate template delineation (standardized β= -0.011, t=-3.410, p<0.001) and both manual delineations (left: standardized β= -0.161, t=-4.901, p<0.001; right: standardized β= -0.108, t=-2.898, p=0.004). Both multivariate delineations showed higher LC intensity was associated with a more rostral slice position (left: standardized β= 0.013, t=6.659, p<0.001; right: standardized β= 0.033, t=3.143, p=0.002). No significant associations were found for the right univariate delineation (standardized β=-0.137, t=0.840, p=0.401)

Slice-wise associations between age and LC intensity

In all cases, nonlinear models provided a better fit and thus only nonlinear models are presented. Slice-wise associations between age and LC intensity are displayed in Figure 4. Separate regression lines for three equidistant sections of the LC are drawn for visualization purposes, however slice number was entered as a continuous variable in the mixed model analyses. In the left univariate delineation, we observed that more rostral sections displayed lower intensity with higher age compared to the other sections (standardized β=0.009, t=-3.628, p<0.001). Both the right univariate (standardized β=0.047, t=3.054 , p=0.002) and right manual (standardized β=0.003, t=4.432, p<0.001) delineations showed an inverted-U curve pattern for LC intensity with age for the caudal section compared to the other sections. No significant interactions were found for the other delineations (left multivariate standardized β=0.001, t=-0.293, p=0.769; right multivariate standardized β=0.017, t=0.780, p=0.435; left manual standardized β=0.039, t=-1.296, p=0.195).

Figure 3. Slice-wise patterns in distribution of locus coeruleus intensities.

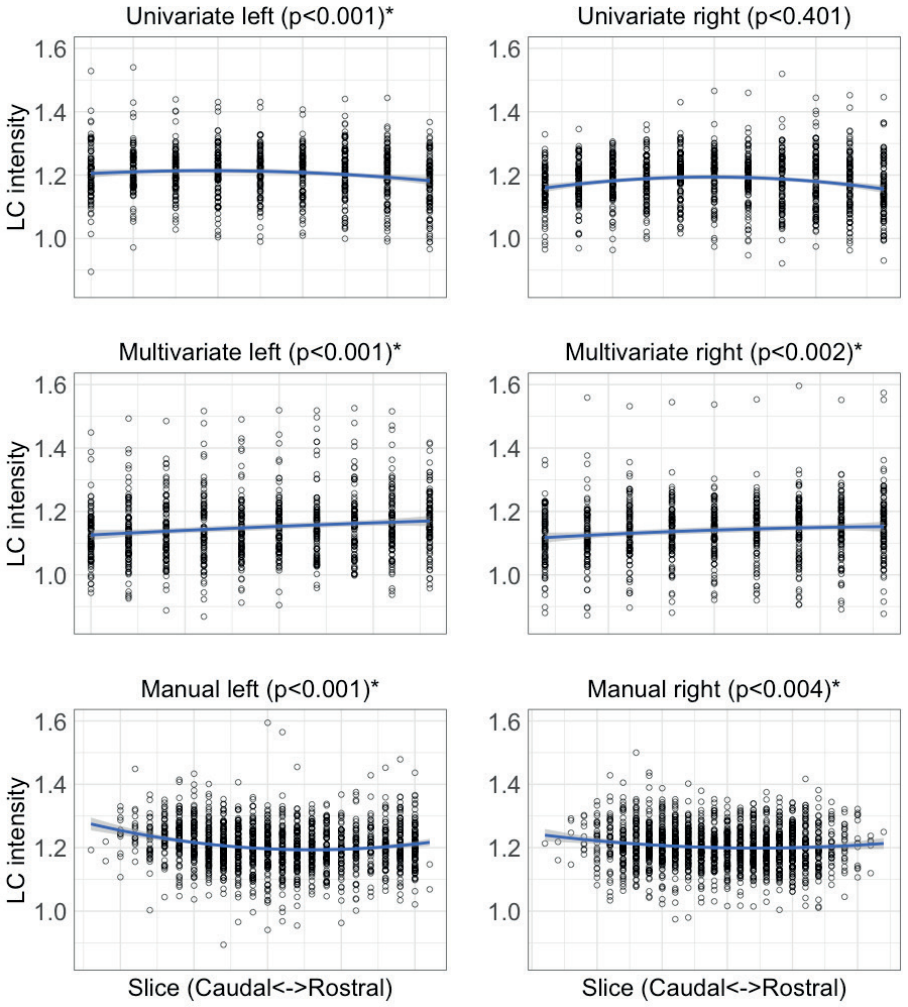

Note. The x-axes represent slice position, where the most caudal slice is the leftmost column of data and the most rostral slice is on the right side of the graph. Y-axes represent normalized intensity. Points represent the median locus coeruleus intensity of a single participant in that slice. Note that due to individualized locus coeruleus masks, the number of datapoints may differ significantly per slice in the manual methodology. Caudal and rostral extremes tend to have fewer datapoints than the central sections. The blue line is a non-linear regression fit, where locus coeruleus intensity is predicted by slice position. Slices are not numbered as the slice numbers are not directly comparable between the different methodologies. Abbreviations: LC: Locus coeruleus.

Figure 4. Slice-wise associations between age and locus coeruleus intensity.

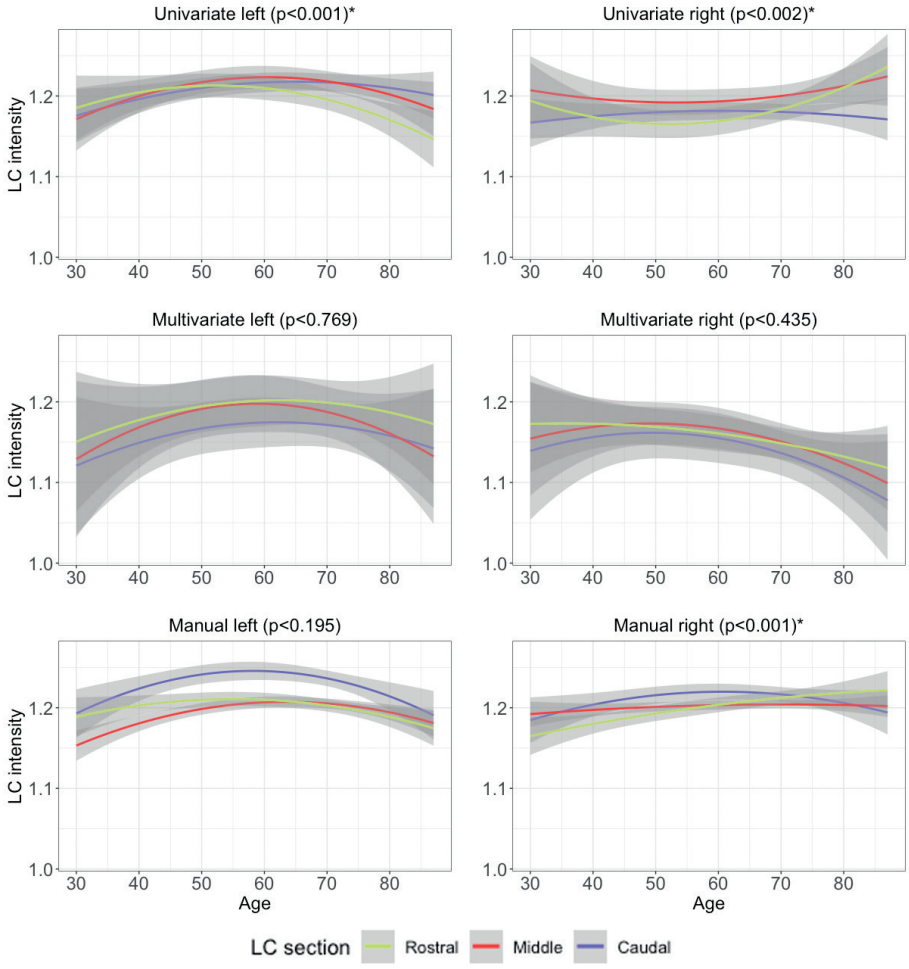

Note. X-axes represent age in years, while the y-axes represent normalized locus coeruleus intensity. The locus coeruleus has been divided in three equidistant sections for the purpose of visualizing the interaction between slice number and age on intensity. Analyses were carried out with a continuous slice number variable. Abbreviations: LC: Locus coeruleus.

Validation of univariate method

Given that we observed the highest reliability metrics in the univariate method compared to the other methodologies, we applied the univariate template to the independent validation dataset previously described.

Intensity across slices in the validation dataset

Nonlinear models provided a better fit and are thus presented. The associations between LC slice and intensity are visualized in Figure 5. Higher LC intensity was associated with a more rostral slice position in the right delineation (standardized β= 0.028, t=6.787, p<0.001) but no association was observed in the left delineation (standardized β= 0.136, t=1.193, p=0.467).

Figure 5. Slice-wise patterns in distribution of locus coeruleus intensities in the validation dataset.

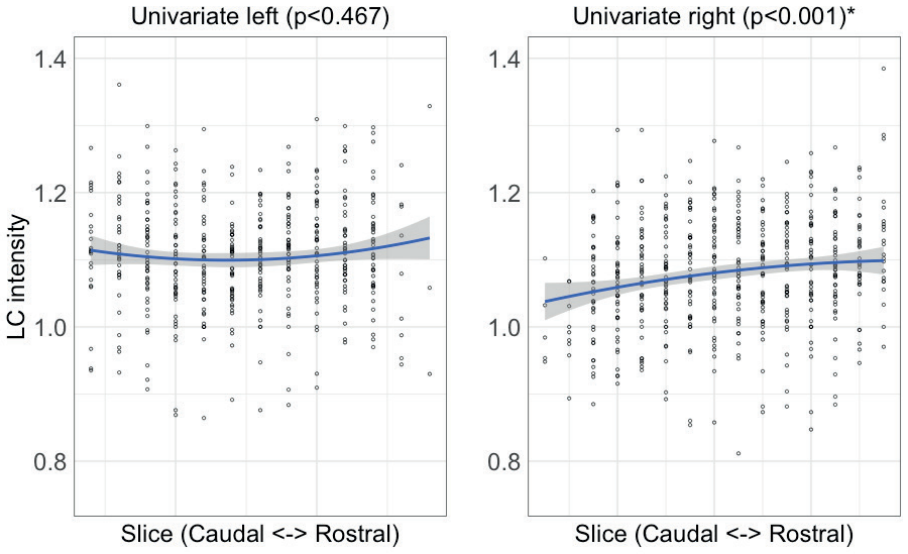

Note. The x-axes represent slice position, where the most caudal slice is the leftmost column of data and the most rostral slice is on the right side of the graph. Y-axes represent normalized locus coeruleus intensity. Points represent the median locus coeruleus intensity of a single participant in that slice. Abbreviations: LC: Locus coeruleus.

Slice-wise associations between age and LC intensity in the validation dataset

Slice-wise associations between age and LC intensity are displayed in Figure 6. No associations between slice position and age were detected for the left (standardized β=0.106, t=1.403, p=0.161) or right LC (standardized β=0.037, t=-1.749, p=0.081), though the right LC intensity shows a trend-level inverted-U curve with age in the rostral LC compared to other sections.

Figure 6. Slice-wise associations between age and locus coeruleus intensity in the validation dataset.

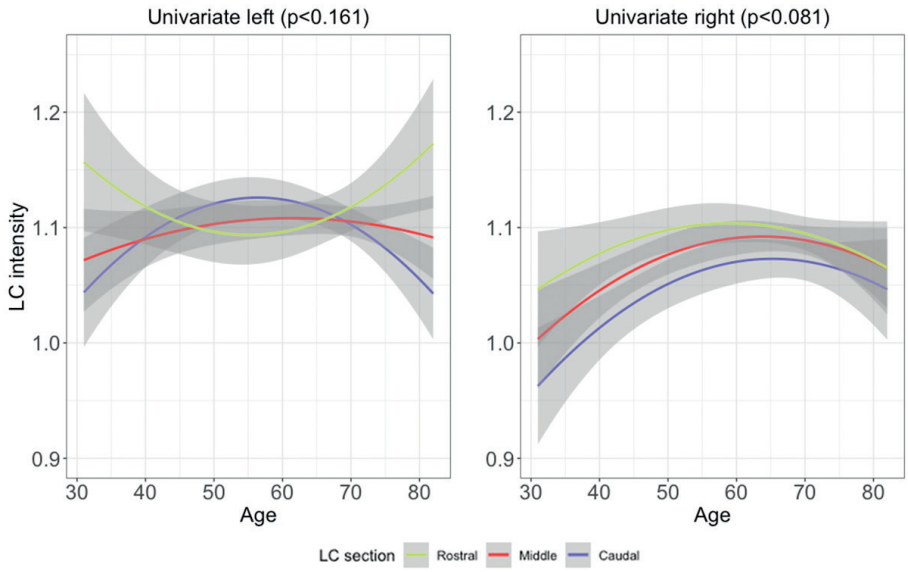

Note. Age is displayed on the x-axes and normalized locus coeruleus intensity is displayed on the y-axes. The template-space locus coeruleus mask from the training set was warped to the individual images in the validation set, resulting in minor variations in the quantity of native-space slices included in the masks. This is represented in the regression lines and confidence intervals of unequal length. Abbreviations: LC: Locus coeruleus.

DISCUSSION

Imaging the LC is a promising marker for early detection of AD [3-5], however there are still substantial challenges in accurately and consistently identifying the anatomy of the LC in vivo. Such challenges include the small size of the LC and confounding factors related to motion of physiology due to the LC's proximity to major blood vessels. These factors complicate the consistent identification of the LC at the individual level, as illustrated by the varying levels of image clarity and LC signal quality. Previous studies have attempted to investigate the LC in vivo using a range of different approaches, such as univariate and multivariate template-based algorithms [12, 14] and manual delineations of the LC [15, 23]. However the lack of a standard has made it difficult to compare and interpret potentially conflicting findings. Here, we aimed to compare several approaches to understand their similarities and differences in LC intensity and their relationship to age. Establishing this method-dependent variability in LC intensity constitutes a critical step for studies focusing on the LC in aging and neurodegenerative disorders using a specific approach.

In terms of reliability, we found excellent reliability metrics for the univariate template approach and mixed reliability measures for the multivariate template approach. By contrast, we found notably worse reliability statistics for the manual approach. The reliability measures, particularly in the univariate template and to a lesser degree in the multivariate template, suggest that the LC signal in template-based approaches is less sensitive to inter-rater variability as compared to the manual approach. Despite this, it should be noted that the template methods do suffer from individual cases of bad registrations (16% for univariate and 13% for multivariate template). Poor registrations are potentially exacerbated when including older participants, which is a concern especially for LC studies in the context of aging and dementia.

Furthermore, we found higher signal intensity towards the more middle and caudally positioned sections of the LC in the left univariate template and bilateral manual methods, which is consistent with post-mortem data reporting higher neuromelanin cell counts in the caudal compared to the more rostral sections of the LC [24]. The reason for the lack of an association between LC slice position and signal intensity in the right univariate template is unclear, however hemispheric asymmetry of LC contrast has been previously reported [25] and requires more detailed investigation in future studies. Conversely, in the bilateral multivariate

template, we found a higher signal intensity as the slice position gets more rostral. This is possibly due to the diffuse anatomical organization of the caudal LC, making it difficult to accurately image the caudal portion of the LC [26]. Supporting this, a previous study which utilized a multivariate template method reported a lower degree of spatial agreement of slice-wise peak intensity voxels across subjects in the caudal section of the LC compared to the other sections [13]. This means that more caution in interpreting the caudal LC values is warranted.

In addition, we were able to confirm a predominantly rostral negative association between age and LC intensity in the left univariate template methodology, corroborating patterns previously described in post-mortem data [27]. Additionally, in the right univariate template and right manual approaches, we found that the caudal section shows an inverted-U curve age-related association compared to the other sections. Post-mortem studies and recent MRI studies also reported greater neuromelanin cell density or LC intensity, respectively, during midlife, while at older ages neuromelanin cell density or LC intensity was lower [15, 28]. The lack of significant associations between age and LC intensity across the rostrocaudal axis in the multivariate approach as well as the left manual approach may be related to the relatively low DSC metrics for these methods, indicating that inter-rater agreement on LC mask is difficult to achieve, which in turn also makes division of the LC into rostral, middle and caudal sections less reliable and consistent.

Finally, we were not able to replicate the univariate results in the independent dataset. This may be due to inherent small interpolation-induced inaccuracies that result from warping the template image to independent native-space images. It is likely that the creation of a study-specific template with a minimal number of interpolation steps may be the best approach to a template-based method.

There are several limitations to the present study. First, our findings underscore the need to further optimize algorithms to increase the accuracy of image alignment in template approaches. One participant was removed due to complete misalignment of the LC mask resulting in zero-values in the multivariate method, but upon visual inspection, we identified more cases in both template approaches where the mask did not seem to provide a great fit. The severity of misaligned data may be exacerbated when applying the template building process to a highly heterogenous sample, such as the sample in the present study. These misalignments can impact further analyses and argue for validating findings

through several methods. Powerful computing units, such as clusters, may be used to increase the number of iterations in the template creation process and thus potentially increase registration accuracy. This has the additional benefit of reducing processing times, providing a more feasible time frame for researchers to analyze data and optimize the template creation process as needed.

Furthermore, many factors, such as lighting conditions, monitor settings, image viewing software settings, and rater bias may influence the outcome of manual delineations, especially when image quality is relatively low. The latter is especially problematic when investigating populations that are more likely to move in the scanner, such as older populations or patient populations. Future studies should aim to standardize the protocol of segmentation of the LC and should investigate the value of applying motion correction to structural images of the LC. Furthermore, ratings from multiple independent raters may reduce biases in manual delineation.

Finally, we did not explore machine-learning based or automated threshold-based methods to identify voxels of the LC. These approaches have been previously described and may provide a rather unbiased method of LC delineation [29, 30]. Therefore, a direct comparison in terms of reliability and validity to template-based and manual approaches would be informative.

Overall, our work provides recommendations for future studies investigating the LC in vivo using structural MRI. Based on our findings, we conclude that the univariate, study-specific template approaches are likely an accurate tool for in-vivo LC delineation, as illustrated by their high reliability metrics. However, we want to signal caution in using template approaches and highlight the need to check the accuracy of LC masks at the individual level, especially when the data contains older participants. Finally, the low reliability of manual delineation and the high operator-dependency indicate that a complete manual approach may constitute the less desired method when refined and accurate template approaches are an available alternative.

REFERENCES:

1. Samuels, E.R. and E. Szabadi, *Functional neuroanatomy of the noradrenergic locus coeruleus: its roles in the regulation of arousal and autonomic function part I: principles of functional organisation.* Current neuropharmacology, 2008. **6**(3): p. 235-253.
2. Holland, N., T.W. Robbins, and J.B. Rowe, *The role of noradrenaline in cognition and cognitive disorders.* Brain, 2021. **144**(8): p. 2243-2256.
3. Braak, H. and E. Braak, *Neuropathological stageing of Alzheimer-related changes.* Acta Neuropathologica, 1991. **82**(4): p. 239-259.
4. Braak, H., et al., *Stages of the Pathologic Process in Alzheimer Disease: Age Categories From 1 to 100 Years.* Journal of Neuropathology & Experimental Neurology, 2011. **70**(11): p. 960-969.
5. Theofilas, P., et al., *Locus coeruleus volume and cell population changes during Alzheimer's disease progression: A stereological study in human postmortem brains with potential implication for early-stage biomarker discovery.* Alzheimer's & Dementia, 2017. **13**(3): p. 236-246.
6. Mouton, P.R., et al., *Absolute number and size of pigmented locus coeruleus neurons in young and aged individuals.* Journal of Chemical Neuroanatomy, 1994. **7**(3): p. 185-190.
7. Oh, J., et al., *Profound degeneration of wake-promoting neurons in Alzheimer's disease.* Alzheimers Dement, 2019. **15**(10): p. 1253-1263.
8. Fernandes, P., et al., *The human locus coeruleus 3-D stereotactic anatomy.* Surgical and Radiologic Anatomy, 2012. **34**(10): p. 879-885.
9. Priovoulos, N., et al., *High-resolution in vivo imaging of human locus coeruleus by magnetization transfer MRI at 3T and 7T.* NeuroImage, 2018. **168**: p. 427-436.
10. Betts, M.J., et al., *Locus coeruleus imaging as a biomarker for noradrenergic dysfunction in neurodegenerative diseases.* Brain, 2019. **142**(9): p. 2558-2571.
11. Jacobs, H.I.L., et al., *In vivo and neuropathology data support locus coeruleus integrity as indicator of Alzheimer’s disease pathology and cognitive decline.* Science Translational Medicine, 2021. **13**(612): p. eabj2511.
12. Liu, K.Y., et al., *In vivo visualization of age-related differences in the locus coeruleus.* Neurobiology of Aging, 2019. **74**: p. 101-111.
13. Ye, R., et al., *An in vivo probabilistic atlas of the human locus coeruleus at ultra-high field.* NeuroImage, 2021. **225**: p. 117487.
14. Betts, M.J., et al., *In vivo MRI assessment of the human locus coeruleus along its rostrocaudal extent in young and older adults.* NeuroImage, 2017. **163**: p. 150-159.
15. Shibata, E., et al., *Age-related Changes in Locus Ceruleus on Neuromelanin Magnetic Resonance Imaging at 3 Tesla.* Magnetic Resonance in Medical Sciences, 2006. **5**(4): p. 197-200.
16. Marques, J.P., et al., *MP2RAGE, a self bias-field corrected sequence for improved segmentation and T1-mapping at high field.* NeuroImage, 2010. **49**(2): p. 1271-1281.
17. Avants, B.B., N. Tustison, and G. Song, *Advanced normalization tools (ANTS).* Insight j, 2009. **2**(365): p. 1-35.
18. Fischl, B., *FreeSurfer.* Neuroimage, 2012. **62**(2): p. 774-781.

19. Jenkinson, M., et al., *FSL.* NeuroImage, 2012. **62**(2): p. 782-790.
20. MATLAB, *version 9.3.0.713579 (R2017b).* Natick, Massachussets: The MathWorks Inc., 2017.
21. Koo, T.K. and M.Y. Li, *A Guideline of Selecting and Reporting Intraclass Correlation Coefficients for Reliability Research.* Journal of Chiropractic Medicine, 2016. **15**(2): p. 155-163.
22. Pajula, J., J.-P. Kauppi, and J. Tohka, *Inter-Subject Correlation in fMRI: Method Validation against Stimulus-Model Based Analysis.* PLOS ONE, 2012. **7**(8): p. e41196.
23. Tona, K.-D., et al., *In vivo visualization of the locus coeruleus in humans: quantifying the test–retest reliability.* Brain Structure and Function, 2017. **222**(9): p. 4203-4217.
24. German, D., et al., *The human locus coeruleus: computer reconstruction of cellular distribution.* The Journal of Neuroscience, 1988. **8**(5): p. 1776-1788.
25. Keren, N.I., et al., *Histologic validation of locus coeruleus MRI contrast in post-mortem tissue.* NeuroImage, 2015. **113**: p. 235-245.
26. Van Egroo, M., R.W.E. van Hooren, and H.I.L. Jacobs, *Associations between locus coeruleus integrity and nocturnal awakenings in the context of Alzheimer's disease plasma biomarkers: a 7T MRI study.* Alzheimer's Research & Therapy, 2021. **13**(1): p. 159.
27. Manaye, K.F., et al., *Locus coeruleus cell loss in the aging human brain: A non-random process.* Journal of Comparative Neurology, 1995. **358**(1): p. 79-87.
28. Mann, D.M.A. and P.O. Yates, *Lipoprotein Pigments - Their Relationship to Ageing in the Human Nervous System: II. The Melanin Content of Pigmented Nerve Cells.* Brain, 1974. **97**(1): p. 489-498.
29. Dünnwald, M., et al., *Fully automated deep learning-based localization and segmentation of the locus coeruleus in aging and Parkinson's disease using neuromelanin-sensitive MRI.* International Journal of Computer Assisted Radiology and Surgery, 2021. **16**(12): p. 2129-2135.
30. Morris, L.S., et al., *Sub-millimeter variation in human locus coeruleus is associated with dimensional measures of psychopathology: An in vivo ultra-high field 7-Tesla MRI study.* NeuroImage: Clinical, 2020. **25**: p. 102148.

SUPPLEMENTARY MATERIAL

Supplementary figure 1. Age and sex distributions in the training and validation datasets.

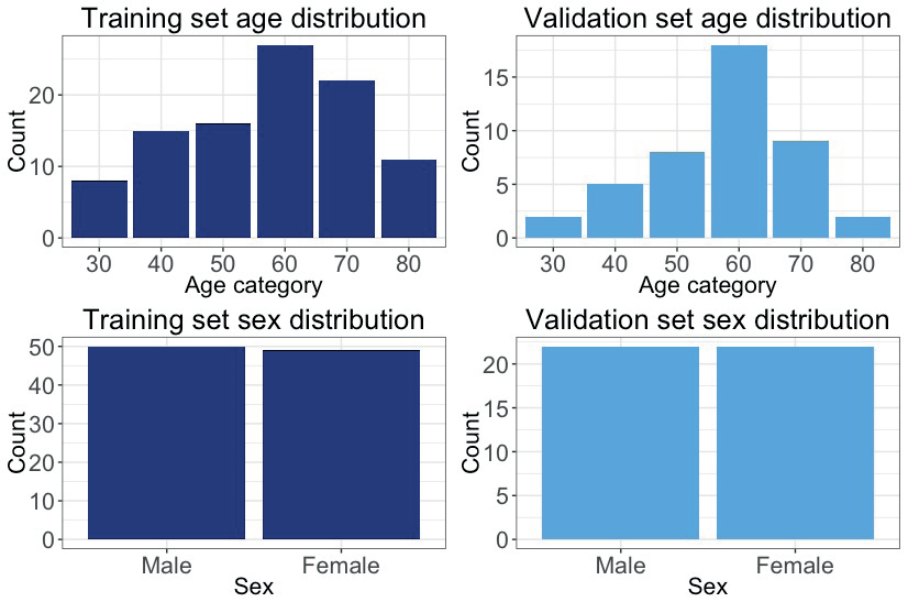

Supplementary figure 2. Surfaces of the locus coeruleus delineations in the different methodologies.

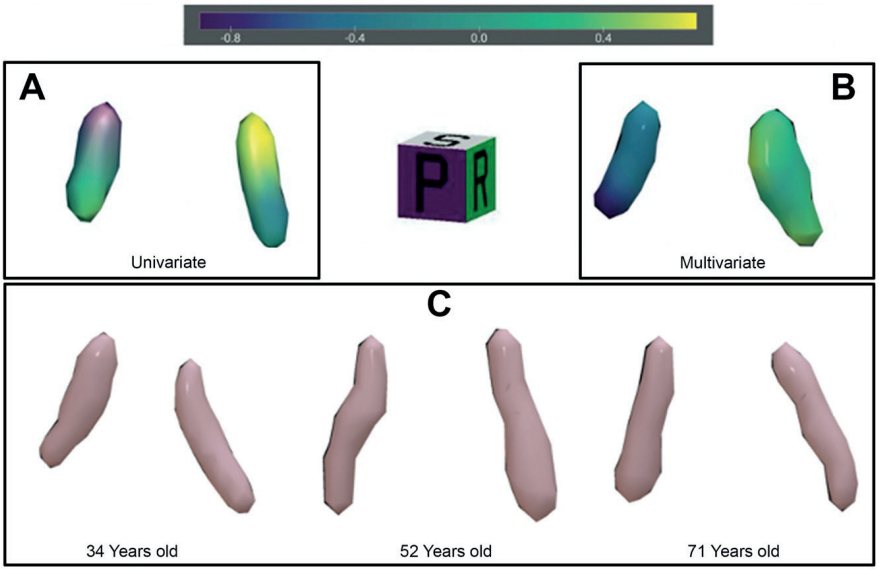

Note. The central cube displays the orientation of the locus coeruleus surfaces (S = superior (rostral), P= posterior (dorsal), R = Right). The colored overlay represents t-values of the age variable resulting from vertex-wise regression of locus coeruleus intensity against age, adjusted for sex in the univariate (A) and multivariate (B) template methodologies. Note that there were no significant age-relationships with locus coeruleus intensity. Since the locus coeruleus masks are different for each manual delineation, vertex-wise analysis was not possible for this methodology and three representative masks for different ages are displayed instead (C). Surfaces were rendered using surfice software.

Supplementary table 1. Dice similarity metrics for the template approaches between all raters.

Univariate				
Left				
	Rater 1	Rater 2	Rater 3	Rater 4
Rater 1	1	0.694	0.735	0.766
Rater 2	0.694	1	0.554	0.615
Rater 3	0.735	0.554	1	0.779
Rater 4	0.766	0.615	0.779	1
Average: 0.691				
Right				
	Rater 1	Rater 2	Rater 3	Rater 4
Rater 1	1	0.741	0.637	0.719
Rater 2	0.741	1	0.495	0.649
Rater 3	0.637	0.495	1	0.703
Rater 4	0.719	0.649	0.703	1
Average: 0.658				

Multivariate				
Left				
	Rater 1	Rater 2	Rater 3	Rater 4
Rater 1	1	0.220	0.213	0.212
Rater 2	0.220	1	0.290	0.711
Rater 3	0.213	0.290	1	0.325
Rater 4	0.212	0.711	0.325	1
Average: 0.329				
Right				
	Rater 1	Rater 2	Rater 3	Rater 4
Rater 1	1	0.331	0.369	0.285
Rater 2	0.331	1	0.387	0.690
Rater 3	0.369	0.387	1	0.393
Rater 4	0.285	0.690	0.393	1
Average: 0.410				

ASSOCIATIONS BETWEEN LOCUS COERULEUS INTEGRITY AND NOCTURNAL AWAKENINGS IN THE CONTEXT OF ALZHEIMER'S DISEASE PLASMA BIOMARKERS: A 7T MRI STUDY

CHAPTER 6

Published in Alzheimer's Research & Therapy (2021)

Maxime van Egroo
Roy W.E van Hooren
Heidi I.L. Jacobs

ABSTRACT

Background: The brainstem locus coeruleus (LC) constitutes the intersection of the initial pathophysiological processes of Alzheimer's disease (AD) and sleep-wake dysregulation in the preclinical stages of the disease. However, the interplay between in vivo assessment of LC degeneration and AD-related sleep alterations remains unknown. Here, we sought to investigate whether MRI-assessed LC structural integrity relates to subjective sleep-wake measures in the context of AD plasma biomarkers, in cognitively unimpaired older individuals.

Methods: Seventy-two cognitively unimpaired older individuals aged 50–85 years (mean age = 65.2 ± 8.2 years, 37 women, 21 *APOE* ε4 carriers) underwent high-resolution imaging of the LC at 7 Tesla, and LC structural integrity was quantified using a data-driven approach. Reports on habitual sleep quality and nocturnal awakenings were collected using sleep questionnaires. Plasma levels of total tau, p-tau$_{181}$, Aβ$_{40}$, and Aβ$_{42}$ were measured using single-molecule array technology.

Results: Intensity-based cluster analyses indicated two distinct LC segments, with one covering the middle-to-caudal LC and displaying lower intensity compared to the middle-to-rostral cluster ($t_{70} = -5.12$, $p < 0.0001$). After correction for age, sex, depression, and *APOE* status, lower MRI signal intensity within the middle-to-caudal LC was associated with a higher number of self-reported nocturnal awakenings ($F_{1,63} = 6.73$, $p_{FDR} = 0.03$). Furthermore, this association was mostly evident in individuals with elevated levels of total tau in the plasma ($F_{1,61} = 4.26$, $p = 0.04$).

Conclusion: Our findings provide in vivo evidence that worse LC structural integrity is associated with more frequent nocturnal awakenings in the context of neurodegeneration, in cognitively unimpaired older individuals. These results support the critical role of the LC for sleep-wake regulation in the preclinical stages of AD and hold promises for the identification of at-risk populations for preventive interventions.

BACKGROUND

In the worldwide effort to identify leverage points to delay the onset of Alzheimer's disease (AD), sleep has emerged as a potent modifiable factor to slow down the characteristic pathophysiological processes of the disease, i.e., the accumulation of amyloid-beta (Aβ) and tau proteins, together with neurodegeneration [1]. Two recent meta-analyses of, respectively, 27 observational and 18 longitudinal studies reported that individuals with sleep-related issues are at a ~1.5 times increased risk of developing AD and that an estimated 15% of AD in the population may be linked to treatable sleep problems [2, 3].

One of the critical brain regions involved in both initial AD pathogenesis and sleep-wake regulation is a small nucleus located in the brainstem: the locus coeruleus (LC). Landmark post-mortem studies have demonstrated that the LC is among the first sites of tau pathology [4], starting as early as age thirty [5]. As part of the complex ascending arousal system, the LC regulates wakefulness periods, arousal, and various cognitive processes, by supplying norepinephrine to the entire cortex [6]. During a typical sleep cycle, LC neurons become progressively silent, which ensures overall consolidation of the sleep period and normal transitions across sleep stages [7], while its activity underlies sleep-to-wake transitions [8, 9].

In animal studies, chronic sleep disruption of 3 days a week during 1 month was enough to induce long-lasting alterations in LC neurons morphology (i.e., reductions in neuronal count and axonal projections) [10, 11] and to promote tau accumulation in the LC [12]. In humans, significant degeneration of wake-promoting LC neurons concomitant with increased tau protein burden was reported at histological investigation of AD brains, which was suggested to contribute to the disrupted sleep-wake pattern commonly experienced by those patients [13, 14]. However, no direct assessments of sleep-wake measures were available in these post-mortem studies, leaving important questions on the interplay between LC alterations, sleep-wake patterns, and AD-related pathophysiological processes unanswered. As both sleep-wake disruption and LC pathologic processes can be detected as early as in the 5th or 6th decade of life [15, 16], addressing these gaps in cognitively unimpaired older individuals may provide new insights into the pathological processes in the earliest stages of AD.

To our knowledge, no studies have directly related in vivo LC measures to sleep-wake variables, most likely because it is challenging to image this brain nucleus, due to its deep location in the brainstem and its small size (~15 mm long and 2 × 2 mm thick).

However, the development of novel MRI methods has enabled in-depth assessment of its properties in vivo [17]. Here, we used state-of-the-art methods in ultra-high field neuroimaging to investigate LC structural integrity in vivo in a cohort of cognitively unimpaired older individuals and to relate it to participants' subjective evaluations of sleep quality and nocturnal awakenings. In addition, we sought to examine interactive effects with early AD-related pathophysiological processes, as measured with recently developed blood-based biomarkers, in order to evaluate LC integrity as a potential early marker for individuals with AD-related sleep disturbances.

MATERIALS AND METHODS

Participants

Seventy-two cognitively unimpaired older individuals aged 50–85 years (mean age = 65.2 ± 8.2 years, 37 women) were recruited to participate in this study (Table 1). The main exclusion criteria were contraindications for ultra-high field neuroimaging, performance on key cognitive tests 2 standard deviations below the mean (according to normative data corrected for age, sex, and education), past or present psychiatric or neurological disorders, major vascular disorders, left-handedness, use of drugs or psychoactive medication, and excessive alcohol consumption (> 15 units/week).

Table 1. Sample characteristics (mean ± SD).

	***N* = 72**
Age (years)	65.2 ± 8.2
Sex (*N*)	37F/35M
Ethnicity	Caucasian
Right-handed (*N*, %)	72 (100)
Body mass index (kg/m^2)	25.5 ± 4.0
MMSE (score)	28.9 ± 1.2
APOE ε4 carriers (*N*, %)	21 (29)
Total tau (pg/ml)	2.5 ± 0.7
P-tau$_{181}$ (pg/ml)	1.7 ± 0.5
Aβ$_{40}$ (pg/ml)	228.9 ± 33.6
Aβ$_{42}$ (pg/ml)	12.1 ± 2.3
Subjective sleep quality (total GSQS score)	3.3 ± 3.6
Nocturnal awakenings (self-reports)	1.8 ± 1.2

7T MRI acquisition and pre-processing

All participants underwent high-resolution imaging of the brainstem on a 7T Magnetom Siemens scanner (Siemens Healthineers, Erlangen, Germany) using a magnetization transfer-weighted turbo flash (MT-TFL) sequence particularly sensitive to LC-related contrast [18, 19], with a field-of-view placed perpendicular to the pons and covering the area between the inferior colliculus and the inferior border of the pons. Importantly, the LC-related MRI signal obtained with this sequence has been established to reflect LC neuronal and fiber projection density [20].

Our 7T LC MRI pre-processing pipeline is summarized in Supplementary Figure 1, and details are available in the Supplementary Methods. In brief, intensity-normalized images were obtained by dividing individual MT-TFL images by the subject-specific mean intensity of a 10 × 10 voxel region-of-interest located in the pontine tegmentum (PT). Next, a study-specific template was built based on all individual intensity-normalized MT-TFL images. The LC was manually delineated on the resulting template in the common space, based on voxel intensities and the known LC anatomy. This LC mask was then applied on each intensity- and spatially normalized individual image on a per hemisphere basis as previously described [18, 21], to extract MRI signal values for subsequent cluster analyses. As in previous work [22], intensity in the PT region served as control in post hoc analyses.

LC MRI signal cluster analysis

Cluster analyses were performed to identify sub-portions within the LC structure in a data-driven manner. We first determined the optimal number of clusters using 'evalcluster' function implemented in MATLAB2017b (The Mathworks Inc., Natick, MA, USA) based on the Calinski-Harabasz criterion. The optimal solution was then used as a prior to run a K-means algorithm ('kmeans' function in MATLAB, Euclidean distance, 100 iterations) on median MRI signal intensity within each slice of the LC mask, separately for left and right hemisphere. Median MRI signal intensity values in each identified cluster constituted our primary measures of interest and were computed for left and right LC and also averaged over both hemispheres. Consistent with previous work [16, 21], we also computed additional LC metrics to conduct post hoc sensitivity analyses, including the mean and peak intensity in each cluster, and mean MRI signal intensity in three manually defined equidistant sections of the LC.

Subjective sleep quality assessment

Sleep quality was investigated through participants' self-reports on the quality of their sleep during a representative night, using the Groningen Sleep Quality Scale (GSQS) [23]. The GSQS is a sleep quality questionnaire widely used in the Netherlands, which comprises 15 dichotomous (yes/no) items related to different dimensions of sleep throughout a habitual night (i.e., sleep latency, sleep duration, feeling of restlessness, etc.). The GSQS scores strongly correlate with the Pittsburgh Sleep Quality Index, another subjective sleep quality scale traditionally used by sleep researchers (unpublished data, n = 61 cognitively unimpaired older individuals, r = 0.79). Subjective sleep quality was computed as the sum of the scores to each GSQS item, with a higher score reflecting an overall worse sleep quality. An additional item was used to measure the habitual number of self-reported nocturnal awakenings ('I wake up on average _ times during the night').

Alzheimer's disease blood-based biomarker assessment

EDTA plasma samples were obtained through venipuncture (fasted). Samples were centrifuged at 2000 × g, aliquoted in polypropylene tubes, and stored at −80°C in our biobank within 60 min of collection. Plasma was analyzed using ultra-sensitive single-molecule array technology of the automated Simoa HD-1 analyzer with the Simoa Human Neurology 3-Plex A assay kit (Quanterix, Lexington, KY, USA) that simultaneously measures plasma concentrations of Aβ40, Aβ42, and total tau. Analyses were performed in duplicates (mean % coefficient of variation [%CV]: Aβ40 3.8%CV, Aβ42 4.1%CV, total tau 6.7%CV) using a 1:4 automated dilution protocol. The levels of tau phosphorylated at threonine 181 (p-tau181) were measured using the Simoa Human tau immunoassay kits on the Simoa HD-1 Analyzer (7.1%CV). APOE genotyping was further performed using polymerase chain reaction based on blood sample DNA extraction. Participants' APOE status was defined as 'ε4 carrier' if they carry at least one ε4 allele.

Statistical analysis

Statistical analyses were conducted in SAS 9.4 (SAS Institute, NC, USA) using generalized linear mixed model (GLMM). Prior to model fitting, the distribution of the dependent variable in each GLMM was determined in MATLAB2017b, and models were adjusted accordingly. All statistical models included age, sex, and

APOE status as covariates. Models with sleep metrics as the dependent variable were further adjusted for depression scores, as measured by the Hamilton Depression Rating Scale [24]. Subject (intercept) was set as a random factor. p-values derived from these main analyses linking sleep-wake metrics to LC intensity were corrected for multiple comparisons using the false discovery rate (FDR) approach. LC intensity variables showing significant associations with sleep metrics were further tested in models including the interaction term with blood-based AD biomarkers. Post hoc control analyses were conducted using subject-specific median intensity in a PT region-of-interest. Post hoc sensitivity analyses were performed using additional LC metrics of peak cluster intensity, mean cluster values, and mean values in three equidistant LC sections. Degrees of freedom were estimated using Kenward-Roger's correction. In all GLMMs, effect sizes for significant effects were estimated with semi-partial R2 (R2β*) values [25].

RESULTS

Association between demographics, subjective sleep measures, and blood-based biomarkers

After adjusting for age, women reported worse sleep quality ($F_{1,69} = 5.54$, $p = 0.02$, $R2\beta^* = 0.07$) and more nocturnal awakenings ($F_{1,69} = 4.75$, $p = 0.03$, $R2\beta^* = 0.06$) compared to men. In addition, higher depression scores, although in the subclinical range for all individuals, were associated with worse sleep quality ($F_{1,68} = 27.22$, $p < 0.0001$, $R2\beta^* = 0.29$) and higher number of nocturnal awakenings ($F_{1,68} = 7.91$, $p = 0.006$, $R2\beta^* = 0.10$), after adjusting for age and sex. With regard to plasma measures, the range of values was consistent with previous Simoa-based studies in cognitively unimpaired older individuals [26, 27]. Older age was associated with higher plasma levels of p-tau181 ($F_{1,66} = 8.36$, $p = 0.005$, $R2\beta^* = 0.11$) and Aβ40 ($F_{1,66} = 12.35$, $p < 0.001$, $R2\beta^* = 0.16$). APOE ε4 carriers (29%) displayed lower levels of Aβ42 ($F_{1,66} = 10.48$, $p = 0.002$, $R2\beta^* = 0.14$) and at-trend level higher plasma levels of p-tau181 ($F_{1,66} = 3.44$, $p = 0.07$) compared to non-carriers (Supplementary Figure 2). No significant relationships were observed between plasma biomarkers and subjective measures of sleep quality or nocturnal awakenings (Supplementary Figure 3 and Supplementary Table 1).

Identification of clusters in LC MRI signal intensity

Cluster analyses on LC MRI signal intensity revealed two clusters, one covering the middle-to-caudal portion (bottom 7 slices for left LC and bottom 5 slices for right LC) and the other cluster covering the middle-to-rostral part (top 12 slices for left LC, top 14 slices for right LC, Fig. 1A). Paired t test analyses showed that median intensity within the middle-to-caudal cluster was significantly lower than in the middle-to-rostral cluster when considered bilaterally ($t(70) = -5.12$, $p < 0.0001$), but also when tested separately for both hemispheres (left: $t(70) = -2.23$, $p = 0.03$; right: $t(68) = -6.46$, $p < 0.0001$, Fig. 1B).

Figure 1. Intensity-based cluster analyses of the LC structure.

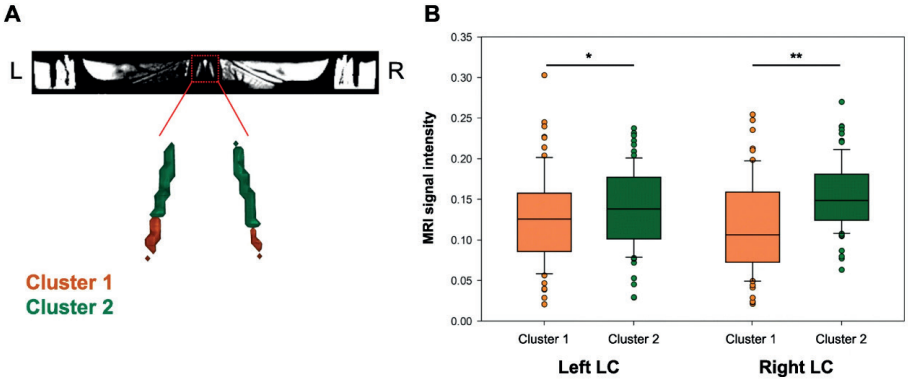

Note. **A** Cluster analyses on MRI signal intensity within the LC mask revealed two distinct clusters along the LC structure, one covering the middle-to-caudal LC (orange, cluster 1) and the other covering the middle-to-rostral LC (green, cluster 2). **B** Box plots of MRI signal intensity within clusters 1 and 2, represented by hemisphere. Paired *t* test analyses showed that MRI signal intensity in cluster 1 is significantly lower than that in cluster 2. ***p* < .05, ****p* < .001.

Association between LC intensity and subjective sleep measures

After adjusting for age, sex, APOE status, and depression scores, subjective sleep quality was not associated with MRI signal intensity values for either of the two LC clusters (Supplementary Table 2). However, we found a significant negative relationship between intensity within the middle-to-caudal LC cluster and participants' reports of nocturnal awakenings ($F_{1,63} = 5.85$, pFDR = 0.03, $R2\beta^* = 0.09$, Figure 2, Table 2), which was strongest in the left hemisphere ($F_{1,63} = 6.73$, pFDR = 0.03, $R2\beta^* = 0.10$). These associations were not observed when investigating the middle-to-rostral cluster (Table 2).

Figure 2. Associations between subjective reports of nocturnal awakenings and middle-to-caudal LC structural integrity, considered bilaterally (top left), in the left hemisphere (top right), and in the right hemisphere (bottom left).

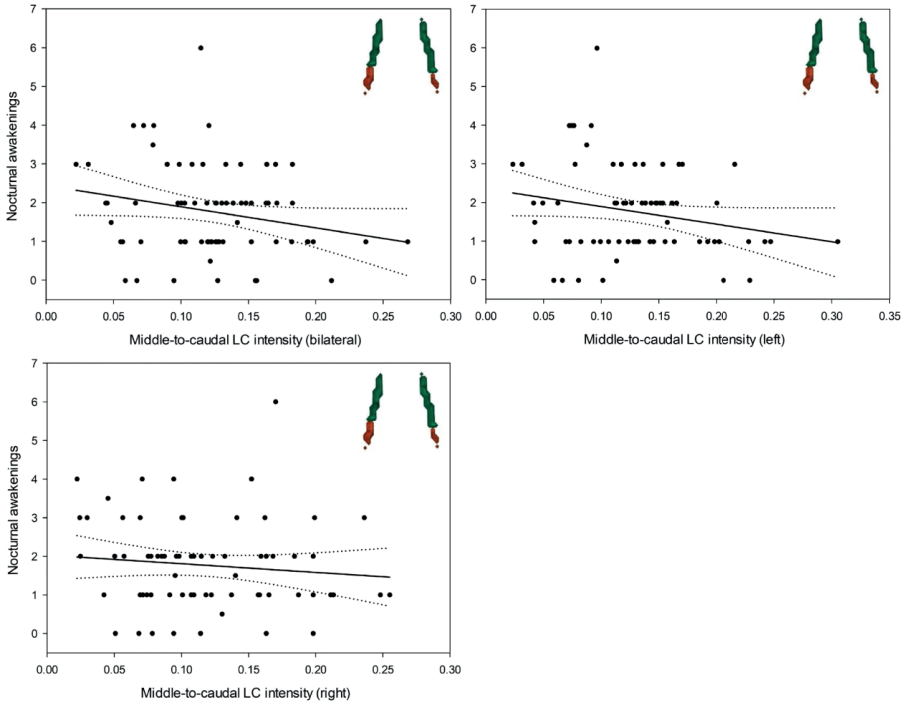

Note. Simple regression lines are used for a visual display and do not substitute the GLMM outputs. Dotted lines represent 95% confidence intervals of these simple regressions.

Table 2. GLMM outputs of the associations between subjective reports of nocturnal awakenings and middle-to-caudal (top) or middle-to-rostral (bottom) LC structural integrity, considered bilaterally (model 1), for left LC (model 2), and for right LC (model 3).

	Model 1	***Model 2***	***Model 3***
Middle-to-caudal LC integrity	$F_{1,63}$ = 5.85 p_{FDR} = 0.03 $R^2_{\beta*}$ = 0.09	$F_{1,63}$ = 6.73 p_{FDR} = 0.03 $R^2_{\beta*}$ = 0.10	$F_{1,63}$ = 0.71 p_{FDR} = 0.40
Age	$F_{1,63}$ = 3.27 p = 0.08	$F_{1,63}$ = 4.08 p = 0.05	$F_{1,63}$ = 2.20 p = 0.14
Sex	$F_{1,63}$ = 6.67 p = 0.01 $R^2_{\beta*}$ = 0.10	$F_{1,63}$ = 7.76 p = 0.007 $R^2_{\beta*}$ = 0.11	$F_{1,63}$ = 6.02 p = 0.02 $R^2_{\beta*}$ = 0.09
Depression	$F_{1,63}$ = 8.07 p = 0.006 $R^2_{\beta*}$ = 0.11	$F_{1,63}$ = 7.26 p = 0.009 $R^2_{\beta*}$ = 0.10	$F_{1,63}$ = 8.42 p = 0.005 $R^2_{\beta*}$ = 0.12
APOE status	$F_{1,63}$ = 2.16 p = 0.15	$F_{1,63}$ = 2.29 p = 0.14	$F_{1,63}$ = 2.46 p = 0.12
Middle-to-rostral LC integrity	$F_{1,63}$ = 1.37 p_{FDR} = 0.37	$F_{1,63}$ = 2.03 p_{FDR} = 0.37	$F_{1,62}$ = 0.36 p_{FDR} = 0.55
Age	$F_{1,63}$ = 2.70 p = 0.11	$F_{1,63}$ = 2.68 p = 0.11	$F_{1,62}$ = 2.43 p = 0.12
Sex	$F_{1,63}$ = 6.09 p = 0.02 $R^2_{\beta*}$ = 0.09	$F_{1,63}$ = 6.60 p = 0.01 $R^2_{\beta*}$ = 0.09	$F_{1,62}$ = 5.53 p = 0.02 $R^2_{\beta*}$ = 0.08
Depression	$F_{1,63}$ = 7.11 p = 0.01 $R^2_{\beta*}$ = 0.10	$F_{1,63}$ = 7.40 p = 0.008 $R^2_{\beta*}$ = 0.11	$F_{1,62}$ = 6.86 p = 0.01 $R^2_{\beta*}$ = 0.10
APOE status	$F_{1,63}$ = 2.38 p = 0.13	$F_{1,63}$ = 2.43 p = 0.12	$F_{1,62}$ = 1.90 p = 0.17

We then performed several sensitivity analyses using different quantifications of LC MRI signal intensity (cluster mean intensity, cluster peak intensity, and mean intensity within three equidistant LC sections), and we found similar associations using mean values within the middle-to-caudal cluster for both bilateral ($F_{1,63}$ = 4.43, p = 0.04, $R^2_{\beta*}$ = 0.07) and left LC ($F_{1,63}$ = 5.04, p = 0.03, $R^2_{\beta*}$ = 0.07). Peak intensity in the middle-to-caudal cluster also yielded comparable results for bilateral ($F_{1,63}$ = 5.17, p = 0.03, $R^2_{\beta*}$ = 0.08) and left LC ($F_{1,63}$ = 6.31, p = 0.01, $R^2_{\beta*}$ = 0.09). Finally, delineation of the LC in three equivalent segments further supports the specific associations between the caudal part of the LC and nocturnal awakenings for both the bilateral ($F_{1,62}$ = 4.15, p = 0.05, $R^2_{\beta*}$ = 0.06) and left LC ($F_{1,63}$ = 5.26, p = 0.03, $R^2_{\beta*}$ = 0.08). In our control analysis, we found no significant association between nocturnal awakenings and median PT values ($F_{1,63}$ = 0.91, p = 0.34), supporting specificity in the relationships observed above with LC intensity metrics.

Interactive effect with blood-based AD biomarkers

Finally, we investigated whether the relationships between LC intensity and nocturnal awakenings are modified by plasma AD biomarkers, and found that the negative relationship between middle-to-caudal LC intensity and nocturnal awakenings was particularly evident in individuals with higher levels of total tau ($F_{1,61}$ = 4.23, p = 0.04, $R^2_{\beta*}$ = 0.06, Fig. 3, Table 3). This interaction was predominantly present in the left hemisphere ($F_{1,61}$ = 4.26, p = 0.04, $R^2_{\beta*}$ = 0.07). No significant interaction was observed with any of the other plasma biomarkers (Supplementary Table 3).

Figure 3. Interactive effect of middle-to-caudal LC structural integrity and plasma total tau levels.

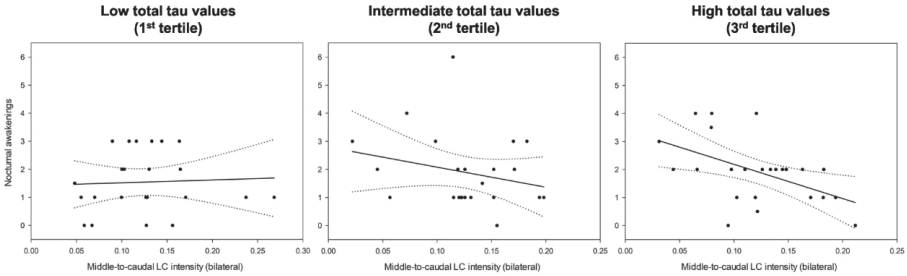

Note. The association between subjective reports of nocturnal awakenings and middle-to-caudal LC structural integrity is represented by tertiles of plasma total tau levels. Simple regression lines are used for a visual display and do not substitute the GLMM outputs. Dotted lines represent 95% confidence intervals of these simple regressions.

Table 3. GLMM outputs of the associations between subjective reports of nocturnal awakenings and the interaction term total tau*middle-to-caudal LC structural integrity, considered bilaterally (model 1), for left LC (model 2), and for right LC (model 3).

	Model 1	***Model 2***	***Model 3***
Total tau*middle-to-caudal LC integrity	$F_{1,61} = 4.23$ $p = 0.04$ $R^2_{\beta*} = 0.06$	$F_{1,61} = 4.26$ $p = 0.04$ $R^2_{\beta*} = 0.07$	$F_{1,59} = 1.96$ $p = 0.17$
Middle-to-caudal LC integrity	$F_{1,61} = 1.47$ $p = 0.23$	$F_{1,61} = 1.55$ $p = 0.22$	$F_{1,59} = 1.20$ $p = 0.28$
Total tau	$F_{1,61} = 3.12$ $p = 0.08$	$F_{1,61} = 3.17$ $p = 0.08$	$F_{1,59} = 1.05$ $p = 0.31$
Age	$F_{1,61} = 4.08$ $p = 0.05$	$F_{1,61} = 5.01$ $p = 0.03$ $R^2_{\beta*} = 0.08$	$F_{1,59} = 2.61$ $p = 0.11$
Sex	$F_{1,61} = 6.84$ $p = 0.01$ $R^2_{\beta*} = 0.10$	$F_{1,61} = 7.90$ $p = 0.007$ $R^2_{\beta*} = 0.11$	$F_{1,59} = 5.59$ $p = 0.02$ $R^2_{\beta*} = 0.09$
Depression	$F_{1,61} = 7.94$ $p = 0.007$ $R^2_{\beta*} = 0.12$	$F_{1,61} = 6.64$ $p = 0.01$ $R^2_{\beta*} = 0.10$	$F_{1,59} = 9.35$ $p = 0.003$ $R^2_{\beta*} = 0.14$
***APOE* status**	$F_{1,61} = 1.83$ $p = 0.18$	$F_{1,61} = 2.19$ $p = 0.14$	$F_{1,59} = 2.24$ $p = 0.14$

DISCUSSION

Sleep-wake disruption constitutes a hallmark of the aging process [28] and contributes to the unfolding of AD, as early as during the preclinical stages of the disease [29, 30]. Given the particular involvement of the LC in both sleep-wake mechanisms and initial AD pathogenesis, it may constitute a strong candidate as a neurobiological correlate of the sleep-wake dysregulation observed in the earliest stages of the disease. Here, we provide in vivo evidence that worse integrity of the middle-to-caudal LC structure is associated with increased number of self-reported nocturnal awakenings in cognitively unimpaired older individuals and that this relationship may be exacerbated in individuals with elevated levels of total tau in the plasma. These results expand on the important contribution of the LC to sleep-wake regulation and have implications for the early detection of sleep disturbances in older individuals at higher risk for dementia.

Our findings that LC structural integrity specifically relates to nocturnal awakenings, but not to a broader metric of sleep quality, corresponds to the role of the wake-promoting LC neurons as a critical component of the ascending arousal system to regulate arousal and wakefulness periods during sleep [9, 31]. While it may seem counterintuitive that worse LC integrity—possibly reflecting volumetric changes including shrinking of wake-promoting neurons—would be associated with an increased number of awakenings, we speculate that compensatory mechanisms are triggered within intact neurons leading to hyperactivity of the LC among the sleep-wake circuitry. Indeed, increased firing frequency and irregular firing patterns have been observed in the remaining neurons following neurotoxin-induced LC reduction in mice [32]. Accordingly, elevated levels of 3-methoxy-4-hydroxyphenylethyleneglycol (MHPG), the principal metabolite of norepinephrine, have been reported after experimental lesions of the LC in rats [33]. Moreover, several studies in humans have suggested that elevated MHPG constitutes a detrimental process contributing to AD-related pathological changes in the early stages of the disease [34,35,36,37]. In that context, we propose that dysregulated norepinephrine release due to aberrant LC activity during sleep, and especially when the LC neurons are supposed to be almost completely quiescent—such as during rapid eye movement sleep [38]—would lead to an imbalance in the interplay between wake- and sleep-promoting neurons [39, 40], resulting in more frequent and inappropriate awakenings.

Through a series of sensitivity analyses, we provided additional evidence that the associations between LC integrity and nocturnal awakenings arise specifically from the cluster-based middle-to-caudal part. Interestingly, a recent study reported similar regional associations between MRI-based assessments of LC structure and subjective measures of daytime dysfunction in 481 older men from the Vietnam Era Twin Study of Aging [22]. It is important to note that the caudal portion of the LC is known to be more difficult to accurately image due to its diffuse anatomical organization [21, 41]. As such, previous work has suggested that caudal sections of the LC on structural MR images likely correspond to the middle part of the actual LC [16]. Consistent with our observation of a stronger negative LC integrity-awakening relationship at elevated total tau levels, autopsy work reported that this middle portion of the LC structure exhibits greater vulnerability to tau accumulation in early Braak stages [42]. Future studies are warranted to replicate this topographical specificity and uncover a potential wakefulness-specific modular architecture in the LC [6]. Nevertheless, our control analysis revealed no significant relationship with MRI signal measured in a PT region-of-interest, located close to the LC. This supports the regional specificity of the LC in the observed associations, thereby reducing the likelihood of having grasped spurious correlations.

Our results suggest that the association between worse LC integrity and higher number of self-reported nocturnal awakenings is more marked in individuals with elevated levels of total tau in the plasma. However, we did not observe similar interactive effects with the more specific blood-based AD biomarkers of p-tau181, Aβ40, and Aβ42. Although plasma total tau values also encompass phosphorylated forms of tau protein, a recent meta-analysis of blood-based biomarkers suggested that total tau is rather a marker of neurodegeneration, with better ability to discriminate between AD patients and controls in studies using Simoa techniques compared to traditional ELISA methods [43]. Even though, based on autopsy studies, we would expect phosphorylated tau accumulation to contribute to the integrity values of our LC assessment, it is possible that the plasma p-tau181 in our cohort of healthy individuals may not be sensitive enough to the earliest tau pathological changes. Plasma p-tau231 has been recently put forward as a promising biomarker to discriminate individuals in early Braak stages and with sub-threshold Aβ markers [44], which cannot be achieved with p-tau181. Taking advantage of these recent, more sensitive plasma tau markers may therefore

reveal distinct associations, especially in studies of healthy older individuals. Our findings should thus be interpreted in the broader context of neuronal injury and increased risk for cognitive decline as well as incident dementia [45], including but not limited to AD.

Limitations

The strengths of our study include state-of-the-art investigation of the LC structure in vivo, using ultra-high field imaging combined with a data-driven approach to examine associations between nocturnal awakenings and fine-grained interindividual variability in LC morphology in cognitively unimpaired older individuals. However, our study also bears limitations. First, the cross-sectional approach restricts causal interpretation, although bidirectional relationships between sleep-wake disruption and LC alteration are likely at play [29]. While longitudinal observations can provide information about the temporal chain of events, interventional designs that interfere with sleep-wake regulation and/or LC activity are needed to address causality. In addition, previous studies reported a female vulnerability to AD pathology and AD-related cognitive decline [46, 47], and a recent review suggested a similar sex-specific vulnerability for the LC-norepinephrine system [48]. While we and others observed more subjective reports of nocturnal awakenings in women compared to men, we did not see sex differences in LC integrity measures, consistent with previous in vivo LC MRI studies in cognitively unimpaired individuals [16, 21, 49]. As the effect of sex may be differentially expressed along the clinical continuum of the disease [50], it will thus be important to further examine the relationships between sex-specific vulnerability to AD, sleep metrics, and LC integrity in populations including cognitively impaired individuals. Finally, future studies should include objective assessments of sleep-wake regulation, such as actigraphy or EEG recordings, alongside subjective measurements, to allow for refined quantification of sleep-wake metrics. This would also contribute to further identifying which characteristics of nocturnal awakenings (e.g., timing, duration) are most closely related to LC structural integrity.

Conclusions

We provide in vivo evidence that more frequent self-reported nocturnal awakenings are associated with worse structural integrity of the LC in cognitively unimpaired older individuals, particularly in those with elevated plasma markers of neurodegeneration. Thus, the investigation of sleep-wake disruption and LC structural integrity in aging may constitute interesting targets to identify individuals at higher risk of developing dementia and holds promises for preventive interventions mitigating the effect of sleep disturbances on brain physiology.

REFERENCES:

1 Van Egroo M, Narbutas J, Chylinski D, Villar González P, Maquet P, Salmon E, et al. *Sleep–wake regulation and the hallmarks of the pathogenesis of Alzheimer's disease*. Sleep. 2019;**42**:1–13https://academic.oup.com/sleep/article/doi/10.1093/sleep/zsz017/5289316.

2 Bubu OM, Brannick M, Mortimer J, Umasabor-Bubu O, Sebastião YV, Wen Y, et al. *Sleep, cognitive impairment, and Alzheimer's disease: a systematic review and meta-analysis*. Sleep. 2017;**40**:1–18.https://academic.oup.com/sleep/sleep/article/2661823/Sleep. https://doi.org/10.1093/sleep/zsw032.

3 Shi L, Chen S-J, Ma M-Y, Bao Y-P, Han Y, Wang Y-M, et al. *Sleep disturbances increase the risk of dementia: a systematic review and meta-analysis*. Sleep Med Rev. 2018;**40**:4–16 https://doi.org/10.1016/j.smrv.2017.06.010.

4. Braak H, Thal DR, Ghebremedhin E, Del Tredici K. *Stages of the pathologic process in Alzheimer disease: age categories from 1 to 100 years*. J Neuropathol Exp Neurol. 2011;**70**(11):960–9.https://academic.oup.com/jnen/article-lookup/doi/10.1097/NEN.0b013e318232a379.

5. Braak H, Del Tredici K. *The pathological process underlying Alzheimer's disease in individuals under thirty*. Acta Neuropathol. 2011;**121**(2):171–81. http://link.springer.com/10.1007/s00401-010-0789-4.

6. Poe GR, Foote S, Eschenko O, Johansen JP, Bouret S, Aston-Jones G, et al. *Locus coeruleus: a new look at the blue spot*. Nat Rev Neurosci. 2020;**21**(11): 644–59. https://doi.org/10.1038/s41583-020-0360-9.

7. Takahashi K, Kayama Y, Lin JS, Sakai K. *Locus coeruleus neuronal activity during the sleep-waking cycle in mice*. Neuroscience. 2010;**169**(3):1115–26. https://doi.org/10.1016/j.neuroscience.2010.06.009.

8. Hayat H, Regev N, Matosevich N, Sales A, Paredes-Rodriguez E, Krom AJ, et al. *Locus coeruleus norepinephrine activity mediates sensory-evoked awakenings from sleep*. Sci Adv. 2020;**6:**eaaz4232 https://advances.sciencemag.org/lookup/doi/10.1126/sciadv.aaz4232.

9. Carter ME, Yizhar O, Chikahisa S, Nguyen H, Adamantidis A, Nishino S, et al. *Tuning arousal with optogenetic modulation of locus coeruleus neurons*. Nat Neurosci. 2010;**13**(12):1526–33. http://www.nature.com/articles/nn.2682. https://doi.org/10.1038/nn.2682.

10. Zhu Y, Fenik P, Zhan G, Somach R, Xin R, Veasey S. *Intermittent short sleep results in lasting sleep wake disturbances and degeneration of locus coeruleus and orexinergic neurons*. Sleep. 2016;**39**:1601–11. https://aca demic.oup.com/sleep/article/39/8/1601/2706358. https://doi.org/10.5665/ sleep.6030.

11. Owen JE, Zhu Y, Fenik P, Zhan G, Bell P, Liu C, et al. *Late-in-life neurodegeneration after chronic sleep loss in young adult mice*. Sleep. 2021;**0**:1–14 https://doi.org/10.1080/07853890.2020.1840620.

12. Zhu Y, Zhan G, Fenik P, Brandes M, Bell P, Francois N, et al. *Chronic sleep disruption advances the temporal progression of tauopathy in P301S mutant mice*. J Neurosci. 2018;**38**(48):10255–70. http://www.jneurosci.org/ lookup/doi/10.1523/JNEUROSCI.0275-18.2018.

13. Oh J, Eser RA, Ehrenberg AJ, Morales D, Petersen C, Kudlacek J, et al. *Profound degeneration of wake-promoting neurons in Alzheimer's disease*. Alzheimer's Dement. 2019;**15**(10):1253–63. http://doi.wiley.com/10.1016/j.ja lz.2019.06.3916.

14. Eser RA, Ehrenberg AJ, Petersen C, Dunlop S, Mejia MB, Suemoto CK, et al. *Selective vulnerability of brainstem nuclei in distinct tauopathies: a postmortem study*. J Neuropathol Exp Neurol. 2018;**77**:149–61. http://academic.oup.com/jnen/article/77/2/149/4783105. https://doi.org/10.1093/jnen/ nlx113.

15. Carrier J, Viens I, Poirier G, Robillard R, Lafortune M, Vandewalle G, et al. *Sleep slow wave changes during the middle years of life*. Eur J Neurosci. 2011;**33**(4):758–66. http://doi.wiley.com/10.1111/j.1460-9568.2010.07543.x.

16. Liu KY, Acosta-Cabronero J, Cardenas-Blanco A, Loane C, Berry AJ, Betts MJ, et al. *In vivo visualization of age-related differences in the locus coeruleus*. Neurobiol Aging. 2019;**74**:101–11. https://linkinghub.elsevier.com/retrieve/pii/S0197458018303786. https://doi.org/10.1016/j.neurobiolaging.2018.10.014.

17. Betts MJ, Kirilina E, Otaduy MCG, Ivanov D, Acosta-Cabronero J, Callaghan MF, et al. *Locus coeruleus imaging as a biomarker for noradrenergic dysfunction in neurodegenerative diseases*. Brain. 2019;**142**:2558–71. https://academic.oup.com/brain/article/142/9/2558/5536581. https://doi.org/10.1093/brain/awz193.

18. Priovoulos N, Jacobs HIL, Ivanov D, Uludağ K, Verhey FRJ, Poser BA. *Highresolution in vivo imaging of human locus coeruleus by magnetization transfer MRI at 3T and 7T*. Neuroimage. 2018;**168**:427–36. https://linkinghub.elsevier.com/retrieve/pii/S1053811917306134. https://doi.org/10.1016/j.neuroimage.2017.07.045.

19. Jacobs HIL, Priovoulos N, Poser BA, Pagen LHG, Ivanov D, Verhey FRJ, et al. *Dynamic behavior of the locus coeruleus during arousal-related memory processing in a multi-modal 7T fMRI paradigm*. Elife. 2020;**9**:1–30. https://elifesciences.org/articles/52059. https://doi.org/10.7554/eLife.52059.

20. Priovoulos N, van Boxel SCJ, Jacobs HIL, Poser BA, Uludag K, Verhey FRJ, et al. *Unraveling the contributions to the neuromelanin-MRI contrast*. Brain Struct Funct. 2020;**225**(9):2757–74. http://link.springer.com/10.1007/s00429-020-02153-z.

21. Betts MJ, Cardenas-Blanco A, Kanowski M, Jessen F, Düzel E. *In vivo MRI assessment of the human locus coeruleus along its rostrocaudal extent in young and older adults*. Neuroimage. 2017;**163**:150–9 https://doi.org/10.1016/j.neuroimage.2017.09.042.

22. Elman JA, Puckett OK, Beck A, Fennema-Notestine C, Cross LK, Dale AM, et al. *MRI-assessed locus coeruleus integrity is heritable and associated with multiple cognitive domains, mild cognitive impairment, and daytime dysfunction*. Alzheimer's Dement. 2021:alz.**12261** https://onlinelibrary.wiley.com/doi/10.1002/alz.12261.

23. Meijman TF, Thunnissen MJ, de Vries-Griever AGH. *The after-effects of a prolonged period of day-sleep on subjective sleep quality*. Work Stress. 1990;**4**(1):65–70. http://www.tandfonline.com/doi/abs/10.1080/02678379008256965.

24. Hamilton M. *A rating scale for depression*. J Neurol Neurosurg Psychiatry. 1960;**23**(1):56–62. https://jnnp.bmj.com/lookup/doi/10.1136/jnnp.23.1.56.

25. Jaeger BC, Edwards LJ, Das K, Sen PK. *An R2 statistic for fixed effects in the generalized linear mixed model*. J Appl Stat. 2017;**44**(6):1086–105. https://www.tandfonline.com/doi/full/10.1080/02664763.2016.1193725.

26. Thijssen EH, La Joie R, Wolf A, Strom A, Wang P, Iaccarino L, et al. *Diagnostic value of plasma phosphorylated tau181 in Alzheimer's disease and frontotemporal lobar degeneration*. Nat Med. 2020;**26**(3):387–97. http://www.nature.com/articles/s41591-020-0762-2. https://doi.org/10.1038/s41591-020-0762-2.

27. de Wolf F, Ghanbari M, Licher S, McRae-McKee K, Gras L, Weverling GJ, et al. *Plasma tau, neurofilament light chain and amyloid-β levels and risk of dementia; a population-based cohort study*. Brain. 2020;**143**:1220–32. https://academic.oup.com/brain/article/143/4/1220/5811096. https://doi.org/10.1093/brain/awaa054.

28. Mander BA, Winer JR, Walker MP. *Sleep and human aging*. Neuron. 2017;**94**(1):19–36. https://doi.org/10.1016/j.neuron.2017.02.004.

29. Wang C, Holtzman DM. *Bidirectional relationship between sleep and Alzheimer's disease: role of amyloid, tau, and other factors. Neuropsychopharmacology*. 2020;**45**(1):104–20. https://doi.org/10.1038/s41386-019-0478-5.

30. Musiek ES, Bhimasani M, Zangrilli MA, Morris JC, Holtzman DM, Ju Y-ES. *Circadian rest-activity pattern changes in aging and preclinical Alzheimer disease*. JAMA Neurol. 2018;**75**(5):582. http://archneur.jamanetwork.com/article.aspx?doi=10.1001/jamaneurol.2017.4719–90.

31. Scammell TE, Arrigoni E, Lipton JO. *Neural circuitry of wakefulness and sleep*. Neuron. 2017;**93**(4):747–65. Cell Press. https://linkinghub.elsevier.com/retrieve/pii/S0896627317300387. https://doi.org/10.1016/j.neuron.2017.01.014.

32. Szot P, Franklin A, Miguelez C, Wang Y, Vidaurrazaga I, Ugedo L, et al. *Depressive-like behavior observed with a minimal loss of locus coeruleus (LC) neurons following administration of 6-hydroxydopamine is associated with electrophysiological changes and reversed with precursors of norepinephrine*. Neuropharmacology. 2016;101:**76**–86 https://doi.org/10.1016/j.neuropharm.2015.09.003.

33. Abercrombie E, Zigmond M. *Partial injury to central noradrenergic neurons: reduction of tissue norepinephrine content is greater than reduction of extracellular norepinephrine measured by microdialysis*. J Neurosci. 1989;**9**(11):4062–7. https://www.jneurosci.org/lookup/doi/10.1523/JNEUROSCI.09-11-04062.1989.

34. Palmer AM, Wilcock GK, Esiri MM, Francis PT, Bowen DM. *Monoaminergic innervation of the frontal and temporal lobes in Alzheimer's disease*. Brain Res. 1987;**401**(2):231–8. https://linkinghub.elsevier.com/retrieve/pii/0006899387914089. https://doi.org/10.1016/0006-8993(87)91408-9.

35. Hoogendijk WJG, Feenstra MGP, Botterblom MHA, Gilhuis J, Sommer IEC, Kamphorst W, et al. *Increased activity of surviving locus ceruleus neurons in Alzheimer's disease*. Ann Neurol. 1999;**45**(1):82–91. https://onlinelibrary.wiley.com/doi/10.1002/1531-8249(199901)45:1%3C82::AID-ART14%3E3.0.CO;2-T.

36. Riphagen JM, van Egroo M, Jacobs HIL. *Elevated norepinephrine metabolism gauges Alzheimer's disease-related pathology and memory decline*. J Alzheimer's Dis. 2021;**80**(2):521–6. https://www.medra.org/servlet/aliasResolver?alias=iospress&doi=10.3233/JAD-201411.

37. Jacobs HIL, Riphagen JM, Ramakers IHGB, Verhey FRJ. *Alzheimer's disease pathology: pathways between central norepinephrine activity, memory, and neuropsychiatric symptoms*. Mol Psychiatry. 2021;**26**(3):897–906. https://doi.org/10.1038/s41380-019-0437-x.

38. Van Someren EJW. *Brain mechanisms of insomnia: new perspectives on causes and consequences*. Physiol Rev. 2020;**51**:physrev.00046.2019 https://journals.physiology.org/doi/10.1152/physrev.00046.2019.

39. Oh J, Petersen C, Walsh CM, Bittencourt JC, Neylan TC, Grinberg LT. *The role of co-neurotransmitters in sleep and wake regulation*. Mol Psychiatry. 2019;**24**(9):1284–95. https://doi.org/10.1038/s41380-018-0291-2.

40. Saper CB, Fuller PM. *Wake–sleep circuitry: an overview*. Curr Opin Neurobiol. 2017;**44**:186–92. https://linkinghub.elsevier.com/retrieve/pii/S095943881630246X. https://doi.org/10.1016/j.conb.2017.03.021.

41. Mäki-Marttunen V, Espeseth T. *Uncovering the locus coeruleus: comparison of localization methods for functional analysis*. Neuroimage. 2021;**224**:117409. https://linkinghub.elsevier.com/retrieve/pii/S1053811920308946. https://doi.org/10.1016/j.neuroimage.2020.117409.

42. Ehrenberg AJ, Nguy AK, Theofilas P, Dunlop S, Suemoto CK, Di Lorenzo Alho AT, et al. *Quantifying the accretion of hyperphosphorylated tau in the locus coeruleus and dorsal raphe nucleus: the pathological building blocks of early Alzheimer's disease*. Neuropathol Appl Neurobiol. 2017;**43**(5):393–408. http://doi.wiley.com/10.1111/nan.12387.

43. Koychev I, Jansen K, Dette A, Shi L, Holling H. *Blood-based ATN biomarkers of Alzheimer's disease: a meta-analysis*. J Alzheimer's Dis. 2021;**79**(1):177–95. https://www.medra.org/servlet/aliasResolver?alias=iospress&doi=10.3233/JAD-200900.

44. Ashton NJ, Pascoal TA, Karikari TK, Benedet AL, Lantero-Rodriguez J, Brinkmalm G, et al. *Plasma p-tau231: a new biomarker for incipient Alzheimer's disease pathology*. Acta Neuropathol. 2021;**141**(5):709–24. https://doi.org/10.1007/s00401-021-02275-6.

45. Pase MP, Beiser AS, Himali JJ, Satizabal CL, Aparicio HJ, DeCarli C, et al. *Assessment of plasma total tau level as a predictive biomarker for dementia and related endophenotypes*. JAMA Neurol. 2019;**76**(5):598. http://archneur.jamanetwork.com/article.aspx?doi=10.1001/jamaneurol.2018.4666–606.

46. Buckley RF, Mormino EC, Rabin JS, Hohman TJ, Landau S, Hanseeuw BJ, et al. *Sex Differences in the association of global amyloid and regional tau deposition measured by positron emission tomography in clinically normal older adults*. JAMA Neurol. 2019;**76**(5):542. http://archneur.jamanetwork.com/article.aspx?doi=10.1001/jamaneurol.2018.4693–51.

47. Koran MEI, Wagener M, Hohman TJ. *Sex differences in the association between AD biomarkers and cognitive decline*. Brain Imaging Behav. 2017;**11**(1):205–13. http://link.springer.com/10.1007/s11682-016-9523-8.

48. Luckey AM, Robertson IH, Lawlor B, Mohan A, Vanneste S. *Sex differences in locus coeruleus: a heuristic approach that may explain the increased risk of Alzheimer's disease in females*. J Alzheimers Dis. 2021;**83**(2):1–18. https://www.medra.org/servlet/aliasResolver?alias=iospress&doi=10.3233/JAD-210404.

49. Trujillo P, Petersen KJ, Cronin MJ, Lin Y-C, Kang H, Donahue MJ, et al. *Quantitative magnetization transfer imaging of the human locus coeruleus*. Neuroimage. 2019;**200**:191–8 https://doi.org/10.1016/j.neuroimage.2019.06.049.

50. Ungar L, Altmann A, Greicius MD. *Apolipoprotein E, gender, and Alzheimer's disease: an overlooked, but potent and promising interaction*. Brain Imaging Behav. 2014;**8(**2):262–73. http://link.springer.com/10.1007/s11682-013-9272-x.

SUPPLEMENTARY MATERIAL

Supplementary methods

Ultra-high field MRI acquisition procedure

MRI data were acquired on a 7T Magnetom Siemens scanner (Siemens Healthineers, Erlangen, Germany). with a 32-channel head coil (Nova Medical, Wilmington, MA, USA). A whole-brain Magnetization Prepared 2 Rapid Acquisition Gradient Echoes (MP2RAGE[1]; TR = 5000 ms, TE = 2.47 ms, flip angle = 5°/3°, voxel size = 0.7 mm^3, number of slices = 240) sequence was first acquired. Then, we performed an in-house developed magnetization transfer-weighted turbo flash (MT-TFL) sequence (TR = 538 ms, TE = 4.08, flip angle = 8°, voxel size = 0.4x0.4x0.5mm, number of slices = 60) with a field-of-view placed perpendicular to the pons and covering the area between the inferior colliculus and the inferior border of the pons. This sequence has been established to be particularly sensitive to LC-related contrast[2,3], likely reflecting its neuronal and fiber projection density[4].

LC MRI processing pipeline

Our 7T LC MRI processing pipeline involved the following steps: first, individual MT-TFL images were intensity-normalized by dividing by the subject-specific mean intensity of a 10x10 voxel region-of-interest in the pontine tegmentum (PT). For each participant, the PT region-of-interest was consistently placed in the axial slice which contained the highest intensity LC voxel. Importantly, no association was found between age and mean intensity in the PT, supporting that no age-related biases would be introduced by this normalization step. Second, a study-specific template was built from these individual intensity-normalized MT-TFL images using the *buildtemplateparallel* function from the Advanced Normalization Tools (ANTs)[5] (transformation model and similarity metric used for registration = greedy SyN with cross-correlation). The LC was then manually delineated on the resulting template, based on voxel intensities and the anatomical properties of the LC. The LC mask was then applied on each individual intensity-normalized MT-TFL images registered to the study-specific template. Finally, median signal intensity across each slice along the vertical axis of the LC structure was extracted on a per hemisphere basis by applying the LC mask on individual intensity- and spatially-normalized images.

Supplementary Table 1. GLMM outputs of the associations between plasma biomarkers and subjective measures of sleep quality or nocturnal awakenings.

	Total tau		***p-Tau 181***	
Age	$F_{1,65} = 0.37$ $p = 0.54$	$F_{1,65} = 0.39$ $p = 0.53$	$F_{1,65} = 8.28$ $p = 0.005$ $R^2_{\beta*} = 0.11$	$F_{1,65} = 9.47$ $p = 0.003$ $R^2_{\beta*} = 0.13$
Sex	$F_{1,65} = 1.02$ $p = 0.32$	$F_{1,65} = 0.88$ $p = 0.35$	$F_{1,65} = 2.17$ $p = 0.15$	$F_{1,65} = 0.48$ $p = 0.49$
APOE status	$F_{1,65} = 1.31$ $p = 0.26$	$F_{1,65} = 1.23$ $p = 0.27$	$F_{1,65} = 3.54$ $p = 0.07$	$F_{1,65} = 4.14$ $p = 0.05$
Subjective sleep quality	$F_{1,65} = 0.01$ $p = 0.93$		$F_{1,65} = 1.81$ $p = 0.18$	
Nocturnal awakenings		$F_{1,65} = 0.02$ $p = 0.89$		$F_{1,65} = 1.56$ $p = 0.22$
	Aβ40		***Aβ42***	
Age	$F_{1,65} = 12.44$ $p < 0.001$ $R^2_{\beta*} = 0.16$	$F_{1,65} = 11.45$ $p = 0.001$ $R^2_{\beta*} = 0.15$	$F_{1,65} = 0.01$ $p = 0.95$	$F_{1,65} = 0.01$ $p = 0.98$
Sex	$F_{1,65} = 2.64$ $p = 0.11$	$F_{1,65} = 3.87$ $p = 0.05$	$F_{1,65} = 1.14$ $p = 0.29$	$F_{1,65} = 1.20$ $p = 0.28$
APOE status	$F_{1,65} = 1.37$ $p = 0.25$	$F_{1,65} = 1.41$ $p = 0.24$	$F_{1,65} = 10.31$ $p = 0.002$ $R^2_{\beta*} = 0.14$	$F_{1,65} = 10.65$ $p = 0.002$ $R^2_{\beta*} = 0.14$
Subjective sleep quality	$F_{1,65} = 0.75$ $p = 0.39$		$F_{1,65} = 0.19$ $p = 0.66$	
Nocturnal awakenings		$F_{1,65} = 0.09$ $p = 0.76$		$F_{1,65} = 0.09$ $p = 0.76$

Supplementary Table 2. GLMM outputs of the associations between subjective sleep quality (GSQS scores) and middle-to-caudal (top) or middle-to-rostral (bottom) LC structural integrity, considered bilaterally (model 1), for left LC (model 2), and for right LC (model 3).

	Model 1	***Model 2***	***Model 3***
Middle-to-caudal LC integrity	$F_{1,63} = 0.65$ $p_{FDR} = 0.63$	$F_{1,63} = 0.69$ $p_{FDR} = 0.63$	$F_{1,61} = 0.23$ $p_{FDR} = 0.63$
Age	$F_{1,63} = 0.01$ $p = 0.098$	$F_{1,63} = 0.01$ $p = 0.93$	$F_{1,61} = 0.03$ $p = 0.85$
Sex	$F_{1,63} = 5.12$ $p = 0.03$ $R^2_{\beta*} = 0.08$	$F_{1,63} = 5.32$ $p = 0.02$ $R^2_{\beta*} = 0.08$	$F_{1,61} = 4.89$ $p = 0.03$ $R^2_{\beta*} = 0.07$
Depression	$F_{1,63} = 25.31$ $p < 0.0001$ $R^2_{\beta*} = 0.29$	$F_{1,63} = 24.69$ $p < 0.0001$ $R^2_{\beta*} = 0.28$	$F_{1,61} = 24.11$ $p < 0.0001$ $R^2_{\beta*} = 0.28$
APOE status	$F_{1,63} = 0.01$ $p = 0.99$	$F_{1,63} = 0.01$ $p = 0.99$	$F_{1,61} = 0.02$ $p = 0.90$
Middle-to-rostral LC integrity	$F_{1,63} = 0.09$ $p_{FDR} = 0.90$	$F_{1,63} = 0.01$ $p_{FDR} = 0.90$	$F_{1,62} = 0.06$ $p_{FDR} = 0.90$
Age	$F_{1,63} = 0.01$ $p = 0.98$	$F_{1,63} = 0.01$ $p = 0.99$	$F_{1,62} = 0.02$ $p = 0.89$
Sex	$F_{1,63} = 4.39$ $p = 0.04$ $R^2_{\beta*} = 0.07$	$F_{1,63} = 4.64$ $p = 0.04$ $R^2_{\beta*} = 0.07$	$F_{1,62} = 5.05$ $p = 0.03$ $R^2_{\beta*} = 0.08$
Depression	$F_{1,63} = 25.26$ $p < 0.0001$ $R^2_{\beta*} = 0.29$	$F_{1,63} = 25.05$ $p < 0.0001$ $R^2_{\beta*} = 0.28$	$F_{1,62} = 24.33$ $p < 0.0001$ $R^2_{\beta*} = 0.28$
APOE status	$F_{1,63} = 0.01$ $p = 0.97$	$F_{1,63} = 0.01$ $p = 0.97$	$F_{1,62} = 0.01$ $p = 0.9$

Supplementary Table 3. GLMM outputs of the associations between subjective reports of nocturnal awakenings and the interaction term plasma biomarker*middle-to-caudal LC structural integrity, considered bilaterally.

	P-tau 181	***Aβ40***	***Aβ42***
Plasma marker*Middle-to-caudal LC integrity	$F_{1,61} = 0.21$ $p = 0.65$	$F_{1,61} = 0.02$ $p = 0.89$	$F_{1,61} = 0.08$ $p = 0.78$
Middle-to-caudal LC integrity	$F_{1,61} = 1.44$ $p = 0.23$	$F_{1,61} = 0.16$ $p = 0.69$	$F_{1,61} = 0.40$ $p = 0.53$
Plasma marker	$F_{1,61} = 0.75$ $p = 0.39$	$F_{1,61} = 0.01$ $p = 0.99$	$F_{1,61} = 0.04$ $p = 0.85$
Age	$F_{1,61} = 3.66$ $p = 0.06$	$F_{1,61} = 1.39$ $p = 0.24$	$F_{1,61} = 2.35$ $p = 0.13$
Sex	$F_{1,61} = 6.83$ $p = 0.01$ $R^2_{\beta*} = 0.10$	$F_{1,61} = 7.54$ $p = 0.008$ $R^2_{\beta*} = 0.11$	$F_{1,61} = 7.41$ $p = 0.008$ $R^2_{\beta*} = 0.11$
Depression	$F_{1,61} = 9.19$ $p = 0.004$ $R^2_{\beta*} = 0.13$	$F_{1,61} = 8.13$ $p = 0.006$ $R^2_{\beta*} = 0.12$	$F_{1,61} = 8.11$ $p = 0.006$ $R^2_{\beta*} = 0.12$
APOE status	$F_{1,61} = 2.32$ $p = 0.13$	$F_{1,61} = 1.50$ $p = 0.23$	$F_{1,61} = 1.41$ $p = 0.24$

Supplementary Figure 1. 7T LC MRI pre-processing pipeline. See **Supplementary Methods** for a full description of acquisition and pre-processing steps. The red square illustrates, for a representative participant, the 10x10 voxel region-of-interest located in the pontine tegmentum and used for subject-specific normalization of MRI signal intensity.

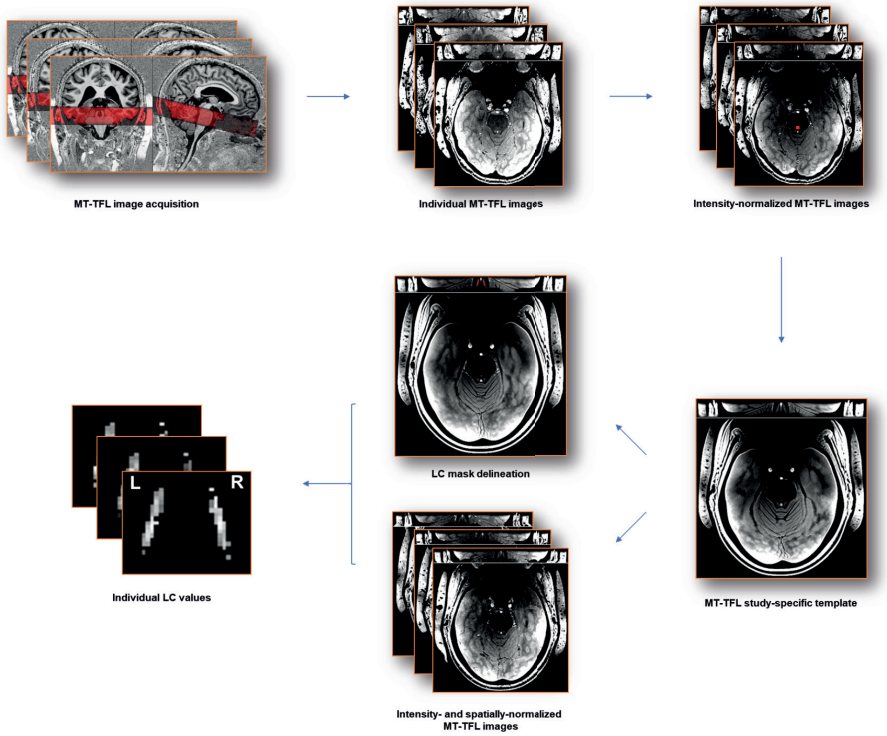

Supplementary Figure 2. *APOE* status vs. plasma biomarkers. * $p < 0.05$. After adjusting for age and sex, *APOE* ε4 carriers (29% of the sample) displayed significantly lower plasma levels of $A\beta_{42}$ ($F_{1,66}$=10.48, p=0.002, $R^2_{\beta*=0.14)}$ and at-trend level higher plasma levels of p-tau_{181} ($F_{1,66}$=3.44, p=0.07).

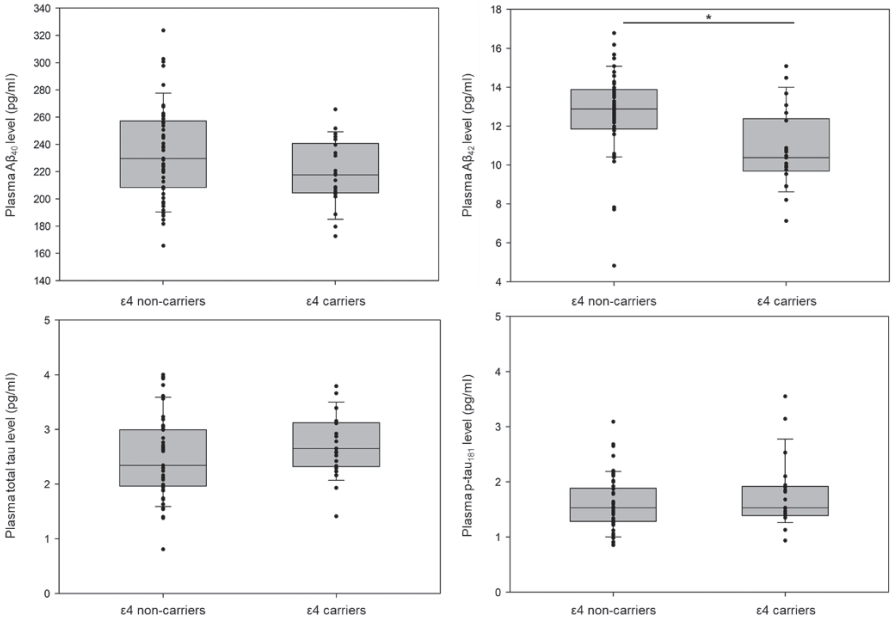

Supplementary Figure 3. Subjective sleep metrics vs. plasma biomarkers. Subjective sleep quality (GSQS score).

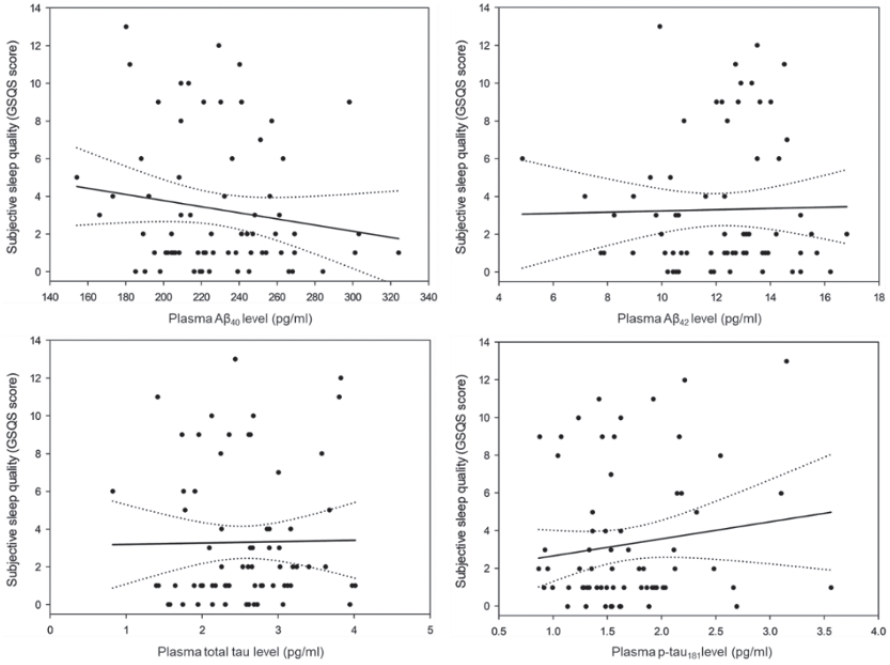

Self-reported nocturnal awakenings

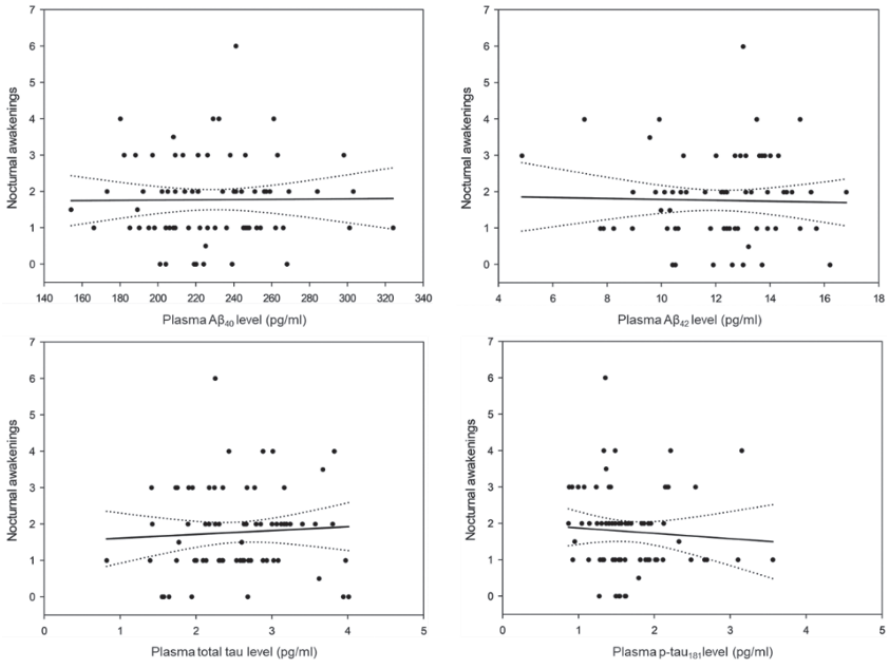

Supplementary References:

1. Marques JP, Kober T, Krueger G, van der Zwaag W, Van de Moortele P-F, Gruetter R. *MP2RAGE, a self bias-field corrected sequence for improved segmentation and T1-mapping at high field.* Neuroimage. 2010;49(2):1271-1281. doi:10.1016/j.neuroimage.2009.10.002
2. Priovoulos N, Jacobs HIL, Ivanov D, Uludağ K, Verhey FRJ, Poser BA. *High-resolution in vivo imaging of human locus coeruleus by magnetization transfer MRI at 3T and 7T.* Neuroimage. 2018;168:427-436. doi:10.1016/j.neuroimage.2017.07.045
3. Jacobs HIL, Priovoulos N, Poser BA, et al. *Dynamic behavior of the locus coeruleus during arousal-related memory processing in a multi-modal 7T fMRI paradigm.* Elife. 2020;9:1-30. doi:10.7554/eLife.52059
4. Priovoulos N, van Boxel SCJ, Jacobs HIL, et al. *Unraveling the contributions to the neuromelanin-MRI contrast.* Brain Struct Funct. 2020;1(0123456789):3. doi:10.1007/s00429-020-02153-z
5. Avants BB, Yushkevich P, Pluta J, et al. *The optimal template effect in hippocampus studies of diseased populations*. Neuroimage. 2010;49(3):2457-2466. doi:10.1016/j.neuroimage.2009.09.062


UM

GENERAL DISCUSSION

CHAPTER 7

RATIONALE

Alzheimer's disease (AD) is the most common cause of dementia [1]. By the time the clinical symptoms of AD emerge [2], the AD pathophysiological process has been evolving for decades [3], suggesting the existence of a preclinical AD phase [4]. The pathophysiological process of AD has been characterized by its hallmark proteinopathies, amyloid-beta (Aβ) plaques and neurofibrillary tau tangles [4-6]. Aβ and tau pathology each have their own unique temporal and topological pattern of progression in the brain, as described in the seminal Thal and Braak stages, respectively; Aβ pathology is first deposited in the associative areas of the neocortex up to 30 years before the onset of clinical symptoms and tau pathology is assumed to be first found in the locus coeruleus (LC) as early as the first decades of life (**footnote A** in **chapter 1**) [7-10]. Specifically, evidence suggests that while Aβ and tau can stimulate each other's neurotoxic properties, tau pathology is more closely associated with neurodegeneration and cognitive deficits [5, 6, 11-14]. The long delay between the first depositions of AD pathology and the onset of clinical symptoms suggests that significant and irreversible neurodegeneration has likely already occurred at the time of diagnosis [3]. Disease-modifying treatments in the clinical phase may therefore occur too late in the AD pathophysiological process [15, 16]. Furthermore, we know from autopsy studies that the deposition of AD pathologies starts before in vivo measurements of Aβ and tau pathology reach the clinical cerebrospinal fluid (CSF) or positron emission tomography detection (PET) thresholds used for the identification of preclinical AD [3, 4] (figure 1 in **chapter 1**). **Therefore, identifying additional *in vivo* pathways for the early recognition of processes related to Aβ and tau pathology, potentially before the preclinical stage, may improve participant selection for clinical trials targeting the earliest stages of the disease.**

OUR KEY FINDINGS

Figure 1. In this hypothetical model, we summarize a possible mechanistic framework for the early pathophysiological processes of AD in the context of the literature and our findings.

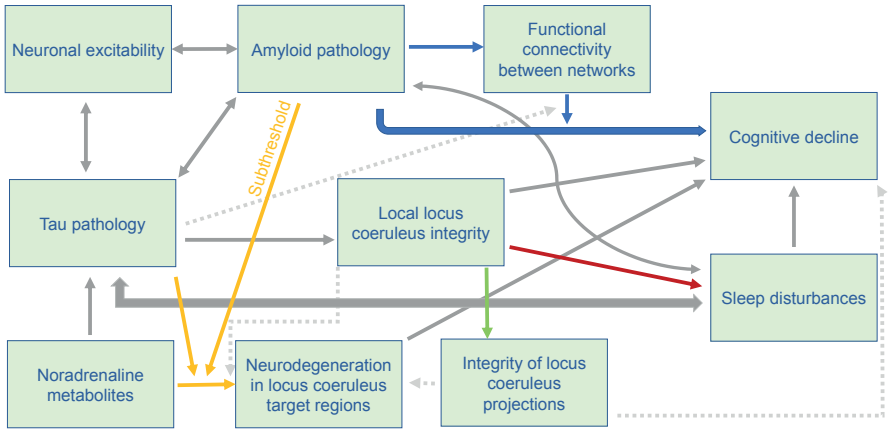

Note. *The purpose of this model is only to highlight the relationships most relevant for the work described here and it is not meant to be exhaustive. The colored arrows indicate the relationships investigated in each corresponding chapter in the legend.*

In vivo MRI markers are modified by AD pathology, potentially in early stages of the disease. Specific MRI features can provide additional information to the early AD-related cognitive and behavioral characteristics, and this information may facilitate patient selection in clinical trials.

Increased levels of neuronal activity are associated with a heightened release of Aβ in mice, indicating that neuronal hyperactivity may play a role in the formation and propagation of this pathology [17]. Importantly, this association may be bi-directional as Aβ has also been shown to drive neuronal hyperactivity [18]. Furthermore, converging evidence in humans suggests that Aβ preferentially accumulates in topographic hubs of functional brain networks that display a high level of baseline activity [19, 20] and that the organization within and between these networks supports cognitive functioning [21-25]. The functional organization of these networks can be investigated in vivo using resting-state functional magnetic resonance imaging (rs-fMRI) as fMRI can measure localized changes in the blood-oxygen level dependent (BOLD) signal, which is coupled to the underlying

neuronal activity [26]. By observing the temporal correlations of changes in the BOLD signal at rest between anatomical hubs of the networks, we can determine the functional connectivity of these networks [27] (**footnote C** in **chapter 1**). Importantly, functional connectivity patterns within and between these networks is altered as a function of Aβ burden, already in cognitively normal adults [28], and patterns within these networks work synergistically with Aβ burden to predict cognitive decline [22]. Furthermore, a dose-response relationship between Aβ and cognition has been reported in cognitively normal adults [29]. *We investigated whether functional connectivity between these large-scale networks is associated with Aβ burden and whether this connectivity conveys information about the Aβ-related rate of cognitive decline (**chapter 2**).*

We found that patterns of inter-network functional connectivity differed depending on the level of Aβ burden, and that the pattern of inter-network connectivity predicted memory decline in an Aβ dose-dependent manner (**figure 1, blue arrows**). Specifically, in the cognitively healthy group, we found that when the temporal correlations between the activation of large-scale brain networks at rest were negative, higher Aβ burden was associated with greater memory decline. However, when inter-network correlations were positive, there was no association between Aβ burden and memory decline. We posit that in the context of accumulating Aβ pathology, cognitively healthy participants with positive inter-network correlations display compensation mechanisms to stave off memory decline that may involve the reconfiguration of large-scale networks [30]. These findings suggest that information about the functional organization between large-scale networks adds additional information about the rate of Aβ-related cognitive decline in preclinical groups and may be used to optimize patient selection in clinical trials. Our power analyses show that sample sizes required to assess efficacy in clinical trials aiming to slow down memory decline by 30% may be reduced by up to 88% with the combined information from functional inter-network connectivity and Aβ burden.

Shifting our focus towards tau as the other hallmark AD proteinopathy, human histology work has shown that the LC is one of the initial sites of aberrant tau accumulation in the brain and the LC shows volume loss in the earliest Braak stages [9, 31] (**footnote A** in **chapter 1**). Furthermore, the LC has widespread projections towards the rest of the brain and is the main source of cerebral NA [32]. Although NA has neuroprotective properties [33], previous research suggests excessive overturn of NA as reflected in the NA metabolite MHPG may occur in

AD [34, 35]. Furthermore, the DOPEGAL metabolite upstream of MHPG in the NA metabolic pathway has been shown to contribute to the production of aggregation- and propagation-prone tau [36, 37], suggesting the LC-NA system may be a catalyst in the spreading of aberrant tau pathology. *We investigated whether these elevations are also associated with downstream effects of tau on brain structure* ***(chapter 3).***

We established that elevated MHPG, together with worse Aβ and tau burden, is associated with neurodegenerative measures in target sites of the LC, including cortical regions and the hippocampus. This association starts at subclinical Aβ levels (**figure 1, orange arrows**) and implies involvement of the LC-NA system in early AD pathophysiological processes.

The LC also modulates cognitive functions and plays an important role in and the sleep-wake cycle [38-42]. Sleep disturbances occur early in life [43] and constitute a risk factor for cognitive decline and (preclinical) AD later in life [44, 45]. Furthermore, sleep is linked to clearance of metabolites like Aβ and tau from the brain [46, 47], Disturbed sleep may therefore lead to a feedback loop, whereby neurodegeneration resulting from the reduced clearance of AD pathology leads to further increased sleep disturbances [48]. Furthermore, animal studies have shown that disturbed sleep induces an acceleration of tauopathy in the LC [49]. Given the predisposition of the LC to early tau pathology and associated volume loss [9, 50] and the important role of the LC in the regulation of sleep and wakefulness [40-42], the combined information about the structural integrity of the LC and sleep disturbances may contain valuable information about early processes related to AD pathology. *We investigated whether we can establish a link between LC degeneration, AD pathology and sleep quality in vivo (****chapter 6****).*

We show that in cognitively healthy individuals, in vivo MRI markers of LC integrity are associated with early behavioral symptoms in the form of increased self-reported nocturnal awakenings (**figure 1, red arrow**), and that this association is particularly strong in the presence of tau pathology. These findings suggest that MRI-based integrity of the LC constitutes an in vivo neurobiological correlate of sleep-wake regulation in preclinical AD. Given that both sleep disturbances and lower LC integrity constitute a risk factor for cognitive decline and AD pathology [51], the combined knowledge about nocturnal awakenings and in vivo LC integrity may help identify individuals at-risk for clinical trials aiming to improve sleep consolidation in the context of AD-related processes.

Furthermore, while direct visualization of the LC in vivo is challenging, modern

MRI developments from our lab allowed us visualize the LC at ultra-high resolution using 7 Tesla MRI scanners utilizing a specialized LC signal-sensitive MRI sequence [52] (**figure 3** in **chapter 1**). This signal has been generally interpreted as a proxy measure of LC integrity [53-57] and recent work indicated converging evidence (**footnote** F **in chapter 1**) between autopsy LC tau tangle density and MRI-based LC integrity, suggesting that LC integrity may signal early tau-related processes [51]. Interestingly, autopsy data reveals volume loss as early as Braak stage a-c, but shows no neuronal loss until Braak stage IV [31] (**Footnote A** in **chapter 1**). It is unclear whether this volume loss may reflect other morphological changes, such as the loss of dendritic arborization or density of projections towards the rest of the brain. The fact that LC integrity was able to correlate early with tau pathology may indicate that LC integrity reflects some of these early morphological changes. *Therefore, we investigated the microstructural correlates of LC integrity to better understand the biological process underlying LC volume loss in preclinical AD (**chapter 4**).* To this end, we use correlational tractography and Neurite Density and Dispersion Orientation imaging [58, 59] (**Footnote G** in **chapter 1**) to investigate the association between LC integrity and microstructural properties of the LC and its projections.

We show that LC integrity is associated with microstructural properties of LC projections to the cortex and cerebellum in a cognitively healthy population (**figure 1, green arrow**). Specifically, we showed that higher MRI-based LC integrity was associated with higher quantitative anisotropy in tracts originating from the LC. These findings suggest that axonal integrity, rather than neurite density or arborization in the LC itself is associated with in vivo measurements of LC integrity. This finding is supported by animal research suggesting that LC projections are affected in early AD model rats before LC neurons themselves show significant deterioration [60] and can be explained by the characteristic vulnerability of the long and poorly myelinated LC axons [32, 61]. Therefore, we conclude that the earliest stages of LC-related neurodegeneration in preclinical AD are likely reflected in MRI measures of LC integrity. This may also tie into our findings from **chapter 3** where we report that AD pathology and metabolites of the LC-NA system are linked to neurodegenerative measures in LC target sites. We speculate that the deterioration of LC projections may be involved in neurodegenerative processes at LC target sites, though this remains to be confirmed.

Finally, LC imaging is a relatively new field where new methods are continuously emerging and researchers are using different approaches to define the LC on MRI images. Diverging findings have been reported about the association between

aging and LC integrity [51, 62-65], and while differences in sample characteristics and MRI field strength may account for some of these discrepancies, it is unclear to what extent the approach to LC delineation may influence these results. *As a first step in order to evaluate and harmonize these efforts, we compared the validity and reliability of several approaches to LC delineation (**chapter 5**).*

We show that template-based approaches for LC delineation, particularly study-specific templates, have the potential to be a powerful tool for reliable LC delineation. When compared to a manual delineation approach, the template-based approaches showed considerably higher reliability scores across the bilateral LC. However, template-based approaches remain vulnerable to registration issues and we recommend further refinement of template-creation pipelines and careful manual quality checks on all registrations.

Methodological limitations and considerations

- In **chapters 4, 5,** and **6**, we draw our data from a cohort of participants from the STRAIN study, representing the adult age span in the general population. While this is a major strength of these chapters, there are also limitations that need to be considered. Our strict exclusion criteria for the STRAIN study preclude the use of psychoactive medication, moderate to severe visual impairments and any contraindications for scanning at the 7T MRI, including the presence of large protheses or implants. This is inherent to these types of research, but may have introduced a potential source of selection bias in our inclusion, as inclusion may be skewed towards the healthiest segment of the population, especially in the older participants. Due to this, our sample may not be entirely representative of the general population.

- The use of the MRI methods described in this thesis comes with inherent challenges and methodological considerations. While **chapter 5** discusses methodological considerations for delineation of the LC in detail, visualization of the LC using MRI remains challenging and the removal of subjects with bad template registrations in **chapter 4** may have influenced our findings. While we took extra steps to optimize the quality of our LC scans, such as minimizing head movement of participants, other advanced techniques such as optical tracking systems inside the MRI bore could further improve data quality. Furthermore, fMRI captures the BOLD signal, which by definition is not a direct measure of neuronal activity, but rather it measures localized changes

in the proportion of deoxygenated and oxygenated blood [66]. It is assumed that the BOLD response is tied to neuronal activity through neurovascular coupling, however it is important to note that there are other components that may contribute to the BOLD signal. In our functional connectivity analyses, we regressed out the signal originating from regions corresponding to large vessels, white matter and CSF, thereby significantly reducing noise unlikely to be of neural origin [67]. However, other potential contributions to the BOLD signal, such as blood pressure and localized differences in neurovascular coupling may not be accounted for [68]. Thus, due to the indirect nature of the association between the BOLD signal and neuronal activity, and functional connectivity by extension, our findings in **chapter 2** should be interpreted with some caution. On a final note related to MRI, it is important to recognize that this thesis contains data obtained on multiple MRI systems with different field strengths. It is unclear to what extent our findings at 7T translate to 3T and vice versa. Given the limited availability and high cost of 7T, our findings may need to be verified at lower field strengths to enhance the feasibility of clinical trials aiming to incorporate these findings.

- We did not directly measure tau in the LC. While convergent patterns have been shown between LC integrity and LC tangle density [51] (see footnote F in **chapter 1**), suggesting that LC integrity may be a proxy for tau pathology, we need to take into account that we have limited information on the influence of potential tau and non-tau related factors in our measurements of LC integrity. It's unclear how factors such as vascular health may affect LC integrity.

- LC degeneration is not unique to AD and occurs in the LC in multiple neurodegenerative diseases, including Parkinson's disease and progressive supranuclear palsy [69-71]. It is still unclear what patterns of LC degeneration are specific to AD and more data is needed on the specificity and sensitivity of LC degeneration as a potential biomarker for AD.

Clinical implications and future directions

An intriguing question raised by the findings of this thesis would be if the definition of preclinical AD should be adapted to recognize early brain changes associated

with AD pathology, before the current threshold for the detection of Aβ and tau pathology is reached? In other words: is there a pre-preclinical phase to AD and can we detect this phase with functional connectivity or LC integrity?

Clinical trials aiming to slow or reverse cognitive decline in symptomatic individuals so far have been disappointing. In **chapter 2**, we provided a power analysis demonstrating that knowledge about the direction of inter-network connectivity patterns can aid considerably in the selection of participants for trials in preclinical populations. Combined with knowledge about Aβ burden, these two factors can improve the selection of cognitively healthy individuals who are more likely to be on an Aβ-related memory decline trajectory. These findings may help to decrease the sample size needed to assess efficacy of clinical trials aimed at mitigating cognitive decline before clinical stages of AD, by minimizing the inclusion of participants whose memory decline may be masked by potential compensation mechanisms linked to functional connectivity. Future studies will need to confirm temporal relationships between Aβ burden and inter-network connectivity using repeated fMRI and PET imaging measures and investigate the predictive value of this information for clinical progression rates. In addition, there is evidence, using recently develop tau PET tracers, which suggests that tau and Aβ levels are synergistically associated with network connectivity [72]. Therefore, future studies may investigate whether the combined prognostic value of inter-network connectivity and Aβ burden may be further improved with the addition of tau information.

Similarly, in **chapter 6**, we show that the combined information about sleep disturbances and LC integrity may facilitate the early detection of AD-related symptoms in cognitively normal individuals and suggests there is potential in interventions that focus on consolidating sleep in the at-risk individuals [73, 74]. More objective measures of sleep-wake regulation through the use of actigraphy or sleep electroencephalograms may provide a better and more detailed assessment of sleep phenotypes and their associations with LC integrity in the context of AD pathology. Furthermore, we speculate that our specific finding relating reduced LC integrity to increased frequency of nocturnal awakenings may be due to compensatory hyperactivity of the intact wake-promoting neurons of the LC in preclinical AD. However, clinical AD has also been linked to additional sleep disturbances, such as insomnia [75]. It is possible that further LC deterioration in more advanced AD [76] is linked to these additional sleep disturbances. Future longitudinal investigations of sleep disturbances and LC integrity in healthy and

cognitively impaired individuals may provide additional insight into the temporal ordering of events across the disease spectrum.

In **chapter 3**, we show that elevated NA metabolites in the context of AD pathology are associated with neurodegeneration at target sites of the noradrenergic LC projections, already at preclinical Aβ levels. Given that the LC is involved early in the disease process, future studies should elucidate the temporal progression of NA metabolite elevations using longitudinal models across the disease spectrum and investigate whether these elevations may be related to clinical symptoms. Future work should also include direct measures of NA in the CSF along with NA metabolites to elucidate whether increased MHPG can be attributed to excessive NA turnover. This information may aid in the development of treatments targeting specific enzymes or metabolites involved in the NA metabolic pathway, such as DOPEGAL, AEP or MAO-A [36]. Lastly, it would be informative to include information about LC integrity to investigate whether in vivo measures of LC integrity can be associated with cortical and subcortical atrophy in the context of MHPG and AD pathology levels.

Furthermore, **chapter 4** suggests that in the context of lower MRI-based LC integrity, the neuropil within the LC may retain relatively normal microstructural properties while the integrity of LC projections is compromised. Longitudinal studies may determine how the association between LC integrity and microstructural properties of the LC evolves with worsening LC integrity and whether there is potentially a tipping point in the process of LC degeneration at which changes to the neuropil of the LC do become involved. Furthermore, it will be informative to note whether clinical symptoms can already be observed before deterioration of the LC neuropil. This information might help determine whether there could be a window for early noradrenergic interventions to restore function of the LC and its projections in early AD, before irreversible frank LC cell deterioration, which has previously been suggested in animal research [60].

Finally, **chapter 5** suggests that study-specific template approaches to LC delineation hold a lot of promise for consistent delineation of the LC in vivo. A more homogenized approach to LC delineation may reduce discrepancies in findings related to methodological differences. Furthermore, divergence in the methods used to determine LC integrity limits the potential of this measure in a clinical setting. A homogenized approach to LC delineation will facilitate future endeavors that may attempt to establish normative values for healthy or pathological LC integrity based on demographic information. We urge future studies to utilize a template-

based approach, though we emphasize that careful inspection of the alignment process of the scans from the individual to the template space is essential and the template creation process may be further refined. In addition, the validity and reliability of template-based and manual approaches needs to be further evaluated in a population with cognitively impaired individuals. More variability in brain morphology may be observed in these populations compared to healthy populations and it is still unclear how this may affect the LC delineation approaches evaluated in this thesis. Finally, we also recommend investigating the reliability and validity of machine-learning based approaches as a tool for consistent LC delineation.

Conclusion

The main goal of this dissertation was to identify brain changes that can signal the earliest accumulation of Aβ or tau in vivo. With this goal in mind, we aimed to identify individuals at-risk for AD earlier in the pathophysiological process, which can benefit clinical trials in the long term. To that end, we examined the associations between these early brain changes, other brain characteristics and early clinical symptoms, as well as the modifying effects of Aβ and tau pathology on these associations. Furthermore, we also aimed to further improve the sensitivity and specificity of methods used to measure these early brain changes.

We found in vivo markers of brain changes associated with the early accumulation of both Aβ and tau pathology. These markers may be useful for the identification of at-risk individuals for AD, already before clinical amyloidosis, suggesting that these markers may be able to recognize AD before the preclinical phase as defined by the current framework. Earlier recognition of preclinical AD processes may be essential for participant selection in clinical trials aiming to improve success rates through earlier intervention. We also provide a better understanding of the specific neurobiological characteristics associated with early AD brain changes and we suggest a homogenized approach to measure these early brain changes.

Much more work will be needed to evaluate the prognostic sensitivity and specificity of our findings for clinical progression rates towards AD dementia. For now, we hope to provide a small piece of the puzzle that may inspire future research towards the earliest stages of the AD pathophysiological process and may eventually allow us to end a streak of disappointing clinical trial results.

REFERENCES:

1. Finder, V.H., *Alzheimer's Disease: A General Introduction and Pathomechanism.* Journal of Alzheimer's Disease, 2010. **22**: p. S5-S19.
2. McKhann, G.M., et al., *The diagnosis of dementia due to Alzheimer's disease: Recommendations from the National Institute on Aging-Alzheimer's Association workgroups on diagnostic guidelines for Alzheimer's disease.* Alzheimer's & Dementia, 2011. **7**(3): p. 263-269.
3. Jack, C.R., et al., *Tracking pathophysiological processes in Alzheimer's disease: an updated hypothetical model of dynamic biomarkers.* The Lancet Neurology, 2013. **12**(2): p. 207-216.
4. Jack, C.R., et al., *NIA-AA Research Framework: Toward a biological definition of Alzheimer's disease.* Alzheimer's & Dementia, 2018. **14**(4): p. 535-562.
5. Bloom, G.S., *Amyloid-β and Tau: The Trigger and Bullet in Alzheimer Disease Pathogenesis.* JAMA Neurology, 2014. **71**(4): p. 505-508.
6. Hardy, J.A. and G.A. Higgins, *Alzheimer's Disease: The Amyloid Cascade Hypothesis.* Science, 1992. **256**(5054): p. 184-185.
7. Braak, H. and E. Braak, *Neuropathological stageing of Alzheimer-related changes.* Acta neuropathologica, 1991. **82**(4): p. 239-259.
8. Thal, D.R., et al., *Phases of Aβ-deposition in the human brain and its relevance for the development of AD.* Neurology, 2002. **58**(12): p. 1791-1800.
9. Braak, H., et al., *Stages of the Pathologic Process in Alzheimer Disease: Age Categories From 1 to 100 Years.* Journal of Neuropathology & Experimental Neurology, 2011. **70**(11): p. 960-969.
10. Jansen, W.J., et al., *Prevalence of Cerebral Amyloid Pathology in Persons Without Dementia: A Meta-analysis.* JAMA, 2015. **313**(19): p. 1924-1938.
11. Ballatore, C., V.M.Y. Lee, and J.Q. Trojanowski, *Tau-mediated neurodegeneration in Alzheimer's disease and related disorders.* Nature Reviews Neuroscience, 2007. **8**(9): p. 663-672.
12. Hanseeuw, B.J., et al., *Association of amyloid and tau with cognition in preclinical Alzheimer disease: a longitudinal study.* JAMA neurology, 2019. **76**(8): p. 915-924.
13. Mattsson, N., et al., *Plasma tau in Alzheimer disease.* Neurology, 2016. **87**(17): p. 1827-1835.
14. Jin, M., et al., *Soluble amyloid β-protein dimers isolated from Alzheimer cortex directly induce Tau hyperphosphorylation and neuritic degeneration.* Proceedings of the National Academy of Sciences, 2011. **108**(14): p. 5819-5824.
15. Knopman, D.S., D.T. Jones, and M.D. Greicius, *Failure to demonstrate efficacy of aducanumab: An analysis of the EMERGE and ENGAGE trials as reported by Biogen, December 2019.* Alzheimer's & Dementia, 2021. **17**(4): p. 696-701.
16. Mehta, D., et al., *Why do trials for Alzheimer's disease drugs keep failing? A discontinued drug perspective for 2010-2015.* Expert Opinion on Investigational Drugs, 2017. **26**(6): p. 735-739.
17. Cirrito, J.R., et al., *Synaptic Activity Regulates Interstitial Fluid Amyloid-β Levels In Vivo.* Neuron, 2005. **48**(6): p. 913-922.
18. Busche, M.A. and A. Konnerth, *Neuronal hyperactivity – A key defect in Alzheimer's disease?* BioEssays, 2015. **37**(6): p. 624-632.

19. Buckner, R.L., et al., *Molecular, Structural, and Functional Characterization of Alzheimer's Disease: Evidence for a Relationship between Default Activity, Amyloid, and Memory.* The Journal of Neuroscience, 2005. **25**(34): p. 7709-7717.
20. Palmqvist, S., et al., *Earliest accumulation of β-amyloid occurs within the default-mode network and concurrently affects brain connectivity.* Nature Communications, 2017. **8**(1): p. 1214.
21. Andrews-Hanna, J.R., et al., *Disruption of large-scale brain systems in advanced aging.* Neuron, 2007. **56**(5): p. 924-35.
22. Buckley, R.F., et al., *Functional network integrity presages cognitive decline in preclinical Alzheimer disease.* Neurology, 2017.
23. Damoiseaux, J.S., et al., *Reduced resting-state brain activity in the "default network" in normal aging.* Cerebral Cortex, 2008. **18**(8): p. 1856-1864.
24. Fornito, A., et al., *Competitive and cooperative dynamics of large-scale brain functional networks supporting recollection.* Proceedings of the National Academy of Sciences, 2012. **109**(31): p. 12788-12793.
25. Kelly, A.M., et al., *Competition between functional brain networks mediates behavioral variability.* Neuroimage, 2008. **39**(1): p. 527-37.
26. Heeger, D.J. and D. Ress, *What does fMRI tell us about neuronal activity?* Nature Reviews Neuroscience, 2002. **3**(2): p. 142-151.
27. Fox, M.D., et al., *The human brain is intrinsically organized into dynamic, anticorrelated functional networks.* Proceedings of the National Academy of Sciences, 2005. **102**(27): p. 9673-9678.
28. Sheline, Y.I. and M.E. Raichle, *Resting State Functional Connectivity in Preclinical Alzheimer's Disease.* Biological Psychiatry, 2013. **74**(5): p. 340-347.
29. Farrell, M.E., et al., *Association of Longitudinal Cognitive Decline With Amyloid Burden in Middle-aged and Older Adults: Evidence for a Dose-Response Relationship.* JAMA Neurology, 2017. **74**(7): p. 830-838.
30. Cabeza, R., et al., *Aging Gracefully: Compensatory Brain Activity in High-Performing Older Adults.* NeuroImage, 2002. **17**(3): p. 1394-1402.
31. Theofilas, P., et al., *Locus coeruleus volume and cell population changes during Alzheimer's disease progression: A stereological study in human postmortem brains with potential implication for early-stage biomarker discovery.* Alzheimer's & Dementia, 2017. **13**(3): p. 236-246.
32. Matchett, B.J., et al., *The mechanistic link between selective vulnerability of the locus coeruleus and neurodegeneration in Alzheimer's disease.* Acta Neuropathologica, 2021. **141**(5): p. 631-650.
33. Counts, S.E. and E.J. Mufson, *Noradrenaline activation of neurotrophic pathways protects against neuronal amyloid toxicity.* Journal of neurochemistry, 2010. **113**(3): p. 649-660.
34. Hoogendijk, W.J.G., et al., *Increased activity of surviving locus ceruleus neurons in Alzheimer's disease.* Annals of Neurology, 1999. **45**(1): p. 82-91.
35. Raskind, M.A., et al., *Norepinephrine and MHPG Levels in CSF and Plasma in Alzheimer's Disease.* Archives of General Psychiatry, 1984. **41**(4): p. 343-346.
36. Kang, S.S., et al., *Norepinephrine metabolite DOPEGAL activates AEP and pathological Tau aggregation in locus coeruleus.* The Journal of Clinical Investigation, 2020. **130**(1): p. 422-437.

37. Eisenhofer, G., I.J. Kopin, and D.S. Goldstein, *Catecholamine metabolism: a contemporary view with implications for physiology and medicine.* Pharmacological reviews, 2004. **56**(3): p. 331-349.
38. Ehlers, M.R. and R.M. Todd, *Genesis and maintenance of attentional biases: The role of the locus coeruleus-noradrenaline system.* Neural Plasticity, 2017. **2017**.
39. Sara, S.J., *The locus coeruleus and noradrenergic modulation of cognition.* Nature Reviews Neuroscience, 2009. **10**(3): p. 211-223.
40. Berridge, C.W. and B.D. Waterhouse, *The locus coeruleus–noradrenergic system: modulation of behavioral state and state-dependent cognitive processes.* Brain Research Reviews, 2003. **42**(1): p. 33-84.
41. Oh, J., et al., *The role of co-neurotransmitters in sleep and wake regulation.* Molecular Psychiatry, 2019. **24**(9): p. 1284-1295.
42. Oh, J.Y., et al., *Subcortical Neuronal Correlates of Sleep in Neurodegenerative Diseases.* JAMA Neurology, 2022. **79**(5): p. 498-508.
43. Carrier, J., et al., *Sleep slow wave changes during the middle years of life.* European Journal of Neuroscience, 2011. **33**(4): p. 758-766.
44. Bubu, O.M., et al., *Sleep, cognitive impairment, and Alzheimer's disease: a systematic review and meta-analysis.* Sleep, 2017. **40**(1): p. zsw032.
45. Shi, L., et al., *Sleep disturbances increase the risk of dementia: a systematic review and meta-analysis.* Sleep medicine reviews, 2018. **40**: p. 4-16.
46. Xie, L., et al., *Sleep drives metabolite clearance from the adult brain.* science, 2013. **342**(6156): p. 373-377.
47. Holth, J.K., et al., *The sleep-wake cycle regulates brain interstitial fluid tau in mice and CSF tau in humans.* Science, 2019. **363**(6429): p. 880-884.
48. Lucey, B.P., *It's complicated: The relationship between sleep and Alzheimer's disease in humans.* Neurobiology of Disease, 2020. **144**: p. 105031.
49. Zhu, Y., et al., *Chronic Sleep Disruption Advances the Temporal Progression of Tauopathy in P301S Mutant Mice.* The Journal of Neuroscience, 2018. **38**(48): p. 10255-10270.
50. Ehrenberg, A.J., et al., *Quantifying the accretion of hyperphosphorylated tau in the locus coeruleus and dorsal raphe nucleus: the pathological building blocks of early Alzheimer's disease.* Neuropathology and applied neurobiology, 2017. **43**(5): p. 393-408.
51. Jacobs, H.I.L., et al., *In vivo and neuropathology data support locus coeruleus integrity as indicator of Alzheimer's disease pathology and cognitive decline.* Science Translational Medicine, 2021. **13**(612): p. eabj2511.
52. Priovoulos, N., et al., *High-resolution in vivo imaging of human locus coeruleus by magnetization transfer MRI at 3T and 7T.* NeuroImage, 2018. **168**: p. 427-436.
53. Keren, N.I., et al., *Histologic validation of locus coeruleus MRI contrast in post-mortem tissue.* NeuroImage, 2015. **113**: p. 235-245.
54. Kitao, S., et al., *Correlation between pathology and neuromelanin MR imaging in Parkinson's disease and dementia with Lewy bodies.* Neuroradiology, 2013. **55**(8): p. 947-953.
55. Priovoulos, N., et al., *Unraveling the contributions to the neuromelanin-MRI contrast.* Brain Structure and Function, 2020. **225**(9): p. 2757-2774.
56. Sasaki, M., et al., *Neuromelanin magnetic resonance imaging of locus ceruleus and substantia nigra in Parkinson's disease.* NeuroReport, 2006. **17**(11).

57. Trujillo, P., et al., *Quantitative magnetization transfer imaging of the human locus coeruleus.* NeuroImage, 2019. **200**: p. 191-198.
58. Zhang, H., et al., *NODDI: practical in vivo neurite orientation dispersion and density imaging of the human brain.* Neuroimage, 2012. **61**(4): p. 1000-1016.
59. Yeh, F.-C., D. Badre, and T. Verstynen, *Connectometry: A statistical approach harnessing the analytical potential of the local connectome.* NeuroImage, 2016. **125**: p. 162-171.
60. Rorabaugh, J.M., et al., *Chemogenetic locus coeruleus activation restores reversal learning in a rat model of Alzheimer's disease.* Brain, 2017. **140**(11): p. 3023-3038.
61. Theofilas, P., et al., *Turning on the Light Within: Subcortical Nuclei of the Isodentritic Core and their Role in Alzheimer's Disease Pathogenesis.* Journal of Alzheimer's Disease, 2015. **46**: p. 17-34.
62. Liu, K.Y., et al., *In vivo visualization of age-related differences in the locus coeruleus.* Neurobiology of Aging, 2019. **74**: p. 101-111.
63. Shibata, E., et al., *Age-related Changes in Locus Ceruleus on Neuromelanin Magnetic Resonance Imaging at 3 Tesla.* Magnetic Resonance in Medical Sciences, 2006. **5**(4): p. 197-200.
64. Betts, M.J., et al., *In vivo MRI assessment of the human locus coeruleus along its rostrocaudal extent in young and older adults.* NeuroImage, 2017. **163**: p. 150-159.
65. Ye, R., et al., *An in vivo probabilistic atlas of the human locus coeruleus at ultra-high field.* NeuroImage, 2021. **225**: p. 117487.
66. Logothetis, N.K. and B.A. Wandell, *Interpreting the BOLD Signal.* Annual Review of Physiology, 2004. **66**(1): p. 735-769.
67. Behzadi, Y., et al., *A component based noise correction method (CompCor) for BOLD and perfusion based fMRI.* NeuroImage, 2007. **37**(1): p. 90-101.
68. Keilholz, S.D., et al., *Noise and non-neuronal contributions to the BOLD signal: applications to and insights from animal studies.* NeuroImage, 2017. **154**: p. 267-281.
69. Kaalund, S.S., et al., *Locus coeruleus pathology in progressive supranuclear palsy, and its relation to disease severity.* Acta Neuropathologica Communications, 2020. **8**(1): p. 11.
70. Marien, M.R., F.C. Colpaert, and A.C. Rosenquist, *Noradrenergic mechanisms in neurodegenerative diseases: a theory.* Brain Research Reviews, 2004. **45**(1): p. 38-78.
71. Ye, R., et al., *Locus Coeruleus Integrity from 7 T MRI Relates to Apathy and Cognition in Parkinsonian Disorders.* Movement Disorders, 2022. **n/a**(n/a).
72. Schultz, A.P., et al., *Phases of Hyperconnectivity and Hypoconnectivity in the Default Mode and Salience Networks Track with Amyloid and Tau in Clinically Normal Individuals.* The Journal of Neuroscience, 2017. **37**(16): p. 4323-4331.
73. McCurry, S.M., et al., *Treatment of sleep disturbance in Alzheimer's disease.* Sleep Medicine Reviews, 2000. **4**(6): p. 603-628.
74. Bretherton, B., et al., *Effects of transcutaneous vagus nerve stimulation in individuals aged 55 years or above: potential benefits of daily stimulation.* Aging (Albany NY), 2019. **11**(14): p. 4836-4857.
75. Gagnon, J.-F., et al., *Chapter 45 - Sleep in Normal Aging, Alzheimer's Disease, and Mild Cognitive Impairment*, in *Handbook of Behavioral Neuroscience*, H.C. Dringenberg, Editor. 2019, Elsevier. p. 677-692.
76. Betts, M.J., et al., *Locus coeruleus MRI contrast is reduced in Alzheimer's disease dementia and correlates with CSF Aβ levels.* Alzheimer's & Dementia: Diagnosis, Assessment & Disease Monitoring, 2019. **11**: p. 281-285.

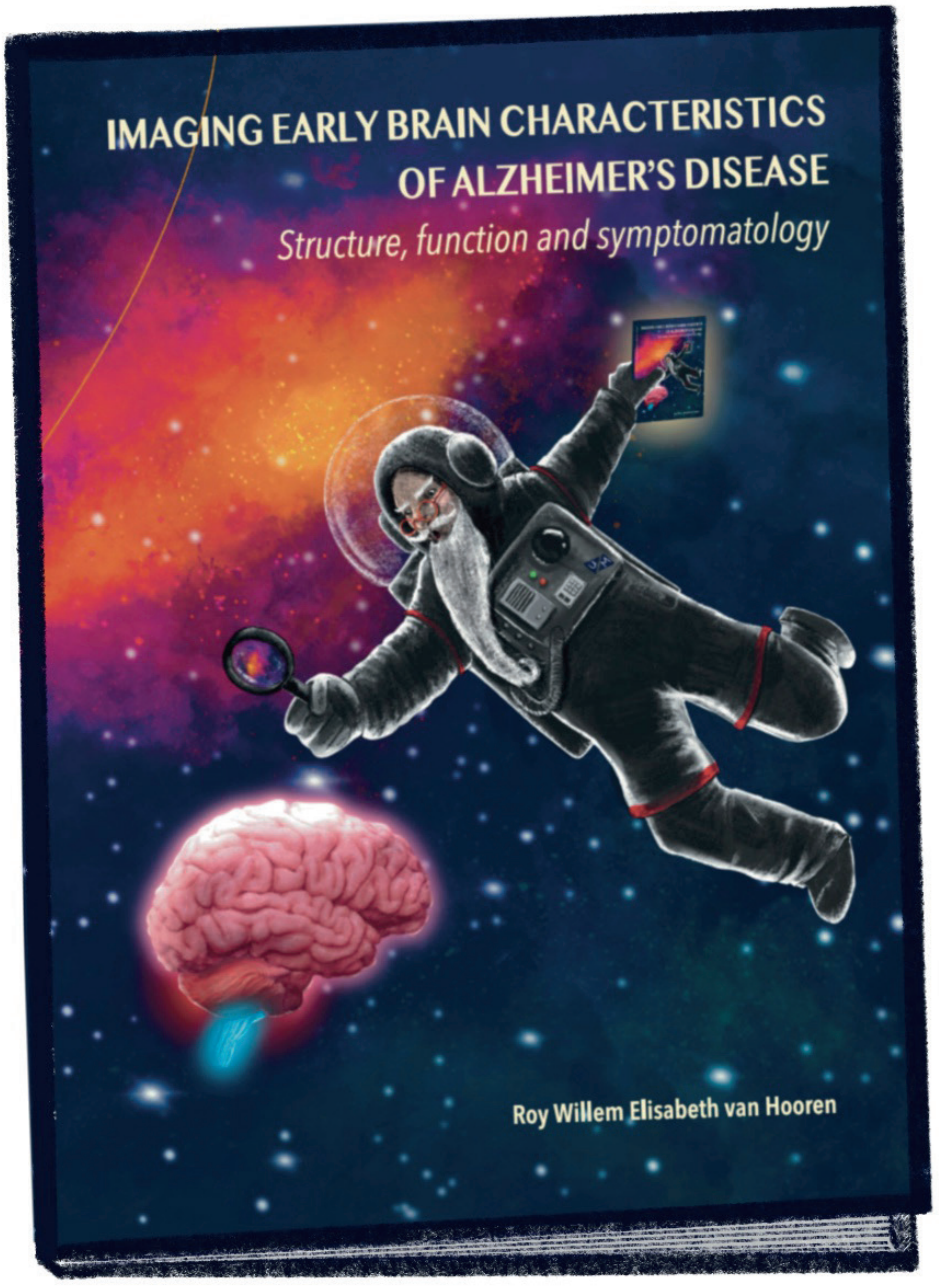
IMAGING EARLY BRAIN CHARACTERISTICS
OF ALZHEIMER'S DISEASE
Structure, function and symptomatology
Roy Willem Elisabeth van Hooren

ADDENDUM

IMPACT PARAGRAPH

SUMMARY

NEDERLANDSE SAMENVATTING

PUBLISHED WORK

PHD DEFENSES AT THE SCHOOL FOR MENTAL HEALTH AND NEUROSCIENCE

DANKWOORD – ACKNOWLEDGMENTS

OVER DE AUTEUR - ABOUT THE AUTHOR

CHAPTER 8

IMPACT PARAGRAPH

Trials attempting to slow down or reverse Alzheimer's disease (AD) in the clinical phase have so far not been successful, which is potentially due to the interventions being applied too late in the disease process. Our main goal in this dissertation was to identify brain changes that can signal the earliest accumulation of amyloid-beta (Aβ) or tau in vivo and to identify individuals at-risk for AD earlier in the pathophysiological process. With this goal in mind, we examined early brain changes associated with Aβ and tau pathology and related them to functional and structural brain characteristics as well as early clinical symptoms. We also aimed assess the validity and reliability of methods used to measure these early brain changes.

Main findings

In this thesis, we show that brain characteristics of early AD pathophysiology can be studied in vivo, even before clinical amyloidosis. We achieved this by utilizing magnetic resonance imaging (MRI) as a non-invasive method for studying these processes in populations across the adult age span as well as in populations in different disease stages. We show functional, as well as structural MRI markers that may be used as indicators of early brain changes associated with Aβ and tau.

We show that Aβ burden is associated with patterns of functional connectivity patterns between large scale networks, and that the direction of inter-network connectivity adds information about the dose-response relationship between Aβ and longitudinal cognitive decline, already at the preclinical stage. The combined information from the direction of inter-network functionality and Aβ burden can reduce the required sample size in clinical trials by 88% to slow down memory decline by 30%.

Shifting our attention to tau, we investigated one of the earliest accumulation sites of tau pathology, namely the locus coeruleus (LC). The locus coeruleus is the main source of cerebral noradrenaline (NA) and we show that in the context of elevated AD pathology, the NA metabolite MHPG is associated with lower cortical thickness in the cortex and hippocampus, even at subthreshold amyloid levels. These findings imply an important role for the LC-NA system in the early AD pathophysiological process and highlight the downstream neurodegenerative

processes occurring at target sites of the long LC projections. This ties into our findings where we report that reduced MRI-based LC integrity is associated with reduced integrity of LC projections towards the thalamus and cerebellum in a cognitively healthy population. This possibly suggests that the deterioration of LC projections is involved in neurodegenerative processes at LC target sites, though this remains to be confirmed.

We also showed that integrity of the LC is associated with nocturnal awakenings in cognitively healthy individuals, especially in the context of tau pathology. The LC is important for sleep-wake regulation and sleep disturbances are associated with an increased risk of developing AD. Furthermore, previous research has suggested that up to 15% of AD-cases may be prevented by the treatment of sleep-related problems. This means that measures of LC integrity, tau burden and sleep disturbances may facilitate the selection of at-risk participants for AD in clinical trials targeting treatable aspects of sleep at the preclinical stage.

Finally, we investigated different methods for the anatomical delineation of the LC in a population covering the adult lifespan. We compared template-based methods to manual delineation and found that overall, a study-specific template approach produces the most reliable results. We argue that manual delineation of the LC is vulnerable to rater bias and the use of a study-specific template has potential to become a standard approach to LC delineation. Such a standard could reduce discrepancies in findings related to LC integrity due to methodological differences between studies. However, future studies should investigate more alternatives to LC delineation, such as a machine-learning based approach and compare measures of reliability and validity to our findings.

Relevance

Worldwide, people are reaching increasingly older ages as a result of our advancing knowledge and technology in the medical field. As a disease typically associated with older age, the prevalence of AD is also increasing and its impact resonates in the lives of patients, caregivers, and society at large. Meanwhile, to date, there is no effective form of treatment to halt, or reverse the AD process, potentially because most clinical trials target the disease in a late, symptomatic stage. With this dissertation, we hope to provide a small piece of the puzzle that may allow us to detect the earliest processes of AD, with the long-term aim to intervene before the disease process reaches a point of no return.

We provide evidence that functional and structural characteristics of the brain combined with established biomarkers of AD, can be used to obtain accurate selection criteria for clinical trials to intervene at preclinical stages of the disease. Ultimately, this knowledge may facilitate the fine-tuned development of primary prevention interventions. Existing treatments for the reduction of Aβ plaques may be utilized in a sample consisting of cognitively healthy participants with negative inter-network correlations, as per **chapter 2**, to investigate its effects on cognitive decline. Similarly, our findings in **chapters 3**, **4** and **6** may support the development of interventions targeting sleep consolidation and the LC-NA system, while **chapter 5** provides a starting point to homogenize future work aimed at studying the LC-NA system.

Target group

The findings presented in this thesis are initially relevant for researchers studying pathophysiological processes in AD. Researchers examining the temporal cascade of AD may investigate the early brain changes we describe in this thesis to further elucidate the temporal ordering of pathological events in AD. Furthermore, researchers trying to understand the neural correlates of sleep may find that LC integrity is potentially an informative measure for in vivo investigations. There are also companies investigating products such as special pillows and wearables to improve sleep quality. These companies may benefit from the findings in this thesis to refine their products and to better identify individuals who may benefit from these treatments. In addition, our findings have value for researchers investigating intervention strategies in AD. Recent work from the university of Cambridge has suggested that localized changes in LC integrity may be used as a biomarker for the selection of participants for clinical trials in Parkinson's disease and progressive supranuclear palsy, which are diseases that also involve significant deterioration of the LC. We encourage similar investigations towards the value of LC integrity as a biomarker for AD, given our findings relating LC integrity to underlying neurobiological characteristics and early sleep disturbances that may have predictive value for AD.

Additionally, our longitudinal work may be relevant to clinicians who may use the findings from **chapter 2** to improve the prognosis of cognitive decline for patients who present with normal cognition on cognitive tests, but report

subjective memory complaints. The AHEAD and A4 trials are focusing on cognitively normal individuals with high Aβ burden. These trials may benefit from information about inter-network connectivity for the selection of participants. Furthermore, we also report that patients with MCI show Aβ-related cognitive decline in the context of positive inter-network correlations, potentially giving clinicians tools to improve the prognosis in MCI patients. This information may help clinicians, patients and their caregivers make better informed decisions about the difficult choices that need to be made in a situation where the future for the patient is uncertain. However, it is important to note that resting-state functional MRI is a difficult tool that requires complex processing, for which the necessary expertise and equipment may not be readily available. Furthermore, the test-retest reliability of functional connectivity is relatively low and its specificity and sensitivity as a marker for cognitive decline needs to be further investigated. This means that careful interpretation is warranted regarding the use of functional connectivity for individualized prognosis, and the clinician should consider multiple other risk factors for cognitive decline in their prognosis.

Dissemination activities

The findings reported in this thesis have been presented to the scientific community through various forms of dissemination. Local disseminations were performed through poster presentations (annual MheNS research days) as well as oral presentations (MheNS external review committee visitation 2021; local working groups). Furthermore, these findings were presented at international conferences and scientific gatherings in the form of poster presentations (MINC 2018, AAIC 2020) and oral presentations (EURON PhD days 2018). In addition, some results from our work have been presented in layman terms through newsletters and other informal communication to the participants of the STRAIN study, who have provided us with a large portion of the data that made this thesis possible. Finally, **chapter 2** and **6** have been published in *Alzheimer's Research & Therapy* (2018 & 2021, respectively) (2021 2-year impact factor = 8.823) and **chapter 3** has been published in *Neurobiology of Aging* (2021) (2021 2-year impact factor = 5.133).

SUMMARY

Disease-modifying treatments acting in the symptomatic phase of the disease may occur too late in the Alzheimer's disease (AD) pathophysiological process, after the occurrence of irreversible brain damage. Guided by recent animal and autopsy studies, we identified specific brain changes that are related to and predict either amyloid-beta (Ab) or tau pathology in the asymptomatic stages of the disease. We aimed to evaluate the corresponding magnetic resonance imaging (MRI) measures of these early brain changes, functional connectivity and locus coeruleus (LC) integrity, by relating them to established AD-related brain changes and cognitive and behavioral symptoms of AD. Early identification of these processes in vivo may enable earlier intervention in the disease process and potentially improve clinical outcomes of clinical trials. Therefore, the aim of this dissertation was to examine imaging measures of these early processes in vivo using MRI and to investigate their potential as markers of AD-related processes.

In **chapter 2**, we investigated whether functional connectivity patterns between large-scale brain networks and Aβ burden are synergistically related to cognition in a longitudinal cohort spanning the disease spectrum from healthy to clinical AD. We found that patterns of inter-network functional connectivity differed depending on the level of Aβ burden and that the directionality of inter-network connectivity predicted memory decline in an Aβ dose-dependent manner. Specifically, in the cognitively healthy group, we found that when inter-network correlations were negative, higher Aβ burden was associated with greater memory decline. However, when inter-network correlations were positive, there was no association between Aβ burden and memory decline. For the mild cognitive impairment group, we found that the dose-dependent association between Aβ and cognitive decline was only present in the group with positive inter-network connectivity. These findings suggest that the direction of functional organization between large-scale networks adds additional information about the rate of Aβ-related cognitive decline in preclinical groups, and may be used to optimize patient selection and reduce the required sample sizes in clinical trials during the presymptomatic phase.

In **chapter 3**, we discovered that the noradrenaline (NA) metabolite 3-Methoxy-4-Hydroxyphenylglycol (MHPG), together with information about Aβ and tau burden, is associated with volume of the hippocampus and cortical thickness in multiple cortical regions. This association was present at preclinical levels of Aβ in the cerebrospinal fluid and involved target sites of LC projections. These

findings imply involvement of the LC-NA system in early AD pathophysiological processes, possibly before clinical amyloidosis, making this system a potential target for pharmaceutical modulation.

In **chapter 4**, we take a closer look at the microstructural correlates of in vivo measures of LC integrity. We show that LC integrity is associated with quantitative anisotropy in tracts originating from the LC, but not with measures of neurite density and arborization within the LC. Specifically, our findings suggest that axonal integrity of projections to the thalamus and cerebellum, rather than changes to the neuropil of LC cells, is associated with in vivo measurements of LC integrity. In accordance with animal research previously suggesting similar patterns in early AD model rats, we conclude that in vivo measures of LC integrity likely reflect early stages of the AD pathophysiological process.

In **chapter 5**, we aimed to make a side-by-side comparison of several approaches to tackle the methodological difficulties that are associated with accurate and consistent delineation of the LC in vivo. We found study-specific template-based approaches for LC delineation to be the most consistent tool for reliable LC delineation. When compared to a manual delineation approach, the template-based approaches showed considerably higher reliability scores across the bilateral LC. However, we recommend caution, as template-based approaches remain vulnerable to registration issues, and further refinement of template creation pipelines and careful manual quality checks on all registrations are to be advised.

In **chapter 6**, we take a closer look at LC integrity and sleep disturbances in the context of AD pathology. The sleep-wake cycle involves the LC-NA system and sleep disturbances are recognized as a risk factor for AD. We find that in vivo MRI markers of LC integrity are associated with the number of self-reported nocturnal awakenings in cognitively healthy older individuals, and that this association is particularly strong in the presence of tau pathology. These findings show an important role for LC integrity in sleep-wake regulation in preclinical AD and suggest that the combined knowledge about nocturnal awakenings and LC integrity may aid in the selection of at-risk individuals for clinical trials targeting AD at an early stage.

Finally, in **chapter 7**, we explore the implications and limitations of our findings, as well as propose directions for future research. Overall, we outline brain changes and clinical symptoms that are associated with the earliest accumulations of Aβ and tau pathology with the aim to facilitate earlier detection of at-risk individuals for clinical trials targeting AD in the preclinical phase.

NEDERLANDSE SAMENVATTING

Behandelingen die proberen de ziekte van Alzheimer (AD) te beïnvloeden worden mogelijk te laat in het ziekteproces toegepast, wanneer onomkeerbare hersenschade al heeft plaatsgevonden. Met behulp van recent dieren- en autopsieonderzoek hebben we specifieke hersenveranderingen geïdentificeerd die verbonden zijn aan amyloid-beta (Ab) of tau pathologie in de asymptomatische fases van de ziekte. We hebben getracht om relevante magnetic resonance imaging (MRI) maten van deze vroege hersenveranderingen, zoals functionele connectiviteit en locus coeruleus (LC) integriteit, te relateren aan gevestigde hersen-, cognitie en gedragsveranderingen in AD. Vroege identificatie van deze processen in vivo kan het mogelijk maken om eerder in het ziekteproces in te grijpen en mogelijk resultaten van klinische trials te verbeteren. Om deze reden was het doel van dit proefschrift om deze vroege processen in vivo in kaart te brengen met behulp van MRI en om het potentieel hiervan te onderzoeken als tekenen van AD-gerelateerde processen.

In **hoofdstuk 2** hebben we gekeken of patronen in functionele connectiviteit tussen grotschalige hersennetwerken en Aβ belasting samen verband houden met cognitie in een longitudinaal cohort overheen het hele gezond tot klinische AD spectrum. We hebben gevonden dat patronen in functionele connectiviteit tussen netwerken verschillen afhankelijk van Aβ belasting en dat de richting van connectiviteit tussen netwerken in staat was om geheugenachteruitgang te voorspellen, afhankelijk van Aβ dosering. Meer specifiek vonden we dat wanneer correlaties tussen netwerken negatief waren, hogere Aβ belasting geassocieerd was met meer geheugenachteruitgang in de cognitief gezonde groep. Echter, wanneer deze correlaties positief waren, was dit verband niet zichtbaar.

Voor de groep mensen met mild cognitieve beperking vonden we de dosis-afhankelijke associatie tussen Aβ en cognitieve achteruitgang alleen in de groep met positieve connectiviteit tussen de netwerken. Deze bevindingen suggereren dat de richting van functionele organizatie tussen grootschalige hersennetwerken informatie toevoegt over de mate van Aβ-gerelateerde cognitieve achteruitgang in preklinische groepen. Deze informatie kan gebruikt worden om de selectie van patiënten voor klinische trials in de preklinische fase te optimaliseren en de benodigde sample sizes te verkleinen.

In **hoofdstuk 3** ontdekten we dat de noradrenaline (NA) metaboliet 3-Methoxy-4-Hydroxyphenylglycol (MHPG), samen met informatie over Aβ en tau

belasting, geassocieerd is met het volume van de hippocampus en corticale dikte in meerdere gebieden van de cortex. Deze associatie bestond al op preklinische niveaus van Aβ in het hersenvocht en was te zien gebieden die projecties van de LC ontvangen. Deze bevindingen impliceren dat het LC-NA systeem vroeg in het AD ziekteproces betrokken is, mogelijk al voor klinische Aβ ophoping. Dit betekent dat het LC-NA systeem een interessant doelwit kan zijn voor farmacologisch ingrijpen.

In **hoofdstuk 4** keken we naar de microstructurele correlaten van in vivo maten van LC integriteit. We lieten zien dat LC integriteit geassocieerd is met quantitative anisotropy in wittestofbanen vanuit de LC maar niet met maten van neuriet dichtheid of vertakking binnen de LC. Specifiek suggereren onze bevindingen dat de integriteit van axonen van de projecties naar de thalamus en het cerebellum, en niet het neuropil van LC cellen, geassocieerd is met in vivo maten van LC integriteit. Dit is consistent met dierenonderzoek dat eerder soortgelijke patronen heeft laten zien in vroege AD model ratten en we concluderen daarom dat in vivo maten van LC integriteit waarschijnlijk vroege stadia van het AD ziekteproces weergeven.

In **hoofdstuk 5** trachtten we een zij-aan-zij vergelijking te maken van meerdere manieren om de methodologische uitdagingen aan te gaan van het accuraat en consistent aftekenen van de LC in vivo. We vonden dat de aanpak waarbij een studie-specifiek sjabloon voor het aftekenen van de LC wordt gemaakt de meest consistente aanpak is. Wanneer we deze methode vergeleken met een handmatige aftekening van de LC, zagen we dat de sjabloon aanpak duidelijk betere betrouwbaarheidsscores liet zien voor de bilaterale LC. Echter is voorzichtigheid geboden omdat sjabloon methodes nog steeds vatbaar zijn voor registratieproblemen. Daarom is handmatige kwaliteitscontrole op de registraties en verdere verfijning van het proces om sjablonen te maken aan te raden.

In **hoofdstuk 6** hebben we gekeken naar LC integriteit en slaapverstoringen in de context van AD pathologie. De LC is betrokken bij de cyclus van het slapen en wakker worden en verstoringen in het slaappatroon zijn genoemd als een risicofactor voor AD. Wij lieten zien dat een vivo MRI maat van LC integriteit verbonden is met de hoeveelheid nachtelijke ontwakingen die cognitief gezonde oudere mensen zelf rapporteren. Deze associatie was bijzonder sterk als ook tau pathologie aanwezig is. Deze bevindingen laten de belangrijke rol van LC integriteit zien in het reguleren van slaap en waken in preklinische AD en suggereren dat de gecombineerde kennis over nachtelijke ontwakingen en LC integriteit kunnen bijdragen aan het vroeg selecteren van individuën met een hoger risico op AD voor klinische trials.

Als laatste keken we in **hoofdstuk 7** naar de implicaties en beperkingen van onze bevindingen en kijken we ook naar opties voor toekomstig onderzoek. Over het algemeen bespreken we hersenveranderingen en klinische symptomen die geassociëerd zijn met de vroegste ophopingen van Aβ en tau met het doel om individuën met een verhoogd risico op AD eerder te herkennen. Klinische trials die de ziekte in de preklinische fase onderzoeken kunnen op deze manier worden geholpen in hun participantenselectie.

PUBLISHED WORK

This thesis

Maxime van Egroo, **Roy W.E. van Hooren,** Heidi I.L. Jacobs, *Associations between locus coeruleus integrity and nocturnal awakenings in the context of Alzheimer's disease plasma biomarkers: a 7T MRI study*, Alzheimer's Research & Therapy (2021), DOI https://doi.org/10.1186/s13195-021-00902-8 (**chapter 6**)

Roy W.E. van Hooren, MSc, Frans R.J. Verhey, PhD, MD, Inez H.G.B. Ramakers, PhD, Willemijn J. Jansen, PhD, Heidi I.L. Jacobs, PhD, *Elevated norepinephrine metabolism is linked to cortical thickness in the context of Alzheimer's disease pathology*, Neurobiology of Aging (2021), DOI https://doi.org/10.1016/j.neurobiolaging.2021.01.024 (**chapter 3**)

van Hooren, R.W.E., Riphagen, J.M., Jacobs, H.I.L., *Inter-network connectivity and amyloid-β linked to cognitive decline in preclinical Alzheimer's disease: a longitudinal cohort study*, Alzheimer's Research & Therapy (2018), DOI https://doi.org/10.1186/s13195-018-0420-9 (**chapter 2**)

Other work

Joost M. Riphagen, **Roy W.E. van Hooren**, Gunter Kenis, Frans RJ, Verhey, Heidi I.L. Jacobs. *Distinct pathways linking the BDNF Val66Met polymorphism to Alzheimer pathologies.* Journal of Alzheimer's Disease (2022), DOI https://doi.org/10.3233/JAD-215353

Linda H.G. Pagen, Benedikt A. Poser, Martin P.J. van Boxtel, Nikos Priovoulos, **Roy W.E. van Hooren**, Frans R.J. Verhey, Heidi I.L. Jacobs, *Worry modifies the relationship between locus coeruleus activity and emotional mnemonic discrimination*. Brain Sciences (2022), DOI https://doi.org/10.3390/brainsci12030381

Joost M. Riphagen, **Roy W.E. van Hooren**, Linda H.G. Pagen, Benedikt A. Poser, Heidi I.L. Jacobs, *Rostro-caudal locus coeruleus integrity differences vary with age and sex using ultra-high field imaging*, Alzheimer's & Dementia (2020), DOI https://doi.org/10.1002/alz.046722

W.M. Freeze, D.N. ter Weele, W.M. Palm, **R.W. van Hooren**, E.I. Hoff, J.F.A. Jansen, H.I.L. Jacobs, F.R. Verhey and W.H. Backes, *Optimal Detection of Subtle Gadolinium Leakage in Cerebrospinal Fluid with Heavily T2-Weighted Fluid-Attenuated Inversion Recovery Imaging*, American Journal of Neuroradiology (2019), DOI https://doi.org/10.3174/ajnr.A6145

PHD DEFENSES AT THE SCHOOL FOR MENTAL HEALTH AND NEUROSCIENCE (MHENS)

Within MHeNS, well over 400 doctoral theses have been successfully defended and this number continues to grow. To save precious paper and energy, they will not be listed in this book, but you can find a continuously updated overview of these defenses from the research school in the Maastricht University repository at:

https://cris.maastrichtuniversity.nl/en/organisations/mhens-school-for-mental-health-and-neuroscience/publications/?type=%2Fdk%2Fatira%2Fpure%2Fresearchoutput%2Fresearchoutputtypes%2Fthesis%2Fdoc

DANKWOORD – ACKNOWLEDGMENTS

Op het moment van schrijven zie ik hier de woordenteller de 50.000 woorden aantikken. Nooit van mijn leven had ik gedacht ooit zo veel worden bij elkaar te zetten en dit was dan ook nooit gelukt zonder de steun van de geweldige mensen om me heen.

Allereerst bedank ik natuurlijk graag mijn promotieteam: Dr. Heidi Jacobs, Prof. Dr. Verhey en Dr. van Egroo.

Heidi, als kersverse alumnus van de Neuropsychology master stuurde ik jou een mailtje met de vraag of je niet toevallig een PhD positie had liggen. Ik in mijn naïviteit dacht dat dat wel eventjes zo gedaan was en jij nam gelukkig uitgebreid de moeite om me uit te leggen dat daar wel het een en ander bij kwam kijken. Je bood toen aan om me als onderzoeksassistent aan te nemen en samen naar een wetenschappelijke publicatie en mogelijk een PhD positie toe te werken, en zie hier het resultaat. Ondanks de luttele ±5.500 kilometer aan oceaan die we meestal tussen ons hadden zitten, heb ik altijd heel prettig samengewerkt met jou als mijn dagelijkse begeleider. Hartelijk bedankt hiervoor.

Frans, naast jouw kundige klinisch perspectief op het onderzoek heb ik ook altijd gewaardeerd hoe veel jij je hebt ingezet om te zorgen dat iedereen op de afdeling zich op zijn gemak voelt. Je bent altijd toegankelijk geweest voor alle collega's en ik heb je nooit gezien als "baas" maar als een echte leider en rolmodel voor de hele afdeling. Het is eigenlijk alleen maar vanzelfsprekend dat zelfs na je pensioen het ACL niet zonder je kan. Hartelijk bedankt voor je begeleiding en steun.

Maxime, your experience with imaging methods, in particular with NODDI, helped out a lot with some of the chapters in this thesis. Sometimes we spent more time dealing with computer issues and waiting for scripts to finish than actual scientific considerations, but nonetheless, we managed to get things rolling. You also piqued my interest in the role of sleep in Alzheimer's disease and I'm very grateful to have you as my co-promotor.

I would also like to extend a big thanks to the assessment committee for taking on the task of evaluating this thesis filled with giant tables and complex figures. Thank you Prof. Dr. David Linden, Dr. Martin van Boxtel, Prof. Dr. Mark van Buchem, Prof. Dr. Ben Poser and Prof. Dr. Kathrin Reetz.

Als volgende wil ik graag mijn kamergenoten overheen de laatste paar jaar bedanken. Elise, Lisa, Whitney, Inge, Nikos, Maxime en Linda, bedankt voor de gezellige tijden en brainstormsessies.

Elise, I am amazed by how well you managed to set up a large international study with such innovative techniques. Even after your house flooded you were determined to keep up your work. You're an incredible source of inspiration and an excellent researcher.

Lisa en Whitney, als onderzoeksassistent op jullie projecten begon mijn tijd bij de UM en heb ik enorm veel geleerd over het reilen en zeilen van MRI onderzoek. Het was dan ook wel erg geinig om een aantal jaar later juist door Whitney aangesproken te worden als "de locus coeruleus expert" die haar vast wel kon helpen bij het vinden van de locus coeruleus in haar post-mortem sample. Bedankt voor deze leuke en leerzame ervaringen.

Inge, de chocolade paaseitjes die we altijd op kantoor hadden staan waren misschien gesmolten door het constante stoken van de computers die stonden te ratelen, maar we waren er toch samen met Linda met z'n drieën erop gebrand om uit te vinden welke kleur nou welke smaak was. Je hebt natuurlijk ook meegeholpen om de sfeer van het kantoor naar een hoger niveau te tillen door de muren en deuren te bedekken met Perkins foto's. Jij en Perkins zijn bedankt voor de gezelligheid.

Nikos, without your hard work and engineer brain laying the foundations for a lot of the imaging work in this thesis, none of this would have been possible. In fact, it is because Leonie (thank you as well!) referred me to you as the expert on MRI that I got in contact with Heidi in the first place. You also pushed me to learn Unix scripting and this skill has paid off many times during my PhD. Thanks for all the good times and may you enjoy many more espressos in your impressive research career. (Also please keep me updated if you receive any more visits from neighbourhood cats).

Uiteraad kan ik dit dankwoord niet schrijven zonder Linda te bedanken. Als een soort yin en yang vulden wij onze sterke en minder sterke kanten aan om het mega STRAIN project voort te trekken en kwam de data sneller binnen dan dat we het konden analyseren. Met je onuitputtelijke werkdrift had je vaak een

klus al handmatig geklaard terwijl ik nog zat te denken: “Hoe zou je dit met een scriptje kunnen doen?”. Daarnaast is natuurlijk de bijdrage van je legendarische kletsvermogen aan ons kantoor niet te vergeten. De lange, soms intense, politieke discussies die je met Inge had zorgden er dan wel weer voor dat ik een fijn achtergrondgeluid had om toch dat scriptje maar te maken. Bedankt voor de gezelligheid en de super samenwerking van de afgelopen jaren en je bent dan natuurlijk ook onmisbaar als mijn paranimf.

Natuurlijk was de studie ook niet van de grond gekomen zonder de enorme inzet van het dynamische STRAIN team van de afgelopen jaren: Lotte, Ann-Kathrin, Wouter, Charissa, Federico, Aafke, Sophie, Jolien en Shelby.

Sophie, Aafke en Jolien, jullie wil ik nog eens extra goed in het zonnetje zetten aangezien onze samenwerking zo goed bevallen was dat jullie na de stage nog eens lekker zijn teruggekomen voor een extra rit op de STRAIN achtbaan. Jullie hebben zelfs meegeholpen bij het opleiden van de nieuwe stagiaires en Sophie heeft ook nog eens bergen verzet om de basis te leggen voor de Bluespot database. Super bedankt voor jullie harde werk.

Lotte en Shelby, jullie verdienen ook een extra pluimpje voor het uitstekend organiseren van het contacteren en testen van vele tientallen deelnemers, ondanks dat jullie de enige stagiaires waren in jullie stageperiodes. Heel erg knap gedaan!

Astrid, Danielle, Nico, Ed, Ron en Joost (Tan), zonder jullie harde werk zou de afdeling niet overeind blijven staan. Of het nou ging om een opstandige Mac computer, een enveloppencrisis, een database opzetten, of het ontcijferen van een script, jullie stonden altijd in de startblokken om te helpen. Enorm bedankt hiervoor.

Ook de mensen van Scannexus en instrumentatie, Kim, Lilian, Job, Rick, Esther, Luc en Chris wil ik graag bedanken voor jullie expertise en de tijd en moeite die jullie hebben gedaan om het onderzoek zo vlot mogelijk te laten verlopen.

Natuurlijk is niet te vergeten dat een mooie studie opzetten leuk en aardig is, maar je er niet zo veel aan hebt zonder de mensen die hun vrije tijd opofferen om mee te doen aan deze studie. Daarom wil ik graag ook mijn enorme waardering en dankbaarheid uiten richting alle mensen die met zo veel enthousiasme en interesse hebben meegedaan aan de STRAIN studie.

Joost (Riphagen), jij hebt me haarfijn de do's en don't's van R uitgelegd in een spoedcursus aan het begin van mijn tijd bij de UM en deze kennis heb ik mijn hele PhD lang kunnen toepassen. Ook je vermakelijke, doch wijze commentaar in de achtergrond van mijn Skypegesprekken met Heidi brachten altijd verse inzichten over het onderzoek. Verder heeft het zien van jouw prestatie tijdens je verdediging me moed gegeven om zelf ook de spotlight te accepteren als mede-introvert.

Niels, bedankt voor de gezellige gesprekken bij het koffieapparaat over alle facetten van het bestuderen van de natuur. Zij het met telescopen, microscopen of door het zelf graven in de ENCI-groeve hier in ons eigen Maastricht. Ik kwam er redelijk snel achter dat het bikkelen in de kou en regen in de vroege zaterdaguren toch andere koek is dan wat je op basis van de Jurassic Park films misschien zou verwachten van de paleonthologie. Desondanks heb ik er nog steeds leuke herinneringen en een mooie collectie fossielen aan overgehouden.

Mignon, als mede-kattengekkie, metalhead en ere-lid van het MRI kantoor kom jij natuurlijk ook niet onder het paranimf zijn uit. Je bracht altijd chille vibes en reminders om even pauze te nemen en de nieuwe soepjes van Banditos te gaan proberen (shoutout naar Banditos voor het voorzien van de caffeïne die dit proefschrift mogelijk heeft gemaakt). Ik ben ook enorm vereerd dat ik als een van de weinige mensen niet op Boesje's hitlist sta dus ik hou me graag te vriend met je om dat zo te houden. Bedankt voor de gezelligheid!

Eoin, without you as my study buddy in the neuropsychology master, I would still be in a fetal position in the library instead of finishing my doctoral thesis. Thank you and best of luck to you in Ireland, Germany, England, or wherever you end up.

Nynke, bedankt voor het ontwerpen van de prachtige cover en voor de fijne samenwerking!

Ado, Jens, Jeff en Rob, bedankt voor de vele late night game sessies, dungeons & dragons avonturen, jamsessies, filosofische discussies en overige nerd hobbies. Ik ken jullie al meer dan 15 jaar en we hebben allemaal vele fases van ons leven doorgemaakt, maar ik weet dat ik jullie nog altijd kan vinden om weer even goed de geek uit te hangen.

Mathilde, thank you for your unwavering support during my PhD. When I sometimes had to work during our weekends together, you simply got cozy and joined me behind my laptop. Even when work required us to live further apart, there was never a moment I didn't feel your love and support. Thank you for all the amazing dinners, city trips, fun activities and your sassy commentary. Even when we're doing nothing at all, you always manage to put a smile on my face and brighten the day. You mean the world to me.

Midas, I could never choose whether I was a dog person or a cat person, but you suddenly made that choice very easy for me. You were a truly unique and wonderful feline companion whose time with us was far too short. So, of course I had no choice but to dedicate my thesis cover to you. I hope you are chasing many bugs in the afterlife and hopefully we meet again some day, buddy.

Natascha, Xavier and Edouard, thank you for the many sunny holiday breaks filled with amazing food, cocktails and companionship. Thank you for always supporting Mathilde, Midas and I and for making me feel like a part of the family. Merci à vous.

Pap en mam, jullie zeiden van kinds af aan al dat ik een onderzoeker zou worden en nu ligt hier dan het bewijs. Met "slechts" modale ouders heb ik dankzij jullie steun en zorgen toch al mijn studies succesvol weten af te ronden en de mogelijkheid gehad om deze PhD te doen. Bedankt voor jullie eeuwige steun en zorgen en ook voor jullie bijdrages aan het Alzheimer onderzoek. Natuurlijk moet ik Bowie en de katten ook niet vergeten te bedanken voor hun emotionele steun. En ja, je mag me dan eindelijk Doctor noemen, pap.

Myrthe, ik ben natuurlijk ook erg trots om jou mijn kleine zusje te mogen noemen. Het is enorm inspirerend om te zien hoe jij als echte powervrouw met je harde werk enorme stukken juridische teksten verslindt en jij de officiers van justitie af en toe misschien wel de les moet lezen. Laat het ook hier zwart op wit staan dat jullie een kat moeten adopteren, trouwens.

Opa, het verschil tussen een doctor en een huisarts is u misschien niet helemaal duidelijk, maar voor mij bent u al vanaf de kindertijd een inspiratiebron geweest met uw kennis, wijsheid en nuchterheid.

OVER DE AUTEUR - ABOUT THE AUTHOR

Roy Willem Elisabeth van Hooren werd geboren op 10 mei 1993, te Valkenburg aan de Geul. Hij groeide in Stein op en haalde zijn vwo-diploma aan het Groenewald college in Stein. Hierna studeerde hij de bachelor Psychologie met biologische minor aan de Universiteit Maastricht en rondde deze af met een these over epigenetische factoren bij schizofrenie onder begeleiding van Prof. Dr. Arjan Blokland. Vervolgens startte hij de master Neuropsychology aan de Universiteit Maastricht, waar zijn interesse werd gewekt voor MRI onderzoek. Tijdens de master deed hij zijn onderzoeksstage, onder begeleiding van Dr. Inge Timmers, over functionele herseneigenschappen bij chronische pijn. Na het afronden van de master startte hij als onderzoeksassistent bij Dr. Heidi Jacobs en begon in 2018 zijn promotietraject. Hierbij werkte hij aan de STRAIN studie en deed hij zijn promotieonderzoek naar vroege herseneigenschappen bij de ziekte van Alzheimer onder supervisie van Dr. Heidi Jacobs, Prof. Dr. Frans Verhey en Dr. Maxime van Egroo.